HOMOGENOUS AND HETEROGENOUS CATALYTIC ACTIVITY OF METALLOPHTHALOCYANINES TOWARDS ELECTROCHEMICAL DETECTION OF ORGANIC COMPOUNDS

THESIS
submitted in fulfilment of the
requirements for the
Degree of

MASTER OF SCIENCE

of Rhodes University

by

TSUKUTLANE J P MAFATLE
B.Sc(NUL), PG Dip. Q.Eng.(Paisley), Ind. Chem.(Intec), B.Sc Hons(Rhodes)

Rhodes University, South Africa
January 1998

To my mum

and

Family

DECLARATION STATEMENT

I hereby declare that this research report is the result of my own investigative study. It is being submitted for the degree of Master of Science at Rhodes University, Grahamstown, and has never been submitted or accepted for any other degree or examination at any other university. Where reference is made to other people's work, this has been duly acknowledged.

Signed: 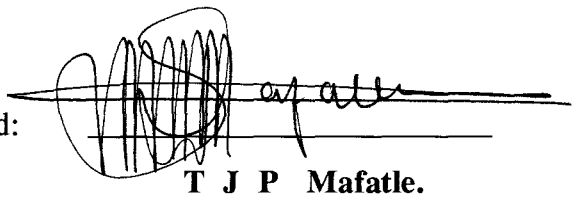

T J P Mafatle.

(30 January 1998)

ACKNOWLEDGEMENTS

With utmost gratitude, I wish to sincerely thank my project supervisor, Prof. T Nyokong, for the guidance and support she provided me with throughout the entire course of this investigative study. Without her, this research undertaking would not have succeeded. Furthermore, a word of appreciation is extended to the following:

- My mother, family and Ms L Rankoane for encouragement and support they have given;
- Mr M S Lesoro for proof-reading this manuscript;
- Lesotho Government, through Manpower Development Secretariat, for the loan bursary;
- Rhodes University for financial assistance in the form of graduate assistantship;
- Chemistry department of Rhodes University and its staff for their assistance in different ways;
- Prof. M Davies-Coleman for assistance with the interpretation of NMR spectra;
- Mr A Adriaan for making the capillary tubes used in fabricating carbon paste electrodes;
- Mr X Nocanda for his help with the NMR; and
- My research group for the support and fruitful discussions, friends and everybody for their various and valuable contributions, and for making my stay comfortable in Grahamstown.

J P T M.
Jan. 1998

ABSTRACT

Cysteine plays an important role in many biological and pharmaceutical systems. Therefore, in view of its importance, it is essential to find means of detecting it at the lowest possible levels. In this regard, electrochemical techniques have been found to be capable of detecting analytes even at micro levels. However, electrochemical determination of cysteine occurs at a very high potentials. These overpotentials makes quantitative analysis or detection of cysteine difficult at most conventional carbon electrodes. On platinum electrode, the oxidation of cysteine has been reported to occur in the potential range 0.7 to 1.45 V (*vs* NHE). Therefore, the object of this investigative study has been to find an active complex that could replace platinum and other expensive metals as electrodes. Such a complex should also be capable of reducing the potential at which the oxidation of cysteine occurs on carbon electrodes. As a result, this manuscript gives a full report on the investigative study of electrocatalytic activity of molybdenum phthalocyanine complexes towards detection of cysteine.

Molybdenum phthalocyanine, OMo(OH)Pc, and its tetrasulfonated derivative, $[OMo(OH)TSPc]^{4-}$ were successfully used to reduce the potential needed to initiate the oxidation of cysteine on carbon paste electrodes (CPE). The oxidation of cysteine on CPE modified with OMo(OH)Pc was found to occur at 0.29 V (*vs* Ag|AgC*l*), and in the presence of $[OMo(OH)TSPc]^{4-}$ species in solution the oxidation occurred at 0.33 V (*vs* Ag|AgC*l*). Molybdenum, in the oxidation states of $Mo^{(IV)}$, $Mo^{(V)}$ and $Mo^{(VI)}$, is found in biological systems as an essential trace element, participating in a number of enzymatic reactions, where it is believed to be coordinated to sulphur-containing ligands in many molybdenum enzymes. This therefore explains why molybdenum phthalocyanines were employed in electroanalytical detection of sulphur containing amino acid, cysteine.

Electrochemical methods have also been successfully used in detection of environmental pollutants such as phenolic compounds. Phenolic compounds are oxidised at readily accessible potentials. However, like cysteine, there are problems associated with the electrochemical detection of these important environmental pollutants. Their electrooxidation is known to form dimeric and/or polymeric oxidation products which adsorb onto the electrode surface, thus

deactivating it. Therefore, to address this problem, cobalt phthalocyanine (CoPc) and its tetrasulfonated derivative, $[CoTSPc]^{4-}$, were employed in electrocatalytic detection of phenolic compounds. These complexes were found to increase the anodic peak currents for the oxidation of o-cresol, m-cresol, p-cresol, phenol, 2-chlorophenol and 4-chlorophenol. In addition, CoPc deposited onto the glassy carbon electrode improved the stability of the electrode, by reducing electrode poisoning caused by the electrooxidation products of the mentioned phenolic compounds. The potential at which the oxidation occurred and the current response of individual phenolic compounds depended on the degree of substitution and the type of substituent on the phenol molecule. In general, the current response was found to be lower for chlorinated phenols compared with the cresols and phenol. To establish the role of the central metal in the catalytic process, comparison of the electrocatalytic activity of some of the first row transition metal phthalocyanines, for the detection of mono-substituted phenolic compounds, showed the following trend:

$Co^{(II)}Pc > Mn^{(II)}Pc > Fe^{(II)}Pc > Ni^{(II)}Pc > Cu^{(II)}Pc > H_2Pc > Zn^{(II)}Pc >$ Bare GCE.

A report is also given on electrocatalysis using $[CoTSPc]^{4-}$ electrochemically deposited on the glassy carbon electrode. This was also found to enhance the anodic peak currents for the oxidation of all phenolic compounds. A report on the effects of scan rate, operating potential, analyte concentration and other variables is also given.

TABLE OF CONTENTS

Page

RESULTS AND DISCUSSION

CHAPTER THREE: CHARACTERISATION OF MPc COMPLEXES

CHAPTER FOUR: ELECTROANALYSIS OF L-CYSTEINE

LIST OF ABBREVIATIONS

2-CLP	=	2-chlorophenol
4-AAP	=	4-aminoantipyrine
4-CLP	=	4-chlorophenol
AE	=	Auxiliary/Counter Electrode
Ar	=	Aromatic
BAS	=	Bio-Analytical System
BE	=	Bulk Electrolysis
C-x	=	Carbon at position x (where x = integer)
CC	=	Chemical Catalysis
$CDCl_3$	=	Deuterium chloroform
CE	=	Catalytic Efficiency
ClN	=	Chloronapthalene
CMCPE	=	Chemically Modified Carbon Paste Electrode
CME	=	Chemically Modified Electrodes
CMGCE	=	Chemically Modified Glassy Carbon Electrode
CPE	=	Carbon Paste Electrodes
CV	=	Cyclic Voltammetry
DIN	=	Germany's Standards Institute (Deutsches Institut für Normung)
DMF	=	N,N-dimethylformamide
DMSO	=	Dimethyl Sulphoxide
DPP	=	Differential Pulse Polarography
DPV	=	Differential Pulse Voltammetry
EC	=	Electrocatalysis/Electrochemical Catalysis
EU	=	European Community/Union
GCE	=	Glassy Carbon Electrode
H-x	=	Hydrogen at position x (where x = integer)
HOMO	=	Highest Occupied Molecular Orbital
H_2TMAP	=	Tetrakis (4-trimethylammoniumphenyl) porphyrin
IR	=	Infrared spectroscopy
LUMO	=	Lowest Unoccupied Molecular Orbital
m	=	Multiplet
MeCN	=	Acetonitrile
MTSPc	=	Metal tetrasulfonated phthalocyanine $[M^{II}(SO_3)_4Pc]^{4-}$

NADH	=	Dihydronicotinamide Adenine Dinucleotide
NHE	=	Normal hydrogen electrode
NMR	=	Nuclear Magnetic Resonance
Pc/Pc(2-)	=	Phthalocyaninato ion $[H_{16}C_{32}N_8]^{2-}$
PCP	=	Pentachlorophenol
pH	=	Hydrogen ion concentration
PSCV	=	Potential Step Cyclic Voltammetry
Py	=	Pyridine
RE	=	Reference Electrode
RSH	=	Cysteine
RSSR	=	Cystine
s	=	Singlet
SCE	=	Saturated Calomel Electrode
TCP	=	2,4,5-trichlorophenol
TBAP	=	Tetrabutylammonium perchlorate $[(C_4H_9)_4NClO_4]$
TEAP	=	Tetraethylammonium perchlorate $[(C_2H_5)_4NClO_4]$
THF	=	Tetrahydrofuran
USEPA	=	United States Environmental Protection Agency
V	=	Volts
WE	=	Working Electrodes

LIST OF SYMBOLS

α	=	Transfer coefficient
Γ	=	Surface coverage
ΔE_p	=	Peak potential difference
A	=	Electrode surface area (cm^2)
Å	=	Angstrom units
C	=	Concentration (mol dm^{-3})
D	=	Diffusion coefficient
E	=	Potential
$E_{½}$	=	Half-wave potential
E^o	=	Formal/standard electrode potential
E_{pa}	=	Anodic peak potential
E_{pc}	=	Cathodic peak potential
F	=	Faraday constant
i_{pa}	=	Anodic peak current
i_{pc}	=	Cathodic peak current
i_{pf}	=	Forward peak current
i_{pr}	=	Reverse peak current
k^o	=	Standard rate constant
n	=	Number of moles of electrons transferred
n_a	=	Number of moles of electrons involved in the charge transfer step
Q	=	Charge under peak (i.e. area under voltammetric peak)
R	=	Gas constant
T	=	Temperature
v	=	Scan rate (V sec^{-1}) or stretching vibrations (IR)
®	=	Registered trade mark
ϵ_{max}	=	Molar extinction coefficient
λ_{max}	=	Wavelength
δ	=	In-plane bending (IR) or Chemical shift (NMR)

LIST OF FIGURES

Figure:

LIST OF TABLES

Table:

LIST OF SCHEMES

Scheme:

CHAPTER ONE: INTRODUCTION

1.1 Electrochemistry

1.2 Theory of electrocatalysis

1.3 Modified electrodes

1.4 Electrochemistry in detection of organic compounds

CHAPTER ONE: INTRODUCTION

1.1 Electrochemistry

General theory and kinetics

During electrolysis, the substrate is consumed in the electrode reaction, and its concentration gets depleted near the electrode surface than in the bulk of the solution. Therefore, if it were not for the mass transfer of the substrate towards the electrode, the substrate concentration would decrease immediately after the initiation of electrolysis. Mass transfer in electrochemical reactions can occur in three ways, namely, through diffusion, convection and migration. Convectional mass transfer occurs when the solution is stirred either by a mechanical device or because of difference in density from one point of solution to another as a result of temperature difference. Diffusion results from the difference in solute concentration from one point of the solution to another.

In a steady solution, mass transfer occurs by diffusion of the substrate toward the electrode. When electrolysis commences, the effect of substrate depletion extends further into the solution. Since the driving force for diffusion is the difference in concentration from one point to another, once the substrate gets depleted around the electrode, this creates a stream flow of substrate from the bulk of solution toward the electrode to compensate for the loss. At the electrode surface, charge transfer occurs. It is this charge transfer that is responsible for the voltammetric peaks, with diffusion current, that are observed. The magnitude of current density is determined by the rate at which the substrate is transferred to the electrode [1]. An increase in scan rate will therefore increase the rate of diffusion, hence increasing conversion of substrate to product at the electrode. To compensate for this rapid loss of the substrate near the electrode, rate of diffusion will increase rapidly too, resulting in increased current density. Therefore, an increase of the rate of electrolysis is directly related to the increasing current

density. This means that a plot of peak current against square root of rate of electrolysis will give a linear relationship, indicating that mass transfer in solution is diffusion controlled [2].

Cyclic voltammetry

In cyclic voltammetry, the potential is scanned linearly from the initial value, $\mathbf{E}_i$, to a second value (irrespective of direction of scan) and then back to the starting potential. Normally, the potential is scanned beyond the oxidation or reduction potential of the analyte under consideration. As the term "cyclic" implies, one or more potential cycles can be performed during cyclic voltammetric scan. **Fig. 1** illustrates a typical cyclic voltammogram of a quasi-reversible reaction. It is apparent from **Fig. 1** that cyclic voltammetry is capable of rapidly generating new oxidation species during the forward scan and then monitors its fate on the reverse scan. Cyclic voltammetric processes can either be classified as reversible, quasi-reversible or irreversible depending on the nature of the reactions.

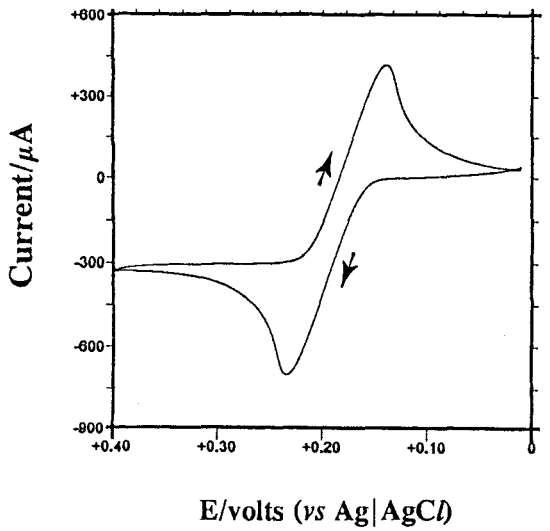

FIGURE 1: *Diagram showing a typical cyclic voltammogram of a quasi-reversible reaction (for illustrative purpose only).*

(i) **Reversible process**

The system is said to be reversible when the oxidized or reduced species are reduced or oxidized, respectively, back to the starting reagent. This is represented by the forward wave which is followed by a corresponding reverse wave upon changing the scan direction. At 25°C

the peak current for a reversible system is given by the **Randles-Sevcik** equation [3]:

$$i_p = (2.69 \times 10^5)\, n^{3/2}\, A\, D^{1/2}\, C\, v^{1/2} \quad \ldots\ldots (1)$$

From equation 1, the peak current (i_p) is found to be directly proportional to concentration (**C**) and increases with increasing square root of scan rate ($v^{1/2}$); n represents the number of moles of electrons transferred, **A** is the electrode surface area and **D** is the diffusion coefficient. The cyclic voltammogram of a simple reversible systems, also termed Nernstian wave, is characterised by a change in peak potential (ΔE_p) less or equal to 0.059 V, and with the ratio of reverse-to-forward peak currents, i_{pr}/i_{pf}, of unity, regardless of scan rate. The number of moles of electrons transferred in the electrode reaction for a reversible couple can be obtained from the separation between peak potentials as given by equation 2, at 25°C [3]:

$$\Delta E_p = E_{pa} - E_{pc} = \frac{2.3\,RT}{nF} = \frac{0.059V}{n} \quad \ldots\ldots (2)$$

The half wave potential, $E_{1/2}$, which is related to the formal potential (E^o), is centred between the anodic peak potential, E_{pa}, and the cathodic peak potential, E_{pc}, as represented by equation 3 below [3]:

$$E_{1/2} = \frac{E_{pa} + E_{pc}}{2} \quad \ldots\ldots (3)$$

Therefore, the peak separation can be used to determine the number of moles of electrons

involved in a redox reaction, and as a criterion for a Nernstian behaviour.

(ii) Irreversible processes

Cyclic voltammograms of irreversible processes are often characterized by a single oxidation or reduction wave, and no reverse wave, indicating non-regeneration of the starting reactant. This may arise from the formation of an electroinactive reduction or oxidation product. Irreversible processes are characterized by a shift of the peak potential with the change in scan rate, and are described by equation 4 [3]:

$$E_p = E^o - (RT/\alpha n_a F)[0.78 - \ln(k^o/D^{1/2}) + \ln(\alpha n_a F v/RT)^{1/2}] \quad \ldots\ldots (4)$$

From equation 4, it is apparent that the peak potential, E_p, occurs at potentials higher than E^o, with the overpotential related to the standard rate constant, k^o, and transfer coefficient, α. Independent of the value of k^o, such peak displacement can be compensated by an appropriate change of the scan rate. The peak potential and half-peak potential (at 25°C) will differ by $48/\alpha n$ (mV). Hence, the voltammogram becomes more drawn out as αn decreases. The peak current is given by equation 5 [3]:

$$i_p = (2.99 \times 10^5)\, n\, (\alpha n_a)^{1/2}\, A\, D^{1/2}\, C\, v^{1/2} \quad \ldots\ldots (5)$$

Equation 5 shows that the peak current is proportional to the bulk of the concentration and square root of scan rate. Irreversible waves are often obtained in voltammetric analysis of organic substances, but they are also encountered in inorganic chemistry, such as in reduction of divalent nickel and cobalt, hydrogen peroxide and iodate ion [1].

For irreversible diffusion controlled processes, the slope of a plot of i_p against square root of scan rate is related to the moles of electrons transferred by equation 6 [4]:

$$\frac{\text{slope}}{Q} = \frac{nF}{4RT} \quad \text{.....(6)}$$

Therefore, knowing the slope of the plot of i_p against $v^{1/2}$ and the charge under the voltammetric peak, Q, the number of moles of electrons transferred, n, can be calculated. Again the charge under the peak gives [3];

$$Q = nFA\Gamma \quad \text{.....(7)}$$

from which the surface concentration of the adsorbed species or surface coverage, Γ, can be estimated. Equation 7 applies to both reversible and irreversible processes.

(iii) Quasi-reversible process

For quasi-reversible processes, the current is controlled by both the charge transfer and mass transport. This applies to systems with k^o in the range $10^{-1} > k^o > 10^{-5}$ cm s^{-1} [3]. In general, quasi-reversible voltammograms are more drawn out, have a large peak potential separation, ΔE_p, and the peaks are more rounded as compared to a reversible process. For quasi-reversible reactions, peak current (i_p) is not proportional to the square root of scan rate, $v^{1/2}$ [5].

1.2 Theory of electrocatalysis

Redox reactions of some electroactive organic compounds, such as cysteine, occur at a measurable rate only at a very high overpotentials [2,6]. To solve this problem, a catalyst can be used to provide alternative reaction pathways which avoid the slow step and allow the reaction to be carried out at an increased current density close to the reversible potential.

A catalyst is a substance which increases the rate at which a chemical reaction attains equilibrium, without itself undergoing any net chemical change. This means that a catalyst enters as a reactant, undergoes chemical transformation, but is ultimately regenerated so that its concentration remains undiminished. Therefore, it is apparent that a catalyst can only increase the rate of a process which is thermodynamically feasible, that is, one in which there is a decrease in free energy of the reaction. However, for a given reaction, there are several permissible reaction paths. The type of catalyst used may selectively determine which path is taken, provide a completely new path for the reaction or act selectively on only one of the reactants present, thus forming the desired product to the exclusion of others.

There are two modes of catalysis involved in electrochemical reactions: homogeneous and heterogeneous catalysis. In homogeneous electrocatalysis, the catalyst and the substrate form an adduct which is transported to the electrode surface where charge transfer occurs. The catalyst is later regenerated by spontaneous decomposition of the adduct. For heterogeneous electrocatalysis, the catalyst that is adsorbed onto the electrode is believed to form an adduct with the substrate, from the solution, to which electron transfer occurs. Therefore, it is clear that the catalyst simply serves as a mediator through which electron transfer takes place, thus playing the role of a charge carrier between the electrode and the substrate [4,7].

As already mentioned, catalysts function by formation of intermediates with the reactants, which subsequently decompose to form a product. Usually, catalysts have a certain degree of valence unsaturation which allows them to form bonds with the reactants and intermediates. The bonds formed must be weak enough to allow ready rupture so that intermediates can form products easily. Where metals are involved, metals make the catalysts to be more selective.

According to Kenball [8], the two major factors which control selectivity are thermodynamic and mechanistic factors. Thermodynamic selectivity factor comes into play when two reactants compete for the same surface active sites, and if the rates of adsorption and desorption of these reactants are rapid compared to the catalytic steps, the relative amounts of the adsorbed species will be determined by equilibrium considerations which constitutes the thermodynamic factors. If the rate of adsorption or desorption of one reactant B is slow compared with the rate of adsorption and desorption of A, and with the rates of catalytic steps, then the concept of thermodynamic factor is no longer applicable. The mechanistic factor then comes into play, and this is applicable where there are other alternative kinetic reaction paths, each with its rate of reaction associated with the mechanism involved. In thermodynamic selectivity factor, competition for surface active site by two reactants leads to poisoning of the electrode and inhibition of the reaction concerned.

Inhibition and poisoning

Even though electrode poisoning has more drastic effect on the rate of reaction than inhibition, these two terms are often used synonymously. The principal way in which the poison operates is by competing for active sites and thereby contributing to deactivation of the electrode. Electrode poisoning can still be observed even if no substances other than one reactant and its products are present in the catalysed reaction system. This occurs when the product(s)

compete strongly with the reactant for the catalytic sites, thus reducing the rate of reaction. Alternatively, the reactant itself may form strongly adsorbed species instead of the formation of a less strongly adsorbed species required for catalytic reaction. This condition is termed self-poisoning. Catalyst specificity can be improved by the presence of a selective poison. In the presence of a selective poison, the poison may cause the catalyst to operate more selectively, than it would have done in its absence.

1.3 Modified electrodes

1.3.1 Methods of modifying electrodes

Most often, the redox reactions at the conventional bare electrodes involves a very weak interaction between the substrate molecule and the electrode, or the reaction involves sluggish electron-transfer kinetics, thus making such reactions to take place only at potentials substantially higher than the expected thermodynamic redox potentials. For instance, oxidation of dihydronicotinamide adenine dinucleotide (NADH) on uncoated platinum is sluggish and occurs at potentials as high as 1.3 V versus normal hydrogen electrode (NHE) [9]. Also the redox reaction of sulfhydryl compounds, such as oxidation of cysteine and reduction of cystine involves a weak interaction with carbon electrodes [10], thus, such reactions need high overpotentials for redox reaction to proceed at a reasonable rate. Therefore, such processes can be easily catalysed by incorporating or attaching suitable surface-bound electron-transfer mediators capable of facilitating interaction of substrate and the electrode, and improving reaction kinetics by accelerating electron transfer.

Electrodes which have an electroactive mediator attached on or incorporated into them are termed chemically modified electrodes (CME) or catalytic electrodes. Ideally, a catalytic

electrode should have a long life, increase current density and reduce the potential required for the redox reaction. The key to electrode modification is to build in chemical sensitivity and selectivity into the electrode so that the analyte of interest is selectively detected by the electrode to the exclusion of other unnecessary constituents and reactions.

Recently a lot of research has gone into chemical modification of electrode surfaces by attaching appropriate organic molecules to conventional electrodes, such as gold, platinum or glassy carbon. Methods such as (1) drop dry, (2) vacuum deposition and, (3) electrochemical deposition have been used to immobilize electrocatalysts onto the electrode surface. Lately, the methods involving (4) incorporation of the catalyst into a conductive matrix such as graphite powder to produce a chemically modified carbon paste electrodes (CMCPE) have been reported [2,6].

Electrochemical deposition (electrodeposition)

Electrodeposition can be achieved by repetitive voltammetric scanning, of appropriate catalyst solution, within the specific range of potential. Electrochemical deposition involves adsorptive interaction between the adsorbate and electrode surface, in which electron density is shared by the adsorbed molecule and the surface [11]. The thickness of the film can be controlled by varying the length of time of electrodeposition. Polymer films electrodeposited this way have been found to be completely insoluble in the analyte solution, even in the solvent used to prepare the solution for electrodeposition. This then prevents loss of polymer materials from the electrode during electrochemical measurements.

Direct adsorption (drop-dry method)

Direct adsorption involves dipping the electrode into the solution of the catalyst, removing it from the solution, and then allowing the solvent to evaporate. This forms a thin uniform layer on the electrode surface. The problem with this method is that it is difficult to control the amount of material deposited on the electrode surface. Alternatively, a known volume of the catalyst solution is transferred onto the electrode surface. This then allows accurate control of the catalyst deposited. This method makes it easy to vary the thickness of the film by increasing the amount or number of depositions, or by increasing the concentration of the catalyst.

Carbon paste electrode

An alternative approach to electrode modification involves incorporating the catalyst into a conductive matrix such as graphite powder to produce a carbon paste electrode (CPE). The chemically modified CPE involves mixing graphite powder with a suitable catalyst and nujol oil to form an electroactive graphite/nujol matrix. CPEs are easy to construct and are capable of producing rapid, reproducible, and easily renewable surfaces. However, despite the potential advantages which might be accrued from their use, only a few instances involving their use have been reported [2,5].

1.3.2 Phthalocyanines in electrocatalysis

Phthalocyanines are a class of porphyrin-like compounds known as tetraazaporphyrins. Metal phthalocyanine (MPc), where Pc is the phthalocyaninato anion, $[C_{32}H_{18}N_8]^{2-}$, contains a ring system made up of four isoindole units. Phthalocyanines and their metal derivatives are characterized by the aromatic π-electrons that resonate through the tetraazaporphyrin ring, in the centre of which various metal ions can be inserted in the place of hydrogens present in non-

metallated phthalocyanine (H_2Pc). They are highly conjugated planar complexes (**Fig. 2**) with the axial coordination sites used for catalytic purposes. They have an aromatic ring system that acts both as an electron donor and acceptor.

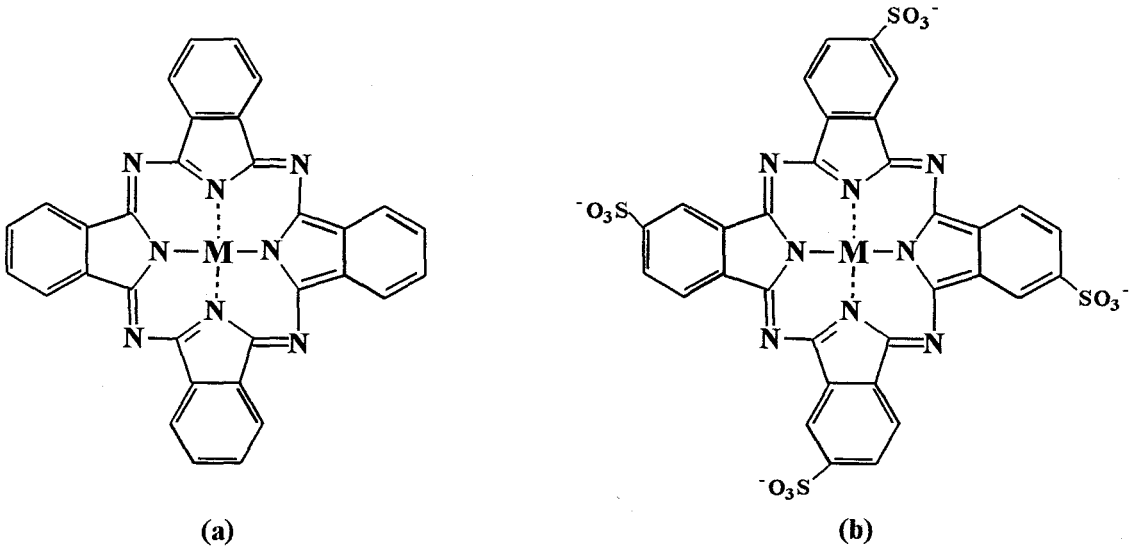

FIGURE 2: *Electronic structure of (a) metal(II) phthalocyanine and, (b) metal(II) tetrasulfonated phthalocyanine.*

Because of their great stability and the intense colour, phthalocyanines have found applications as catalysts and as dyes, respectively. Incorporating different metals into the core of the phthalocyanine ring and addition of various substituents on the periphery of the ring results in complexes that have varying properties. For example, MPc (**Fig. 2(a)**) is insoluble in aqueous solvents, but soluble in some organic solvents. However, attaching substituents such as sulphate groups (**Fig. 2(b)**) to the phthalocyanine ring renders them to be more soluble in water or any other aqueous solvents. Phthalocyanines generally have an electrochromic property, that is, changes in their oxidation numbers often results in reversible and dramatic colour changes. Therefore, these complexes have a potential application in visual display and optical data storage systems [12].

To understand the electronic constitution of the different metal phthalocyanines, Taube [13] suggested that there are 9 s-, p- and d-orbitals of the central metal atom, the 4 σ-hybrid orbitals from the inner nitrogen atoms of the Pc ring and the 40 π-orbitals of the ring. For the metal, the most important orbitals are $\mathbf{b_{2g}}$, $\mathbf{6e_g}$, $\mathbf{2a_{1g}}$ and $\mathbf{2b_{1g}}$ arising from the 3d-orbitals and the 4s-orbitals. Occupation of any of these orbitals determines the oxidation state of the central metal atom. Reduction or oxidation can occur either at the central metal or the phthalocyanine ring. Ligand or metal reduction can simply be described as an occupation of the lowest unoccupied ligand or metal orbital and oxidation as the removal of an electron from the highest occupied ligand or metal orbital **(Fig. 3)**. Taube [13] further states that the stability of the central metal improves along the transition series of the periodic table (from left to the right of the periodic table). These stability results from the increasing nuclear charge of the central atom, meaning that in the same way the oxidation potential of the MPc must increase with the increasing nuclear charge of the central metal.

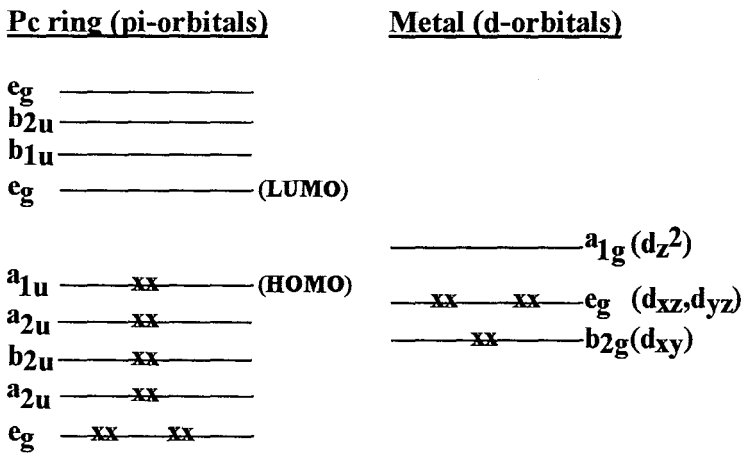

FIGURE 3: *Energy level diagram of a typical MPc, using a low spin d^6 metal (Fe^{2+}) as an example (where LUMO = Lowest unoccupied molecular orbital and, HOMO = highest occupied molecular orbital) [12].*

When dissolving MPc complexes in organic solvent such as pyridine, a bispyridine complex ($(Py)_2MPc$) is formed by pyridine molecules coordinating to the axial coordination sites of the central metal atom. For example, the bispyridine complexes are formed with chromium, manganese and iron phthalocyanines. In chromium, manganese and iron, the $2\mathbf{a}_{1g}$-orbital becomes unoccupied due to electron pairing and a strong attraction between the pyridine's bonding orbital, with the metal's $3\mathbf{d}_z^2$ and $4\mathbf{p}_z$-orbitals occurs **(Table 1)**. In nickel and copper phthalocyanines, spin pairing cannot be realized, and from the doubly occupied $2\mathbf{a}_{1g}$-orbital **(Table 1)** results a strong electronic repulsion preventing any further complex formation with pyridine. Cobalt has one electron occupying $2\mathbf{a}_{1g}$-orbital **(Table 1)** and zinc has a strongly contracted d-shell. Therefore, cobalt and zinc form a weak complex with one pyridine ligand [13].

TABLE 1: *Electronic configuration of some of the first row transition metal(II) ions in metal phthalocyanines and their pyridine complexes [13].*

M(II)Pc / Py	d-electrons	Electronic configuration
[CrPc] [CrPc.Py]	d^4	$(6e_g)^2\ (b_{2g})^1\ (2a_{1g})^1$ $(6e_g)^3\ (b_{2g})^1$
[MnPc] [MnPc.2Py]	d^5	$(b_{2g})^2\ (6e_g)^2\ (2a_{1g})^1$ $(6e_g)^4\ (b_{2g})^1$
[FePc] [FePc.2Py]	d^6	$(b_{2g})^2\ (6e_g)^3\ (2a_{1g})^1$ $(b_{2g})^2\ (6e_g)^4$
[CoPc] [CoPc.Py]	d^7	$(b_{2g})^2\ (6e_g)^4\ (2a_{1g})^1$ $(b_{2g})^2\ (6e_g)^4\ (2a_{1g})^1$
[NiPc]	d^8	$(b_{2g})^2\ (6e_g)^4\ (2a_{1g})^2$
[CuPc]	d^9	$(b_{2g})^2\ (6_{eg})^4\ (2a_{1g})^2\ (2b_{1g})^1$
[ZnPc] [ZnPc.Py]	d^{10}	$(b_{2g})^2\ (6e_g)^4\ (2a_{1g})^2\ (2b_{1g})^2$ ----------

MPc uses the axial coordination sites for catalysis. Their catalytic action is similar to that of enzymes as can be expected from their structures similar to that of metalloporphyrin in heme-enzyme [14]. For this to be possible, the central metal of the MPc needs an empty or half-filled $\mathbf{2a_{1g}}$-orbital with proper symmetry to interact with the substrate. This is characteristic of manganese, iron and cobalt [13,15]. This explains why manganese, iron and cobalt phthalocyanines have been found to exhibit higher catalytic activity towards electrooxidation of cysteine and electroreduction of cystine [16,17], and electrooxidation of hydrazine [15]. Nickel, copper and zinc (in NiPc, CuPc and ZnPc) on the other hand have $2\mathbf{a_{1g}}$-orbital filled with two electrons and these does not favour axial ligation of the substrate for catalytic purposes. This then makes NiPc, CuPc and ZnPc to be weak catalysts because of their inability to axially coordinate the substrate. Oxidation and reduction of these species takes place on the ring, rather than on the central metal atom [17-19]. Zinc(II), with an electronic configuration of $[Ar]3\mathbf{d^{10}}$, is also not known to form compounds in which the 3d-orbital looses an electron [20]. Cobalt, compared to iron and manganese phthalocyanines, has proved to be the best catalyst towards reduction of carbon dioxide [21]. This can be attributed to the presence of partly occupied $\mathbf{a_{1g}}$ orbital **(Table 1 above)** with an excess of π-electrons in cobalt, suggesting that the partially occupied $\mathbf{a_{1g}}$ orbital of the central metal atom in the phthalocyanine complexes play a central role in electrocatalysis. It is believed [21] that the ligand π-electrons simply enhances the activity of the $\mathbf{a_{1g}}$ orbital . On the other hand, low spin manganese and iron have empty $\mathbf{a_{1g}}$ orbital [21]. The empty $\mathbf{a_{1g}}$ orbital implies that there are no electrons to interact with the axially coordinated substrate, thus making manganese and iron phthalocyanines to be weaker catalysts than cobalt.

Randin [14] correlates the catalytic behaviour with the first oxidation potential of the MPc, suggesting that the electrocatalytic activity of MPcs increases with the ease at which an

electron can be electrochemically extracted from the MPc modified electrode.

For heterogeneous catalysis, the electrocatalytic activity of the MPc critically depends on the solvent from which it is deposited onto the electrode. Pyridine, which is a stronger ligand than tetrahydrofuran (THF) if used as a solvent for depositing MPc onto the electrode, will not be easily replaced by the substrate during catalysis. This is because of strong coordination between the central metal and the pyridine molecule. This strong bonding is possible with manganese and iron phthalocyanines. A weak bonding between pyridine and cobalt is formed [13], thus making substitution of pyridine ligand by the substrate easier in CoPc deposited from pyridine. And for better catalytic action, there should not be strong bonding between the solvent, substrate and redox products. This therefore explains why pyridine was the solvent used for depositing CoPc onto the glassy carbon electrode for electroanalysis of phenolic compounds in this work.

1.3.3 Absorption spectral properties of metal phthalocyanines

Metallophthalocyanines are $\mathbf{D_{4h}}$ complexes with intense $\pi \rightarrow \pi^*$ transition between 230 and 800 nm [22], which is responsible for the intense colour exhibited by MPc solid complexes and solutions. According to Stillman and Nyokong [22], the highest occupied molecular orbital (HOMO) of the phthalocyanine ring is $\mathbf{a_{1u}}$ (π) and the next low lying orbital is $\mathbf{a_{2u}}$ (π). The lowest unoccupied molecular orbital (LUMO) is the doubly degenerate $\mathbf{e_g}$ (π^*) and the next is $\mathbf{b_{1u}}$ (π^*). The $\pi \rightarrow \pi^*$ transition comprise of $\mathbf{a_{1u}}$ to $\mathbf{e_g}$ transition which produces the intense band called the Q band around 670 nm, and the $\mathbf{a_{2u}}$ and/or $\mathbf{b_{2u}}$ to $\mathbf{e_g}$ transitions which yield the Soret or B band envelope between 300 and 450 nm **(Fig. 4 below)**.

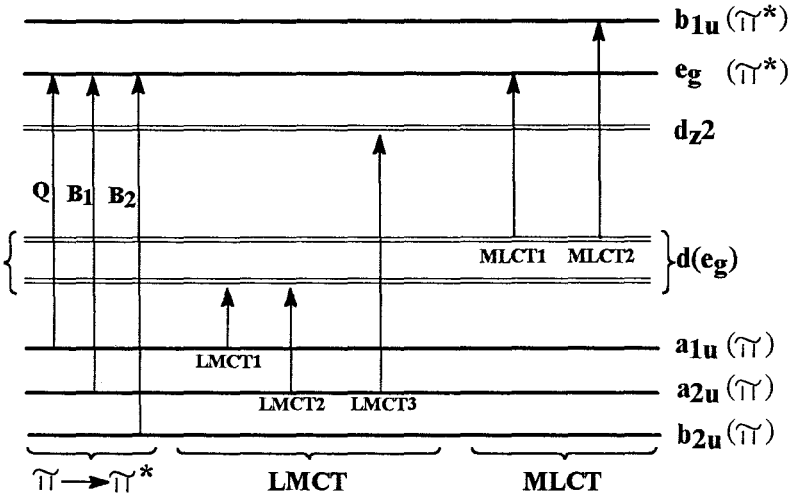

FIGURE 4: *Diagram showing different energy levels and the origin Q, B and charge transfer bands of a typical MPc complex [22,23].*

The phthalocyanines absorb strongly between 600 and 700 nm, with a fairly constant and well resolved intense wavelength (λ_{max}) around 670 nm. Therefore, within this region the red light is absorbed while the blue and green parts of the visible spectrum are less absorbed. This explains why the phthalocyanines appear blue to green, depending on the location of their visible absorption bands [24]. The Soret or B band around 300 nm is not easy to identify because the band in that region of the spectrum is much broader and less well defined. The Q band is sharp and its intensity is relatively insensitive to changes in axial ligand or central metal, whereas the wavelength is sensitive to changes in axial ligand and the change of the central metal. For the absorption spectra of phthalocyanines, the region below 450 nm comprises of several overlapping bands that change considerably with a change of axial ligand or the central metal [22].

Additional bands which appear in the same region as the $\pi \rightarrow \pi^*$ (230 - 800 nm) are usually assigned to metal to ligand (MLCT) or ligand to metal (LMCT) charge transfers, and this

involve molecular orbitals of the phthalocyanine π-system and the metal's d-orbitals. For the ligand to metal charge transfer, the electronic transition is from the ring to the metal. For the metal to ligand charge transfer, the electronic transition is from the metal to the phthalocyanine ring. The most well-known charge transfer bands lie between 450 and 600 nm, but additional weak ones are also found to the red end of the Q band between 700 and 1500 nm. With the exception of $\mathbf{d^0}$ and $\mathbf{d^{10}}$ metals, charge transfer transitions from the metal to the ligand or ligand to the metal occur in the spectral region 200 to 1000 nm. The direction and the resultant energies of these charge transfer bands depends on both the spin and oxidation state of the central metal.

For many peripherally substituted MPc complexes, aggregation occurs readily at low concentrations, and these are the concentrations which are often used to record absorption spectra of MPc complexes. The aggregation effect makes the spectral data more difficult to interpret. Rollman and Iwamoto [18] reported the occurrence of aggregation at concentrations above 10^{-5} mol dm^{-3}. In this cases, quite different absorption spectra are often observed in water, when compared to a solvent like DMF, which usually indicates the presence of extensive aggregation. For example, tetrasulfonated derivatives of phthalocyanines are generally soluble in aqueous solutions, and in many cases their spectra in the Q band region show aggregation effects, with a typical blue-shift of the maximum absorbance from 670 towards 630 nm and an overall broadening of the envelope with a loss of resolution of the vibrational components [25,26].

The appearance of a strong band around 630 nm results from coupling between the two π systems of the dimerized phthalocyanines which leads to a blue-shifting of the Q band. The absorption bands around 630 and 670 nm energies can therefore be explained in terms of

dimeric and monomeric species of the phthalocyanine complexes, respectively [25].

1.4 Electrochemistry in detection of organic compounds

1.4.1 Cysteine

Amino acids are organic substances which form the basic unit of proteins. They have the same core structure but with varying side chain (represented as **R** in equation 8 below). It is the sequence of this side chain that gives each amino acid, hence the protein, its characteristic set of properties.

Amino acids are insoluble in non-polar solvents like petroleum ether, benzene, or ethers, and are appreciably soluble in water. Their aqueous solutions behave like solutions of substances of high dipole moments. They are both acidic and basic in nature, hence their electrochemistry depends on the acidity or basicity of the medium in which they are dissolved in [27]. The occurrence of different ionic species of cysteine when dissolved in basic or acidic media is as presented in equation 8 below:

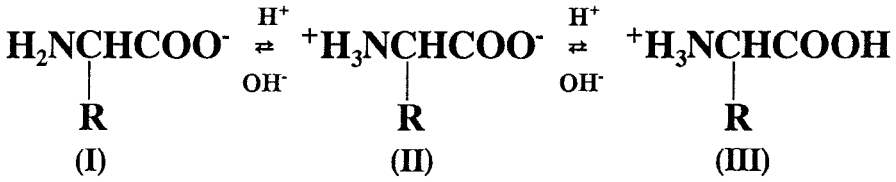

..... (8)

Where: **R** = $HSCH_2$ (for cysteine)

The hydrogen ion concentration of the solution in which compound **I** and **III** (equation 8) are in equilibrium is called the **isoelectric point** of that particular amino acids. Cysteine, which

is monoammino monocarboxylic acid (compound **II**), is more acidic than basic, with an isoelectric point of **5.02** [26]. Therefore, when dissolved in water (pH 7.0), the resulting solution contains more of the anion **I** than the cation **III** [27]. This excess ionization of ammonium ion can be repressed by addition of the acid, to reach the isoelectric point. At pH 5.02, the dipolar ion cysteine (compound **II**) exists in high concentration. Therefore, as the solution is made more acidic or more alkaline, the concentration of the more soluble and mobile ions **III** or **I** increases, respectively. This explains why acidic medium (0.05 mol dm^{-3} sulphuric acid) was used for investigative study of cysteine in this work. From the above discussion, it is therefore important to know the isoelectric point of the amino acid under consideration, so as to be able to predict which ions are present in solution, before any electrochemical analysis.

Electrochemical detection of cysteine

A lot of research into polarographic study of cysteine and cystine, using mercury electrodes, has been documented [28]. This was later followed by the use of noble metals, gold and platinum, as electrodes [29]. For the mechanism followed by polarographic detection of cysteine at pH 7.0 using mercury electrodes, oxidation of cysteine leads to an adsorbed mercuric cysteinate [$Hg(RS)_2$], which is preceded by mercury oxidation [28], as in equation 9 and 10 below;

$$Hg \rightarrow Hg^{2+} + 2e^- \quad \text{..... (9)}$$

$$2RSH_{aq} + Hg^{2+} \rightarrow [Hg(SR)_2]_{ads} + 2H^+ + 2e^- \quad \text{..... (10)}$$

Thus, electrooxidation of cysteine on mercury electrode can best be described as mercury

oxidation to form the adsorbed mercuric cysteinate, $Hg(RS)_2$. Electroreduction of cystine at the mercury electrode is highly reversible and occurs at an $E_{1/2}$ of about -0.50 V (*vs* NHE, with anodic and cathodic reduction potentials of -0.47V and -0.52 V, respectively) at concentrations below 3×10^{-4} mol dm^{-3}. This reversible process exhibits a notable shift of anodic and cathodic peak potentials with changes in cysteine concentration [28]. The shift in potential was attributed [28] to the attainment of monolayer coverage of $Hg(RS)_2$ species and the formation of a tight film when lateral interactions between the adsorbed molecules occur. Oxidation of cysteine on noble metals has been observed at easily accessible potentials. For example, on platinum electrode the chemisorbed cysteine species are oxidized in the potential range 0.7 to 1.45 V (*vs* NHE), to cysteic acid.

As reported by Pradáč and Koryta [29], electrooxidation of cysteine involves strong interaction of the sulphur atom with the active sites on the electrode surfaces of the noble metals. This is because the amino acids alanine and serine, which have similar structure as cysteine but lack S-H and S-S groups, were found to be electroinactive, indicating that sulphur is the only electroactive group in the electrooxidation of cysteine and electroreduction of cystine.

Generally, for electrochemical detection to be possible, the major property required for useful application of electrochemical methods is that the analyte of interest be oxidizable or reducible at potentials comparatively lower than the potential required for electrolysis of the solvent, otherwise electrolysis of the analyte will be masked by that of the solvent [2]. Unfortunately, at most conventional carbon electrodes, such as glassy carbon and graphite, cysteine and other sulfhydryl compounds exhibit irreversible oxidation requiring extreme positive potentials [2,6,30]. This is often compromised by slow electron-transfer kinetics at the electrode surface, which is a result of very weak interaction between cysteine sulphur atom and carbon

electrodes [10]. This weak interaction causes the oxidation to occur at a potential that exceeds the expected thermodynamic potential. The selectivity and limits of detection in electrochemical measurements depends, to an extent, on the magnitude of the oxidation or reduction overpotential [6]. The lower the potential required, the better is the sensitivity and selectivity that is expected thereof [2].

Therefore, efforts have gone into finding the catalyst(s) capable of lowering the potential needed for oxidation of cysteine and other sulfhydryl compounds so as to make the electrochemical determination of these species feasible. As a result, electrodes with surface bound redox mediators have demonstrated to have distinct advantages over conventional electrodes in detection of cysteine. For example, cobalt(II) tetrasulfonated phthalocyanine, $[CoTSPc]^{4-}$, adsorbed onto graphite electrodes has been found to result in a substantial decrease of overpotential needed for electrooxidation of cysteine [16,17]. It is therefore apparent that the presence of adsorbed layers of metal tetrasulfonated phthalocyanine (MTSPc) substantially improves the activity of the electrode, and the catalytic activity has been found to depend on the nature of the central metal ion of the MTSPc. For electrooxidation of cysteine, catalytic activity of MTSPc decreases as follows; Co > Fe > Mn > Ni > Cu, which indicates correlation between the catalytic activity and the ability of the metal to bind extraplanar ligands, such as cysteine [17]. However, on cobalt phthalocyanine ($Co^{(II)}Pc$) modified electrodes, the potential for the oxidation of cysteine is still high, about 0.77 V (*vs* SCE) [2]. As a result, in this study, other metal phthalocyanines and their tetrasulfonated derivatives were were investigated, in an attempt to lower the potential needed for the oxidation of cysteine. The oxidation potential of cysteine is related to the redox potential of metal phthalocyanine, hence why molybdenum phthalocyanines with low oxidation potential were used as electrocatalysts for the oxidation of cysteine in this study, as it will be discussed later.

1.4.2 Cresols, mono-chlorinated phenols and phenol

Analysis of phenols in natural and waste waters is of prime importance due to their persistent occurrence in the environment, where they pollute air, water and soil. Phenolic compounds, especially halogenated ones, are of concern in the environment because of their toxicity to humans, fish and other aquatic life, and their adverse effects on the taste and odour of water and fish, even at micro levels [31,32].

Phenolic compounds are introduced into the environment in various ways. For example, 4-chlorophenol, found in industrial effluents, arises from its use as an intermediate in the manufacture of quinazarin, trichlorophenol from its use as a fungicide and as a pollutant found in paper mill effluents when wood pulp is delignified by chlorine bleaching, and pentachlorophenol from its use as a wood preservative and as a moth-proofing agent [33]. Phenol, is a widely used industrial chemical, and its pollution effect arise from its use in the manufacture of products ranging from plastic resins to pesticides. Irrespective of the type of exposure, phenols are easily adsorbed by human skins, and at high levels they have been proven to have detrimental effects on animals and human health [34]. Due to hazardous effects they have on terrestrial and aquatic life, some phenols, especially nitrophenols and chlorophenols, have been listed by United States Environmental Protection Agency (USEPA) and European Community (EU) as priority pollutants. The current admissible level for phenol in drinking water is set, by USEPA and EU, at 0.5 μgL^{-1} for total content and 0.1 μgL^{-1} for the individual content, and 5 μgL^{-1} in bathing water [31,35].

Owing to their toxicity and environmental impact, analysis of phenolic compounds is of major environmental, industrial and clinical significance. Therefore, it is essential to have a cheap, rapid, sensitive and selective way of monitoring their levels at lowest possible amounts in the

environment. For quantitative analysis of phenolic compounds, use of colorimetric analysis based on 4-aminoantipyrine (4-AAP) [36], multicomponent analysis by means of UV-spectrometry [37], high performance liquid chromatography (HPLC) by linear gradient and gas chromatography with electron capture preceded by derivatization with halogenated reagents have been reported [35,38,39]. There are many problems associated with the use of some of these techniques. For example, 4-AAP method which is used as Germany's quality standard (in DIN 38409H16) for determination of phenolic compounds is based on oxidative coupling of phenolic compounds with 4-AAP, producing a quinoneimine dye that absorbs at around 510nm (equation 11) [37]. The method does not give the actual amounts of individual phenols, instead the results are expressed as "total phenols". The major problem with 4-AAP is that it does not form any dyes with nitro- or any para-substituted phenols because coupling of 4-AAP with phenols requires an unoccupied para-position [32,37]. The problem associated with other methods is that the equipment involved lacks portability, and therefore cannot be used for field monitoring and the samples, in most cases, need pretreatment prior to analysis, and the methods are slow and expensive to operate. Electrochemical methods surpasses these methods by providing improved quality, efficiency, sensitivity and selectivity of analysis, and routine field monitoring of phenols [40].

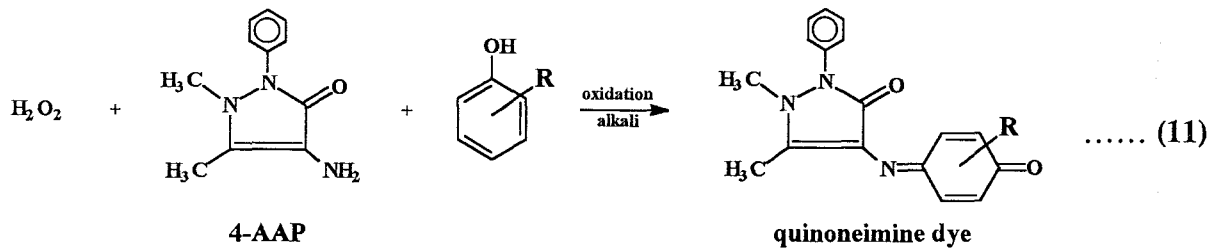

4-AAP quinoneimine dye ..... (11)

Since most phenols are oxidized at readily accessible potentials, electrochemical methods have been used successfully in their detection. However, the problem associated with their electrochemical detection is that their electrooxidation at solid electrodes produces dimeric or

polymeric products which causes electrode deactivation, resulting in a decrease in response on repetitive scans [41-46]. The mechanism for the formation of polymeric oxidation products of cresols and phenol has been established [41,45]. It is reported that cresols and phenol undergo one-electron oxidation to form a phenoxy radical. This free radical then undergoes resonance stabilization to give different phenoxy radicals which couple together to form dimeric and/or polymeric products. For example, electrooxidation of phenol follows the following route towards the formation of different phenoxy radicals **(scheme 1)** [41];

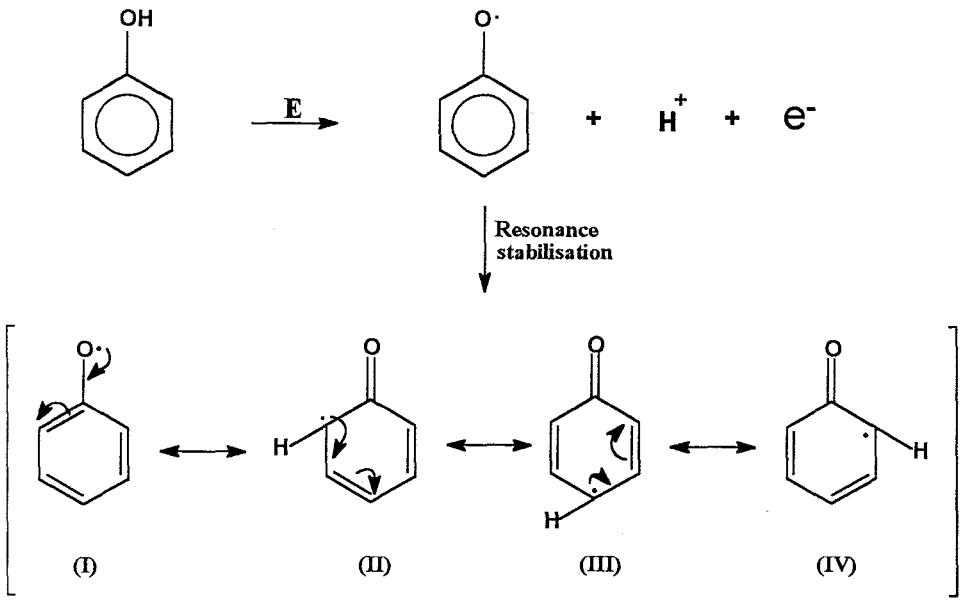

Scheme 1

Coupling of phenoxy radicals occurs through oxygen, using unpaired electrons, or through ortho or para-carbon atoms. Head-head coupling, through oxygens, does not generally occur because of instability of the resultant peroxide. Normally, coupling occurs at a position para to the hydroxyl group **(Fig. 5 below)**; if occupied, as in p-cresol, coupling takes place at one of the ortho positions. It is this polymers which are responsible for electrode deactivation

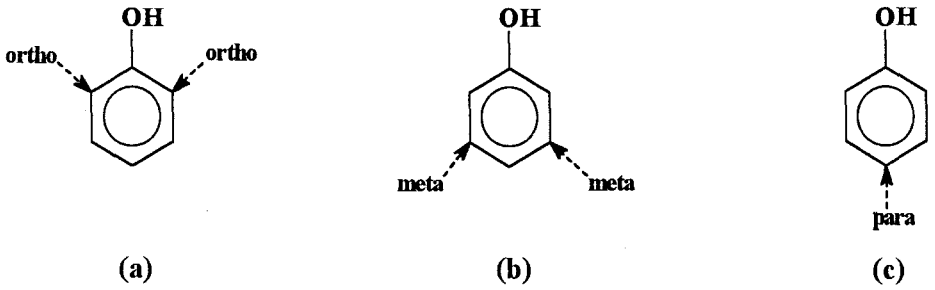

FIGURE 5: *Structural presentation of phenol showing;* ***(a)*** *ortho positions, where occupation of one of the positions by methyl or chlorine gives o-cresol or 2-chlorophenol, respectively,* ***(b)*** *shows meta positions, occupation of one of the positions by methyl gives m-cresol and* ***(c)*** *shows para position which is occupied by methyl or chlorine in the case of p-cresol and 4-chlorophenol, respectively.*

[41]. To avert this problem, different strategies have been employed in reactivating and improving the stability of the electrode. For example, anodic polarization in acidic solution of ferric chloride has been employed in removal of phenol polymeric film from the platinum electrode [47]. In-situ electrochemical renewal of glassy carbon electrode by running differential pulse voltammetry (DPV) of an electrolyte solution only (without the analyte) after the voltammetric analysis of phenol [48], flame treatment by burning off polymer film on the electrode in the bunsen burner flame for 30 seconds prior to the next voltammetric scan [42] and laser reactivation [49] have been reported. However, electrodes modified with polymeric substance have successfully been found to minimise electrode fouling in detection of phenol [46], amino acids [2,6,17,50], and nitrates and nitrites [51], thus improving sensitivity and selectivity of the electrode. This then enables routine detection and analysis of such compounds. In this work, MPcs have been used to improve the activity and stability of the glassy carbon electrode (GCE) towards detection of some phenolic compounds.

1.4.3 Polychlorinated phenols

Many environmental pollutants, including some phenolic compounds, can be converted into easily degradable compounds by hydrolysis, reduction, and/or oxidation pathways by microorganisms that utilize intra- and extracellular enzymes. However, polychlorinated aromatics are extremely persistent in the environment because of their halogen content, which contribute to their low solubility in water and resistance to oxidation under aerobic conditions. For example, natural degradation of trichlorophenol and pentachlorophenol is very slow, and can only occur by a reductive dechlorination route in anaerobic conditions or by an oxidative pathway catalyzed by ligninase or cytochrome P-450 of *Rhodococcus chlorophenolians* [52]. As a result, research into the use of catalytic and photochemical methods of oxidative and reductive degradation of these halogenated aromatic compounds has been reported [52-55].

Little information is available on an electrochemical behaviour of polychlorinated phenols. However, Christophersen and Cardwell [31] report that in an electrochemical detection of phenolic compounds, individual compounds exhibit current responses which depends on the degree of substitution and the type of substituent. In general, an increase in chloro or nitro substitution leads to a decrease in response at the electrochemical detector [31].

Trichlorophenol and pentachlorophenol are expected to undergo one-electron oxidation to form different phenoxy radicals as in the electrooxidation of phenol [41] and cresols [45]. However, coupling of these radicals, using ortho and para-carbon atoms, is likely to be sterically hindered by electron-rich chlorines occupying both para and ortho positions. This means that the electrooxidation of these compounds is unlikely to result in dimeric or polymeric oxidation products, unless if dechlorination occurs prior to coupling.

CHAPTER TWO: EXPERIMENTAL

2.1 Materials

2.2 Methods

2.3 Working electrode pretreatment

CHAPTER TWO: EXPERIMENTAL

2.1 Materials

2.1.1 Reagents

(i) Analytes

L-cysteine (98%, Sigma), phenol and o-cresol (BDH), m-cresol and p-cresols (99.5%, Saarchem), 2-chlorophenol, 4-chlorophenol, 2,4,6-trichlorophenol and pentachlorophenol (99%, Aldrich) solutions were freshly prepared in 0.05 mol dm^{-3} sulphuric acid before use. 0.05 mol dm^{-3} sulphuric acid was prepared from a concentrated acid of analytical grade (98%, Saarchem) and triply distilled-deionised water. 1.0 mol dm^{-3} sodium hydroxide was added to improve the solubility of less soluble pentachlophenol and trichlorophenol in water.

(ii) Catalysts

Phthalocyanine complexes of manganese (MnPc), iron (FePc), copper (CuPc), nickel (NiPc), zinc (ZnPc) and metal-free phthalocyanines (H_2Pc) were purchased from Eastman Kodak or Aldrich. Cobalt(II) phthalocyanine ($Co^{(II)}Pc$) was either synthesised according to the procedure outlined in section 2.1.2(iii) or purchased from Kodak. Solutions of these complexes were prepared from freshly distilled pyridine (Saarchem). Cobalt(II) tetrasulfophthalocyanine, $Na_4[Co^{(II)}TSPc]\cdot 2H_2O$ [56], oxomolybdenum(V) phthalocyanine, $OMo^{(V)}(OH)Pc$ [57,58] and oxomolybdenum(V) tetrasulfophthalocyanine, $Na_4[OMo^{(V)}(OH)TSPc]\cdot 5H_2O$ [56,59], were synthesised and purified according to the published procedures; see section 2.1.2 for detailed synthetic procedure.

(iii) Phosphate buffer

Phosphate buffer solutions were prepared from potassium dihydrogen phosphate (Eltec) and potassium hydroxide (Saarchem). For electrochemical measurements, phosphate served as a

supporting electrolyte.

(iv) Other reagents

Other reagents used include: sodium hydroxide, sodium chloride, cobalt chloride, ammonium molybdate, molybdenum hexacarbonyl, anhydrous sodium sulphate, perchloric acid (60%) and glacial acetic acid (99.5%), which were all purchased from Saarchem. Sodium perchlorate (BDH), ammonium chloride (N.T. Lab), urea and naphthalene purchased from PAL, cobalt sulphate and silver nitrate were purchased from Holpro, tetrabutylammonium perchlorate, tetraethylammonium perchlorate and phthalimide were all from Aldrich. Monosodium salt of 4-sulfophthalic acid was prepared as per the procedure in section 2.1.2(i).

All the purchased reagents and catalyst complexes were either of reagent or analytical grade, and were therefore used without further purification. All aqueous solutions were prepared from triply distilled-deionized water. Pyridine, dimethylsulfoxide (DMSO), chloronaphthalene (C*l*N) and acetonitrile were freshly distilled, DMSO was distilled under reduced pressure, before use. Tetraethylammonium perchlorate (TEAP), tetrabutylammonium perchlorate (TBAP) and ferrocene were recrystallized from ethanol before use. TEAP and TBAP were synthesised as in section 2.1.2(v) and were used as electrolytes, and ferrocene was used as an internal reference in non-aqueous electrochemical experiments.

2.1.2 Synthesis

(i) Preparation of tetrasodium salt of cobalt(II) 4,4',4'',4'''-tetrasulfophthalocyanine 2-hydrate - Na_4 [CoTSPc] · $2H_2O$

The sodium salt of cobalt(II) tetrasulfonated phthalocyanine was prepared according to the procedure adopted from the method reported by Weber and Busch [56]. That is, 6.48g of

monosodium salt of 4-sulfophthalic acid, 0.71g of ammonium chloride, 8.71g urea, 0.11g ammonium molybdate and 2.04g cobalt (II) sulphate-7-hydrate ($CoSO_4 \cdot 7H_2O$) were ground together until a homogenous mixture was obtained. Nitrobenzene (40 ml) was added to a 250 ml three-necked round bottomed flask fitted with a thermometer, a condenser and a stopper. First the nitrobenzene was heated to 180°C. Then the solid mixture was added slowly, with stirring, maintaining the temperature between 160°C and 190°C. This heterogenous mixture was then heated for 6 hours at about 190°C. The crude product obtained was ground and washed with methanol until the smell of nitrobenzene could no longer be detected. The remaining solid was added to 1000 ml of 1.0 mol dm^{-3} hydrochloric acid saturated with sodium chloride. The solution was briefly heated to boiling, allowed to cool down to room temperature, and then filtered. The resulting solid was dissolved in 300 ml of 0.1 mol dm^{-3} sodium hydroxide. The solution was then heated to 80°C and insoluble material separated by filtering the solution while still hot. 40.5g of NaCl was added to the filtrate. The slurry was continuously bubbled with air, stirred and heated to a constant temperature of about 80°C until ammonia evolution stopped. The product obtained was then washed with 80% aqueous ethanol until the filtrate was chloride-free (tested with 1.0 mol dm^{-3} silver nitrate). The product was then refluxed for 4 hours in 100 ml absolute ethanol, allowed to cool down to room temperature and a pure, blue product was obtained by filtration and dried in vacuo over silica gel (in a dessicator) to a constant weight.

Preparation of monosodium salt of 4-sulfophthalic acid

The monosodium salt of 4-sulfophthalic acid was prepared according to the literature procedure [18] by the reaction of sodium hydroxide with 30% aqueous sulfophthalic acid (Eastman), followed by evaporation giving pinkish-white crystals.

(ii) Preparation of tetrasodium salt of oxomolybdenum(V) tetrasulfonated phthalocyanine - $Na_4[OMo^{(V)}(OH)TSPc] \cdot 5H_2O$

Pentahydrate oxomolybdenum(V) tetrasulfonated phthalocyanine complex, abbreviated as $[OMo^{(V)}(OH)TSPc]^{4-}$, was prepared by the procedure similar to that detailed for the synthesis of cobalt(II) tetrasulfonated phthalocyanine above (section 2.1.2(i)), except that molybdenum hexacarbonyl was used as the starting material, instead of cobalt sulphate.

(iii) Preparation of crude cobalt(II) phthalocyanine (Co(II)Pc) complex

Crude cobalt(II) phthalocyanine ($Co^{(II)}Pc$) was synthesised following the method proposed by Farrel *et al* [60]. That is, 0.58g of cobalt (II) chloride-hexahydrate ($CoCl_2 \cdot 6H_2O$), 7.26g of O-cyanobenzamide and 2.92g of naphthalene were mixed, ground together, then transferred to a round bottomed flask and refluxed (with a water condenser) for 1 hour at 290°C. The crude product was cooled, washed with absolute ethanol, filtered, and allowed to dry. The dried residue was soxhlet-extracted with glacial acetic acid until the washings were colourless. The product obtained was dried in the oven at 90°C to remove excess acetic acid, and later dried and allowed to cool down in vacuo over silica gel.

Preparation of O-cyanobenzamide

O-cyanobenzamide, used for cobalt(II) phthalocyanine preparation, was synthesized by dissolving 31.72g of phthalamide in 100 ml of acetic anhydride, heating the mixture as fast as possible to the boiling point and then refluxing the solution (with a water condenser) for 3 hours. After cooling, yellowish-white crystals were formed. These were then washed with cold absolute ethanol and dried at 100°C overnight. Yield of 7.26g was obtained. The melting point range was 170 - 190°C, as expected.

Preparation of phthalamide.

Phthalamide used in the synthesis of o-cyanobenzamide was prepared by adding 30g phthalimide to 90 ml of 25% ammonia solution and stirred at room temperature for 24 hours. The resulting product was filtered and the white crystals obtained were dried in the oven at 100°C overnight. Yield of 31.72g was obtained. The melting point temperature range was 220 - 230°C, as expected.

(iv) Preparation of oxomolybdenum(V) phthalocyanine (OMo(OH)Pc) complex

Oxomolybdenum(V) phthalocyanine complex, $OMo^{(V)}(OH)Pc$, was prepared by following the procedure of Edmondson and Mitchell [57] by mixing ammonium molybdate and phthalodinitrile in the ratio **1:4**, respectively. The mixture was ground together and heated in air at 270°C for 45 minutes. The blue solid formed was purified by soxhlet-extraction with butanone for 6 hours. The product was then washed with 0.1 mol dm^{-3} sodium hydroxide and water to remove any unreacted molybdate, molybdenum oxide or phthalimide. The product was then further washed with ethanol and acetone until the washings were colourless.

(v) Preparation of tetrabutylammonium perchlorate (TBAP) and tetraethylammonium perchlorate (TEAP)

TEAP was prepared by mixing equal volumes of hot solutions of 1.0 mol dm^{-3} sodium perchlorate and 1.0 mol dm^{-3} tetraethylammonium chloride. The mixture was cooled in ice cold water. The precipitate formed was then filtered and washed with ice cold ethanol and later recrystallised from hot absolute ethanol, giving white crystals. TBAP was prepared in a similar manner, except that 1.0 mol dm^{-3} tetrabutylammonium chloride was used instead of tetraethylammonium chloride.

2.2 *Methods*

2.2.1 Electrochemistry

Voltammetric measurements were done in a conventional three electrode system, using micro-cell kit (Model K0264) from EG and G electrochemical systems. For aqueous solutions, silver|silver chloride (Ag|AgC*l*, 3 mol dm^{-3} KC*l*) and platinum wire were used as reference and counter electrodes, respectively. The uncoated or MPc modified glassy carbon electrode (GCE) were the working electrodes in the analysis of phenolic compounds, whereas, unmodified carbon paste, $OMo^{(V)}(OH)Pc$ or $Co^{(II)}Pc$ chemically modified carbon paste electrodes were used as the working electrodes in the detection of cysteine. The use of CoPc-CMCPE towards detection of L-cysteine has been reported by Halbert and Baldwin [2]. Therefore, in this work CoPc-CMCPE was used only for comparison purposes.

For the determination of half-wave potentials ($\mathbf{E}_{½}$) of $Na_4[OMo(OH)TSPc]\cdot 5H_2O$ (in DMSO), OMo(OH)Pc (in C*l*N), $Co^{(II)}Pc$ (in DMSO) and $Na_4[CoTSPc]\cdot 2H_2O$ (in water and DMSO) complexes, a glassy carbon electrode (GCE) was the working electrode. A platinum wire was employed as the counter electrode and a silver wire coated with silver chloride was the pseudo-reference electrode. In organic solvents, the potentials were referenced internally to the ferrocenium|ferrocene ($fc^+|fc$) couple [58,61]. The half-wave potential of $fc^+|fc$ couple has been reported to be 0.45 V *vs* saturated calomel electrode (SCE) in DMSO and C*l*N containing TEAP and TBAP, respectively [23,58]. For the determination of $\mathbf{E}_{½}$ values for the redox reactions of MPcs in organic solvents, potentials were referenced against SCE to make it easier to compare with literature values, whereas for electroanalysis of cysteine and phenolic compounds the potentials are reported against Ag|AgC*l*.

For electrochemical analysis, unless stated otherwise, solutions were prepared in aqueous solvent, with 0.05 mol dm^{-3} sulphuric acid as the supporting electrolyte and to suppress ionization of phenolic compounds [32]. 1.0 mol dm^{-3} sodium hydroxide was used to assist dissolving less soluble 2,4,6-trichlorophenol and pentachlorophenol. All solutions were deoxygenated with high-purity nitrogen (Fedgas), which was further purified by bubbling it through ¼ inch gas filter packed with 50:50 of self-indicating anhydrous calcium sulphate (drierite® 8mesh, Saarchem) and Molecular sieve (3Å, Merck) prior to measurements. Thereafter, a stream of nitrogen gas was continuously blown over the solution to prevent oxygen from redissolving back into the solutions. All studies were conducted at room temperature.

2.2.2 Apparatus

Cyclic voltammograms were recorded with a BioAnalytical Systems (BAS) CV-50W Voltammetric Analyser. Electronic absorption spectra were recorded with a Cary 1E UV-vis spectrophotometer, at 1800 nm/min. The concentrations of $Na_4[OMo(OH)TSPc]\cdot 5H_2O$ and $Na_4[CoTSPc]\cdot 2H_2O$ were of the order of 10^{-5} mol dm^{-3} for electronic absorption spectral studies and 10^{-3} mol dm^{-3} for cyclic voltammetric studies. $[Co^{(II)}TSPc]^{4-}$ forms aggregates in aqueous solutions. Therefore, for electronic absorption spectral studies, the concentration of dimeric $(CoTSPc)_2$ was calculated from the published molar extinction coefficient of 5.6×10^4 $dm^3\ mol^{-1}\ cm^{-1}$ [25]. Fourier transform infra-red (FTIR) spectra were collected with a computerized Perkin Elmer Spectrum 2000 IR spectrometer using a potassium bromide disk for solid products, or as a neat liquid on cesium iodide (CsI) salt windows for analysis of some of the oxidation products of chlorophenols. Elemental analysis was done at the University of Natal, and proton (^{1}**H**) and carbon-13 (^{13}**C**) nuclear magnetic resonance (NMR) spectra were recorded on a Bruker AMX400 MHz NMR spectrometer.

2.2.3 Bulk electrolysis

To investigate for the possible ring cleavage and/or oxidative dechlorination during electrooxidation of chlorinated phenols, bulk electrolysis experiments using a glassy carbon electrode was undertaken. 0.1 mol dm^{-3} solutions of chlorophenols (trichlorophenol, pentachlorophenol, 2-chlorophenol and 4-chlorophenol) were made by dissolving the right amounts in doubly distilled acetonitrile containing 0.1 mol dm^{-3} perchloric acid to acidify the medium and 0.1 mol dm^{-3} sodium perchlorate as a supporting electrolyte. The solution was exhaustively electrolysed for 48 hours using CV 27 BAS analyser at a constant potential of 1.35 V (*vs* Ag|AgC*l*) with uncoated glassy carbon electrode (A = 0.07 cm^2) as a working electrode, and a platinum foil (A = 1.44 cm^2) as a counter electrode. Electrolysis was carried out in a two-compartment cell separated by glass frit **(Fig. 6)**. The counter electrode was separated from the compartment housing the working and reference electrodes to prevent oxidation products from being reduced at the counter electrode. Compartment (**B**) contained

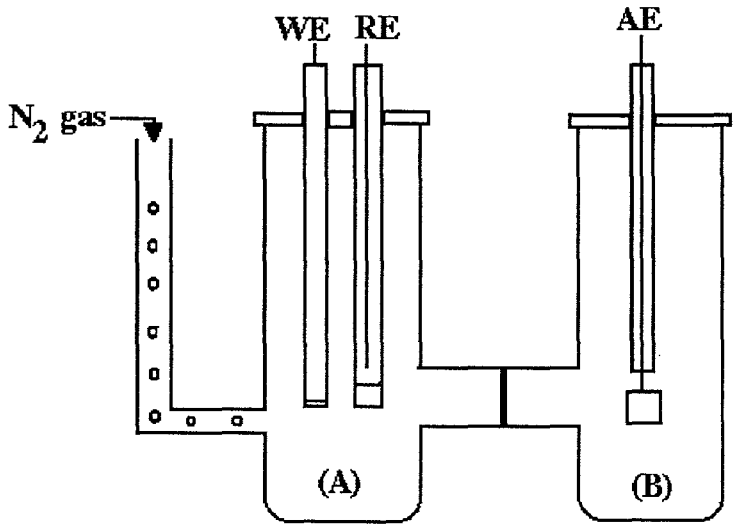

FIGURE 6: *Schematic diagram of H-type cell used in controlled potential coulometry, with two compartments separated by a glass frit (where; RE = reference, AE = counter/auxiliary and, WE = working electrodes).*

electrolyte solution only, whereas compartment (**A**) contained chlorophenols dissolved in electrolyte solution. Electrosynthesis in aqueous media was impossible due to electrode poisoning by what is believed to be the oxidation products of phenolic compounds. The solutions were constantly stirred throughout the electrolysis time.

At the end of 48 hours, the solution was evaporated to dryness by removing acetonitrile in a rotary evaporator (Buchi R-114). Chloroform (20 ml) was then added to dissolve the resulting solid product, followed by 40 ml of water to dissolve the water soluble components. The mixture was shaken for 5 minutes in a separating funnel and allowed to separate. The organic phase was separated, dried with anhydrous sodium sulphate, filtered and then evaporated to dryness with a rotary evaporator at 40°C. The products were then subjected to FTIR using KBr disk or as a neat liquid on CsI salt windows and NMR spectra with deuterium chloroform ($CDCl_3$) as a solvent. For NMR analysis, ^{1}**H** and ^{13}**C** chemical shifts are reported in δ units (ppm) and are referenced to trimethylsilane (TMS).

(i) Product(s) of electrolysis of 2-chlorophenol

Following electrolysis and separation of the oxidation products of 2-chlorophenol, a yellowish-brown solid product was obtained. Proton NMR analysis in chloroform gave: ^{1}**H** NMR (400MHz, $CDCl_3$) δ/ppm = 5.11 (1H, *s*, OH), 7.29 (4H, *m*, ArH), where *m* = multiplet and *s* = singlet resonance signals.

(ii) Product(s) of electrolysis of 4-chlorophenol

A dark brown product was obtained from electrolysis of 4-chlorophenol. ^{1}**H** NMR (400 MHz, $CDCl_3$) δ/ppm = 5.11 (1H, *s*, OH), 6.76 (2H, *s*, ArH), 7.18 (2H, *s*, ArH). ^{13}**C** NMR (400 MHz, $CDCl_3$) δ/ppm = 116.67 (2C-2+6), 125.75 (C-1), 129.53 (2C-3+5), 154.00 (C-4).

IR (neat) ν_{max}/cm^{-1}: 3340 (O-H), 2928 (ArC-H), 2685, 2068, 1591, 1494, 1435, 1374, 1358, 1232, 1167, 1094, 1009, 825, 698, 644, 504.

(iii) Product(s) of electrolysis of 2,4,6-trichlorophenol

Electrolysis of 2,4,6-trichlorophenol gave a brown oily product. ^{1}**H** NMR (400 MHz, $CDCl_3$) δ/ppm = 5.72 (1H, *s*, OH), 7.25 ($CDCl_3$), 7.52 (2H, *s*, ArH). ^{13}**C** NMR (400 MHZ, $CDCl_3$) δ/ppm = 117.78 (2C-2+6), 124.27 (C-1), 129.62 (2C-3+5), 150.51 (C-4). IR (neat) ν_{max}/cm^{-1}: 3517 (O-H), 2929 and 2718 (ArC-H), 1655, 1591, 1561, 1459, 1384, 1352, 1293, 1246, 1187, 1127, 1079, 875, 782, 734, 678, 571, 530, 445.

(iv) Product(s) of electrolysis of pentachlorophenol

Following electrolysis of pentachlorophenol, a white crystalline product was obtained. ^{13}C NMR (400 MHz, $CDCl_3$) δ/ppm = 119.73 (2C-2+6), 125.09 (C-1), 131.50 (2C-3+5), 148.14 (C-4). IR (KBr) ν_{max}/cm^{-1}: 3514 (O-H), 1545, 1418, 1381, 1305, 1192, 985, 769, 705, 648, 514.

2.3 Working electrode pretreatment

2.3.1 Carbon Paste Electrodes (CPE)

(i) Unmodified electrode

An unmodified carbon paste electrode was made by thoroughly mixing 1.70g finely ground graphite powder (Saarchem) with 1.0 ml nujol mineral oil (Fluka). For both unmodified electrodes and chemically modified carbon paste electrodes, the paste was packed into one end of a fused silica capillary tube of 1.0 mm outside diameter. Electrical contact was established by embedding a nichrome wire (0.5 mm diameter) into the carbon paste, ensuring that the wire

did not come out through the surface of the electrode. Finally, the electrode was smoothed by polishing the surface on a filter paper.

(ii) Chemically modified carbon paste electrode

Chemically modified carbon paste electrodes (CMCPE) were prepared in a similar manner as the unmodified electrode. However, prior to the addition of nujol mineral oil, an appropriate amount of OMo(OH)Pc or CoPc was mixed with graphite powder, finely ground with a mortar and a pestle until thorough mixing was obtained. The concentration of OMo(OH)Pc or CoPc in the carbon paste was expressed as a percentage of MPc added to the graphite powder. The OMo(OH)Pc content was varied from 3 to 8% to find the percentage content which exhibits optimum catalytic activity. Best results were obtained with 4% OMo(OH)Pc. The use of 5% CoPc chemically modified carbon paste electrode (CoPc-CMCPE) has been reported by Halbert and Baldwin [2]. In this work, 4% CoPc-CMCPE was used for comparison with 4% OMo(OH)Pc-CMCPE used for voltammetric studies of cysteine.

2.3.2 Pretreatment of glassy carbon electrode

(i) Drop-dry method

MPc was adsorbed onto the surface of a glassy carbon electrode (A = 0.07 cm^2) by applying a known volume ($\approx$ 3 μL) of 10^{-3} mol dm^{-3} of MPc, dissolved in pyridine, with a microsyringe and allowed to dry in air. Upon drying, the MPc is believed to form a thin, uniform layer on the electrode surface. The electrode was then ready for use. Prior to coating, the electrode was cleaned by polishing on a buehler felt pad, coated with alumina slurry (Al_2O_3, Merck), and then rinsed with triple distilled-deionized water.

(ii) Electrochemical deposition (electrodeposition)

Electrochemical deposition of $[Co^{(II)}TSPc]^{4-}$ onto the glassy carbon electrode was done according to the method reported in literature [16,50,62]. That is, after precleaning, the glassy carbon electrode was electrochemically-coated by repetitively scanning in unstirred deaerated aqueous 10^{-3} mol dm^{-3} solution of $[Co^{(II)}TSPc]^{4-}$ in the potential range of 0.0 to 1.3 V (*vs* Ag|AgC*l*), under nitrogen degassed condition, using 0.05 mol dm^{-3} sulphuric acid as the supporting electrolyte. To ensure maximum deposition, the electrode was scanned until no significant change in peak height was noted (i.e up to 25 scans). The electrode was then rinsed in absolute ethanol, distilled water and finally in 0.05 mol dm^{-3} sulphuric acid, and was then ready for use.

RESULTS AND DISCUSSION

CHAPTER THREE: CHARACTERISATION OF MPc COMPLEXES

3.1 Tetrasodium salt of cobalt(II) tetrasulfophthalocyanine

3.2 Cobalt(II) phthalocyanine

3.3 Tetrasodium salt of oxomolybdenum(V) tetrasulfophthalocyanine

3.4 Oxomolybdenum(V) phthalocyanine

3.1 Tetrasodium salt of cobalt(II) tetrasulfophthalocyanine

3.1.1 Synthetic route for $[Co^{(II)}TSPc]^{4-}$

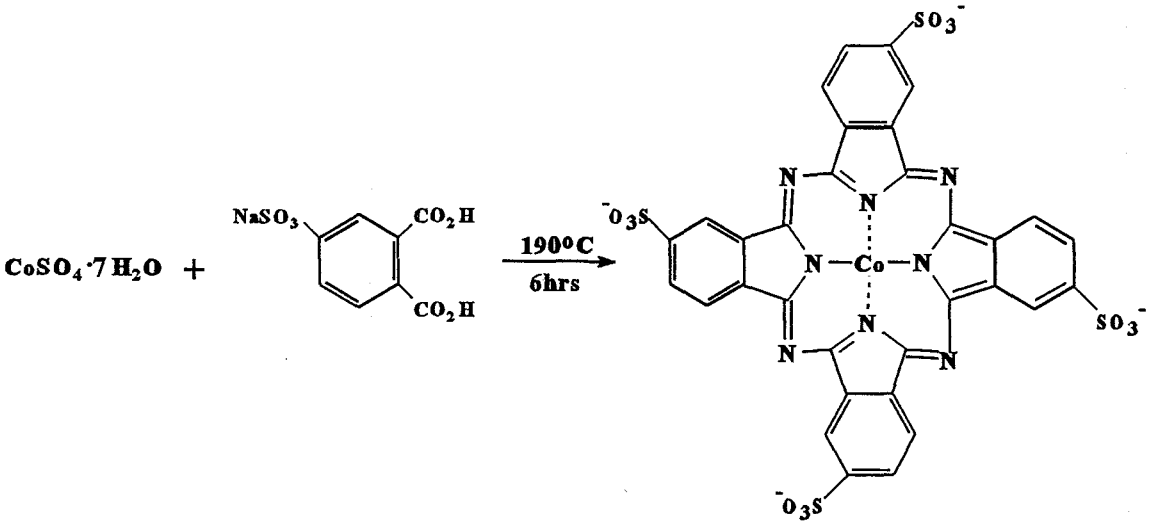

SCHEME 2

Scheme 2 shows the simplified synthetic route for the preparation of $[Co^{(II)}TSPc]^{4-}$, prepared by heating the mixture of cobalt(II) sulphate and monosodium salt of 4-sulfophthalic acid in the presence of nitrobenzene, detailed experimental procedure is in section 2.1.2.

3.1.2 Redox properties of $[Co^{(II)}TSPc]^{4-}$

To understand the redox properties of $[Co^{(II)}TSPc]^{4-}$, the electrochemical characteristics of $[Co^{(II)}TSPc]^{4-}$ complex in 0.05 mol dm^{-3} sulphuric acid and in dimethylsulfoxide (DMSO) were investigated via cyclic voltammetry. In organic solvents, half-wave potentials ($E_{½}$) were determined against saturated calomel electrode (SCE) for easier comparison with the established literature values which are mostly reported against SCE. For catalytic purposes the potentials were determined against silver|silver chloride (Ag|AgC*l*).

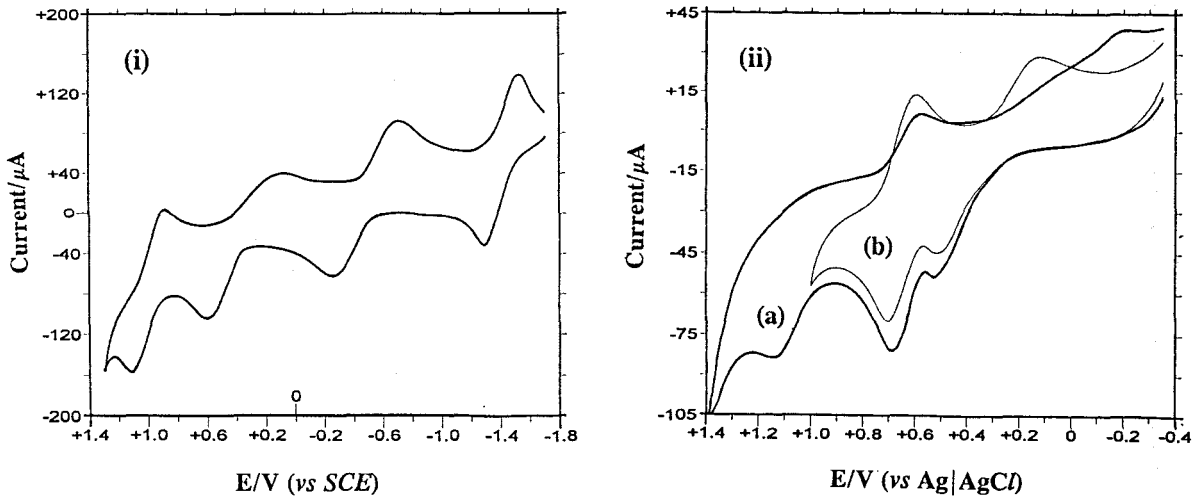

FIGURE 7: *Cyclic voltammograms of $[Co^{(II)}TSPc]^{4-}$ in (i) DMSO containing 0.1 mol dm^{-3} TEAP (vs SCE, scan rate = 200 mV s^{-1}) and, (ii) in 0.05 mol dm^{-3} sulphuric acid with (a) scanned from -0.4 to 1.4 V and (b) scanned from -0.4 to 1.0 V (vs Ag|AgCl), scan rate = 100 mV s^{-1}; all on glassy carbon electrode.*

Fig. 7(i) shows the cyclic voltammogram of $[CoTSPc]^{4-}$ in DMSO with TEAP as the supporting electrolyte. Two quasi-reversible reduction peaks with half-wave potentials of -0.50 and -1.40 V (*vs* SCE) were observed. From literature [16], the first reduction is known to be at the central metal, followed by reduction of the phthalocyanine ring. Therefore, the two reduction couples at -0.50 and -1.40 V are assigned to the metal reduction of $[Co^{(II)}TSPc(2-)]^{4-}$ to $[Co^{(I)}TSPc(2-)]^{5-}$ followed by the phthalocyanine ring reduction of $[Co^{(I)}TSPc(2-)]^{5-}$ to $[Co^{(I)}TSPc(3-)]^{6-}$. In addition to these two reduction couples, two oxidation waves were observed at 0.59 and 1.09 V (*vs* SCE). The first wave showed a very weak return peak, while the second was quasi-reversible. Earlier electrochemical studies of $[Co^{(II)}TSPc]^{4-}$ have assigned the first anodic oxidation to be due to involvement of cobalt metal in $Co^{(II)}/Co^{(III)}$ transition and the couple at higher potentials to be due to Pc(2-)/Pc(1-) transition [17,23]. Therefore, in **Fig.7(i)**, the anodic oxidations at 0.59 V and at $E_{½}$ = 1.09 V (*vs* SCE)

corresponds with the central metal oxidation of $[Co^{(II)}TSPc(2-)]^{4-}$ to $[Co^{(III)}TSPc(2-)]^{3-}$ followed by the phthalocyanine ring oxidation, represented by oxidation of $[Co^{(III)}TSPc(2-)]^{3-}$ to $[Co^{(III)}TSPc(1-)]^{2-}$. The first wave, due to the metal oxidation, exhibited what looks like a very weak cathodic return wave whose height depended more on the magnitude of the scan rate. The first oxidation wave of $[Co^{(II)}TSPc]^{4-}$ has been reported to be irreversible in DMF [16].

In 0.05 mol dm^{-3} sulphuric acid, two irreversible anodic oxidation waves were observed at 0.54 and 1.10 V (*vs* Ag|AgC*l*) and a third, quasi-reversible oxidation peak was observed at $\mathbf{E}_{½}$ = 0.68 V (*vs* Ag|AgC*l*) **(Fig. 7(ii))**. The wave with $\mathbf{E}_{½}$ of 0.68 is assigned to the central metal oxidation [2], represented by the oxidation of $[Co^{(II)}TSPc(2-)]^{4-}$ to $[Co^{(III)}TSPc(2-)]^{3-}$. The wave at 1.10 V is due to the ring oxidation of $[Co^{(III)}TSPc(2-)]^{3-}$ to $[Co^{(III)}TSPc(1-)]^{2-}$ [23]. According to Lever *et al* [23], cobalt phthalocyanine complexes are capable of exhibiting additional redox waves which are associated with redox reactions of mixed-valence species. These redox active mixed-valence species may be of the metal-centred type, such as $[Co^{(II)}Pc(2-)]_2/[Co^{(I)}Pc(2-)\bullet Co^{(II)}Pc(2-)]^-$ or of the ring-centred type, represented by $[Co^{(II)}Pc(1-)]_2^{2+}/[Co^{(II)}Pc(1-)\bullet Co^{(II)}Pc(2-]^+$. The $\mathbf{E}_{½}$ for the redox potentials arising from splitting of mixed-valence intermediates for $Co^{(II)}Pc$ is reported to be 0.45 V (*vs* SCE) in dimethylformamide (DMF) [23]. These were assigned to mixed-valence splitting of $[Co^{(III)}Pc(2-)\bullet Co^{(II)}Pc(2-)]^+/[Co^{(II)}Pc(2-)]_2$ species. $[Co^{(II)}TSPc]^{4-}$ readily forms dimeric species in aqueous solution. Therefore, the wave at 0.54 V **(Fig. 7(ii))**, which is very close to the peak assigned to the metal oxidation, may arise from splitting due to stabilisation of $[Co^{(II)}TSPc]^{4-}$ mixed-valence species. These may be of the metal-centred type, such as $[Co^{(III)}TSPc(2-)\bullet Co^{(II)}TSPc(2-)]^{7-}/[Co^{(II)}TSPc(2-)]_2^{8-}$. It is therefore suggested that the redox active polynuclear species with splitting at 0.54 V arises from the stabilisation of mixed

valence intermediate from the reaction represented as [23]:

$$[Co^{(II)}TSPc(2-)]_2^{8-} + [Co^{(III)}TSPc(2-)]_2^{6-} \rightarrow 2[Co^{(II)}TSPc(2-)\bullet Co^{(III)}TSPc(2-)]^{7-} \quad .....(12)$$

The difference in potentials from the splitting of mixed-valence of $[Co^{(II)}TSPc]^{4-}$ and $Co^{(II)}Pc$ may arise from the effect of peripheral sulphonate groups in the former. The anodic currents of the waves at 0.54, 0.68 and 1.10 V were found to depend on the concentration of $[Co^{(II)}TSPc]^{4-}$ and the scan rate, suggesting diffusion controlled reaction. A small undefined reduction wave was seen on the reverse scan and its position and intensity was found to depend on the positive potential limit of the forward scan. When the potential was scanned from 0.0 to 1.40 V the peak was observed at -0.20 V **(Fig. 7(ii)(a))** but when scanned up to 1.0 V these cathodic wave shifted to -0.12 V (*vs* Ag|AgC*l*) **(Fig. 7(ii)(b))**. In non-donor solvents, such as chloronaphthalene, metal or ring reductions of $[Co^{(II)}TSPc]^{4-}$ are not usually observed [23]. Similarly, in sulphuric acid, reduction of either the cobalt central metal or the phthalocyanine ring, for $[Co^{(II)}TSPc]^{4-}$, was not observed **(Fig. 7(ii))**. Presumably, this is due to the oxidising nature of sulphuric acid. It is also reported [23] that cobalt(II) phthalocyanine complexes in donor solvents is solvated (five or six coordinated) while in non-donor solvents it is unsolvated, with four-coordination, and has a different spin.

3.1.3 Elemental and spectral analysis

Elemental analysis for carbon, hydrogen and nitrogen in $Na_4[CoTSPc]\cdot 2H_2O$, when calculated for $Na_4CoS_4C_{32}O_{13}H_{16}N_8$ gave: H, 2.58%; C, 33.84% and N, 9.78%, whereas were found to be: H, 2.56%; C, 32.37% and N, 9.73%.

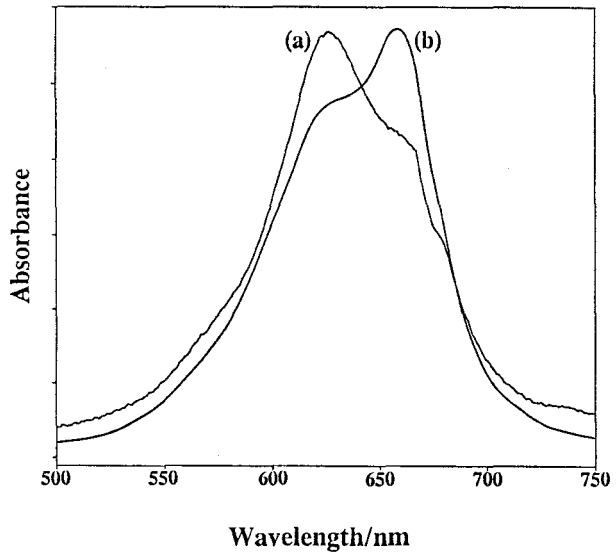

FIGURE 8: *Electronic absorption spectrum of $[Co^{(II)}TSPc]^{4-}$ in (a) 0.05 mol dm^{-3} sulphuric acid and, (b) in water.*

Absorption spectral analysis of $[Co^{(II)}TSPc]^{4-}$ in water revealed a broad Q band **(Fig. 8(b))**. The split Q band exhibited an intense absorption with λ_{max} at 659 nm and a band with lower absorbance at 630 nm. The higher-wavelength band (at 659 nm) is attributed to the absorption of monomeric and, the lower-wavelength band (at 630 nm) is associated with the absorption of dimeric species **(Fig. 8(b))**. These observations are consistent with those of Gruen and Blagrove [25,26]. In 0.05 mol dm^{-3} sulphuric acid, $[Co^{(II)}TSPc]^{4-}$ was found to exist mainly in a dimerized form, with an intense Q band absorption at 627 nm (dimeric species) and a less intense absorption due monomeric species around 660 nm **(Fig. 8(a))**. The aggregation of $[Co^{(II)}TSPc]^{4-}$ is a result of its labile axial water molecule [63]. Dimerization is exemplified by blue shifting of the Q band absorption, where a usually sharp Q band is replaced by a broad envelope centred at higher energies.

Table 2 compares the Fourier transform infrared (FTIR) absorption frequencies of cobalt(II) and molybdenum(V) phthalocyanines, and their tetrasulfonated derivatives together with the main frequencies of copper and molybdenum phthalocyanines as reported in literature [64,65]. Frequency bands assigned in **Table 2** are based on the work of Shurvell and Pinzuti [64]. From **Table 2**, cobalt(II) tetrasulfonated phthalocyanine, $[Co^{(II)}TSPc]^{4-}$ and molybdenum tetrasulfonated phthalocyanine, $[OMo^{(V)}(OH)TSPc]^{4-}$, exhibits fewer FTIR bands than cobalt(II) and oxomolybdenum(V) phthalocyanines, $Co^{(II)}Pc$ and $OMo^{(V)}(OH)Pc$, respectively. The bands not shown were too weak and some appeared as fused broad or split bands, as

TABLE 2: *Infrared absorption bands of phthalocyanines in the range 4000 to 500 cm^{-1} - using potassium bromide (KBr) disk (wavenumbers in cm^{-1}).*

CoPc	MoPc	MoTSPc	CoTSPc	CuPc[64]	MoPc[65]	Assignment
518m	---	---	---	506w		
---	532m	---	---			
573m	570m	583m	591m	574w		
642m	643m	634m	634m	641vw		
---	---	688m	699s			ν(S-O)
733vs	729(716)s	---	---	730vs	731s	π(C-H)
756s	752s	745w	750vs	755s	752m	
781s	774s	770w	762w	771m	769m	
876m	---	841s	831s	871w	872w	(C-H)
914s	896vs	894s	904w	900m	896m	
956w	---	929w	934s	949w	953w	
---	973s	967vw	---		972m	ν(Mo=O)
---	1030m	1034vs	1028vs			δ(C-H)
1075w	---	1073w	1059s	1069m	1065m	(C-H)

Table 2: continued

CoPc	MoPc	MoTSPc	CoTSPc	CuPc[64]	MoPc[65]	Assignment
1089vs	1087vs	1089w	1081w	1091vs	1088s	
1122vs	1117vs	1125w	1118m	1121vs	1117s	(C-C)
1165s	1159s	1140w	1143m	1168s	1163m	
---	1183m	1191s	1189m			
1202w	1209w	1209w	---			
1290s	1289w	---	---	1288s	1289m	ν(C-C)
---	1306m	1315w	---			
1333vs	1332vs	1332m	1328vs	1334vs	1332s	
1385w	1383m	1389m	---			
1426s	1410m	1405m	1402vs	1421s	1116m	ν(C-C)
1457m (1468)m	1467m (1472)m	1459m	1460m	1457w (1465)w	1479w	
1500w	1509m	1509m	1509m	1505m	1498m	ν(C-C)
1524s	1525m	1527m	1523s	1509		
1544m	1543	1545w	1543m			
1562m	1561	1561w	1561m			
1609	1606m	---	---	1611w	1612m	ν(C-C)
1642m	1645s	1636m	1638w			ν(C-N)
1718m	1718vs	1719w	1718w			
---	1775s	---	---			
3045w	3050m	3161w	3081sh			ν(C-H)
---	3450m	3436m	3429		3420s	ν(O-H)

Where: *ν = stretching vibrations, π = out-of-plane bending vibrations, δ = in-plane bending or deformation, **vs** = very strong, **s** = strong, **sh** = shoulder/hump-like band, **m** = medium, **w** = weak, **vw** = very weak and frequencies in brackets represents split bands.*

shown in FTIR spectrum of $[Co^{(II)}TSPc]^{4-}$ in **Fig. 9**. This behaviour may be due to the effect of sulfonate groups on the phthalocyanine ligand. Reports show that MPcs with substituent groups attached to the ligand are dominated by fused broad bands in the 1600 to 1000 cm^{-1} region [64]. From **Table 2**, the absence of bands at 1000 cm^{-1} indicates that the complexes are free from contamination by metal-free phthalocyanine (H_2Pc) [65]. H_2Pc exhibits a band characteristic of N-H stretching vibrations at 1000 cm^{-1} [65].

From IR spectral analysis, bands which are characteristic of phthalocyanine ligand absorption are assigned as follows: the 3030 cm^{-1} band is due to aromatic C-H stretching vibrations, the 1670 and 1610 cm^{-1} bands to C-C benzene ring skeletal stretching vibrations, the 1640 cm^{-1} to C-N stretching vibrations, the 1030 cm^{-1} to C-H in-plane bending or deformation, and the 730 cm^{-1} band is due to C-H out-of-plane bending vibrations [64,66-69].

The additional vibration noted at ν3429 cm^{-1} is assigned to O-H stretching vibrations, indicating that the complex is in a hydrated form. For sulfonated phthalocyanines, the sulfur bonded S-O stretching vibrations were observed around 699 to 660 cm^{-1} [69,70]. However, the occurrence of S-O vibrations at higher frequencies have been reported before [69,70]. The bands due to metal-nitrogen vibrations are reported to occur in the far-IR region [69].

In view of the similarity of electrochemical properties and spectral properties of the synthesised $[CoTSPc]^{4-}$ with the literature data [10,16,17,23,25,64-69], this led to the conclusion that the synthesised $[CoTSPc]^{4-}$ complex was pure enough and can therefore be conveniently written as $Na_4[Co^{(II)}(SO_3)_4Pc]\bullet 2H_2O$. This was also supported by elemental analysis results.

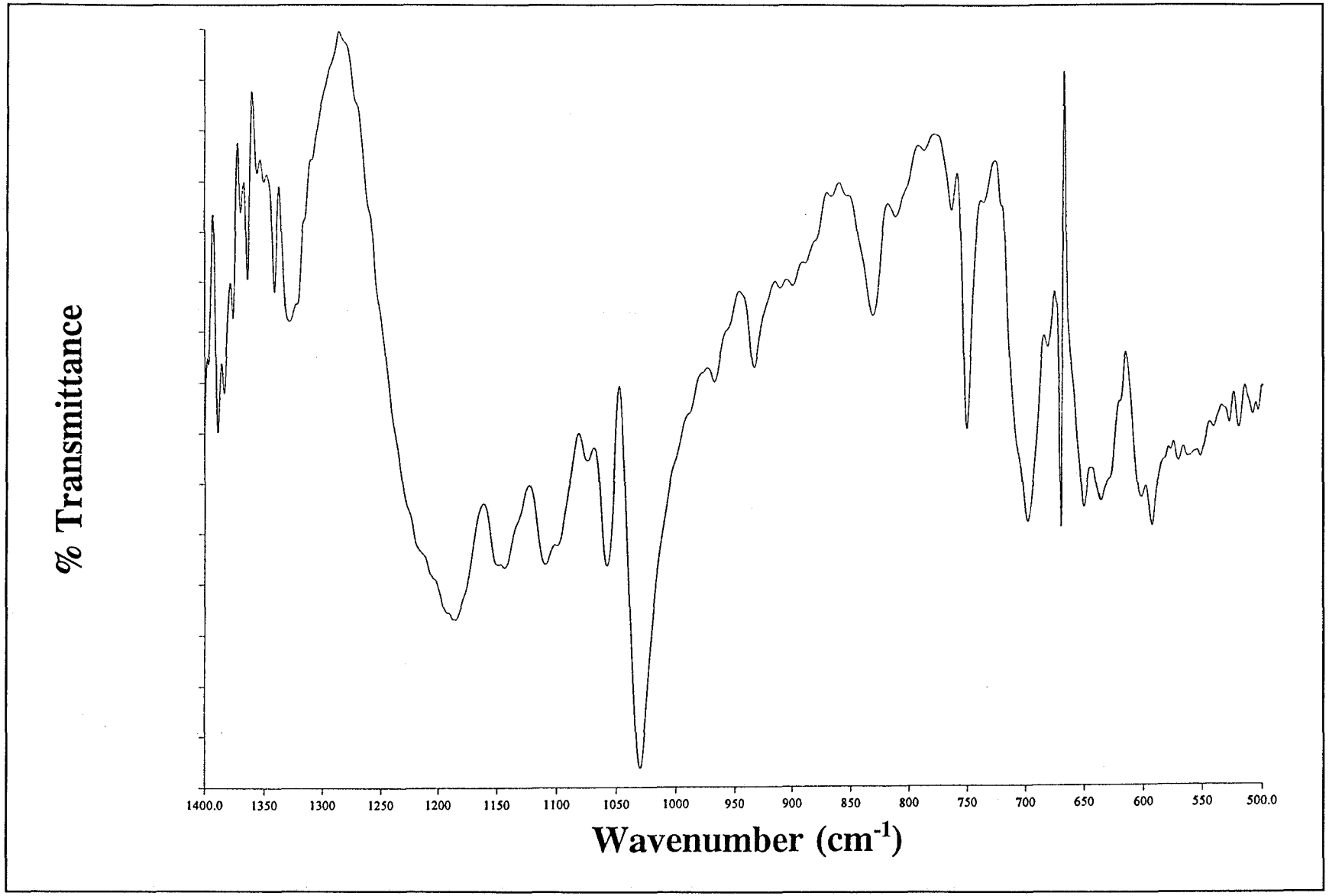

FIGURE 9: *Infrared spectrum of Cobalt(II) tetrasulfonated phthalocyanine, [$Co^{(II)}TSPc]^{4-}$, using potassium bromide disk.*

3.2 *Cobalt(II) phthalocyanine*

3.2.1 Synthetic route for $Co^{(II)}Pc$

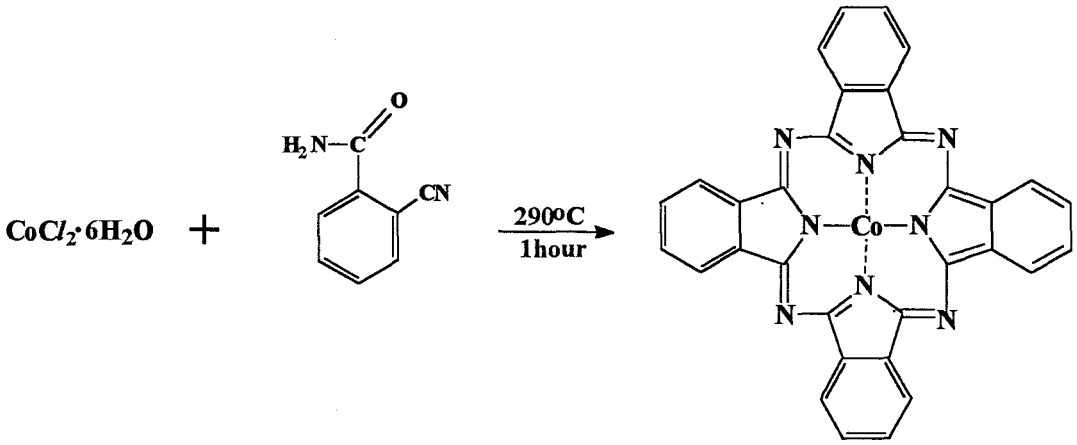

SCHEME 3

Scheme 3 shows the simplified synthetic route followed towards the preparation of cobalt(II) phthalocyanine, which was prepared by heating the mixture of o-cyanobenzamide and cobalt(II) chloride as explained in the experimental section, giving the complex whose structure is as shown above.

3.2.2 Redox properties of $Co^{(II)}Pc$

Electrochemical behaviour of $Co^{(II)}Pc$ was investigated in DMSO with TEAP as the supporting electrolyte. A typical cyclic voltammogram of $Co^{(II)}Pc$ is shown in **Fig. 10** below. Three quasi-reversible couples with $E_{½}$ of -0.36, 0.14 and 0.37 V (*vs* SCE) were observed. Metal reduction involving $Co^{(II)} \rightarrow Co^{(I)}$ has been reported to be at -0.37 V (*vs* SCE) [23]. Therefore, the cathodic peak at -0.36 V **(Fig. 10)** is attributed to the metal reduction involving $Co^{(II)} \rightarrow Co^{(I)}$ transition as reported by Lever *et al* [23]. The quasi-reversible couple at $E_{½} = 0.14$ V is duly assigned to $Co^{(II)}/Co^{(III)}$ transition, which is consistent with the results of Li and Guarr [71],

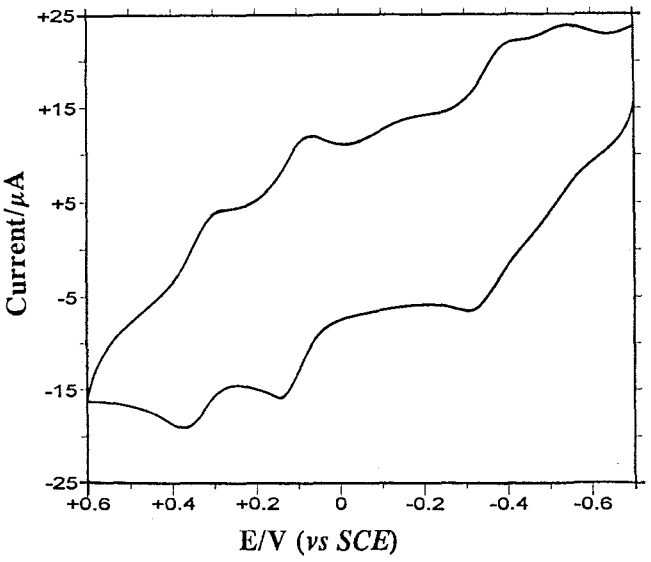

FIGURE 10: *Cyclic voltammogram of $Co^{(II)}Pc$ in DMSO containing 0.1 mol dm^{-3} TEAP as an electrolyte on glassy carbon electrode (vs SCE, scan rate = 300 mV s^{-1}).*

who observed the same couple at 0.17 V(*vs* SCE, in DMSO at GCE). The anodic peak at 0.37 V is tentatively assigned to Pc(2-)→Pc(1-) couple in accordance with the bulk of the literature and with results obtained on other metallophthalocyanines [23,71]. An additional undefined peak was observed at -0.55 V on the return scan. These peak a very weak corresponding wave on the forward scan. However, it is likely to arise from Pc(2-)/Pc(3-) transition.

3.2.3 Elemental and spectral analysis

Elemental analysis of $Co^{(II)}Pc$ calculated for $CoC_{32}H_{16}N_8$ gave H, 2.80%; C, 67.30% and N, 19.60%, whereas analysis found H, 2.70%; C, 66.10% and N, 18.90%.

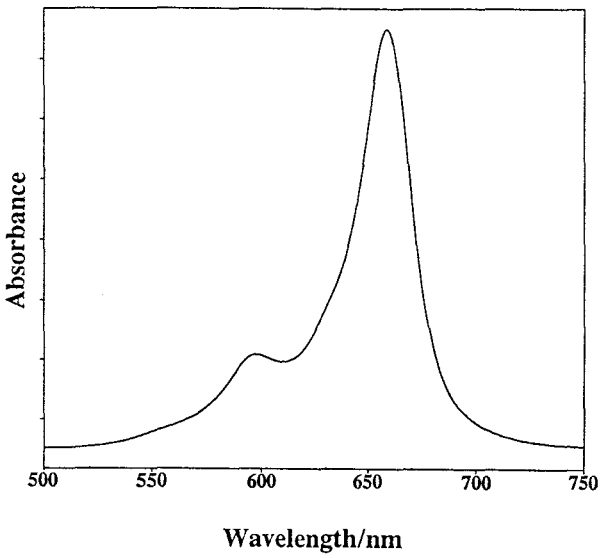

FIGURE 11: *Electronic absorption spectrum of $Co^{(II)}Pc$ in pyridine, showing an intense Q band absorption and vibronic transition.*

The UV-visible absorption spectrum of $Co^{(II)}Pc$ dissolved in dimethylformamide (DMF) showed the absorption bands characteristic of MPc complexes **(Fig. 11)**. The spectrum showed an intense Q band at 659 nm, arising from the absorption of monomeric species. A less intense absorption band was observed at lower wavelength (598 nm). This wavelength is too low to be due to dimeric species. It is therefore always assigned to vibronic transitions because $Co^{(II)}Pc$ does not dimerize. The intense absorption at 659 nm indicates that $Co^{(II)}Pc$ exists as monomeric species when dissolved in strong coordinating solvents, such as pyridine. Possibly, the complex exists as $(Py)Co^{(II)}Pc$ (pyridine-CoPc), with pyridine molecule axially coordinated to the central metal.

Fig. 12 shows the IR spectrum of $Co^{(II)}Pc$, with well resolved absorption bands. The bands are assigned as discussed before, and comparison with bands observed from other

phthalocyanines is showed in **Table 2.** The spectrum closely resemble that of α-form of cobalt phthalocyanine as reported by Ebert and Gottlieb [72]. Additional weak absorption bands at 3034, 2864, 2656 and 2586 cm^{-1} were observed. The one at 3034 cm^{-1} appears to be too low to be an O-H vibration. It is probably an aromatic C-H stretch vibration.

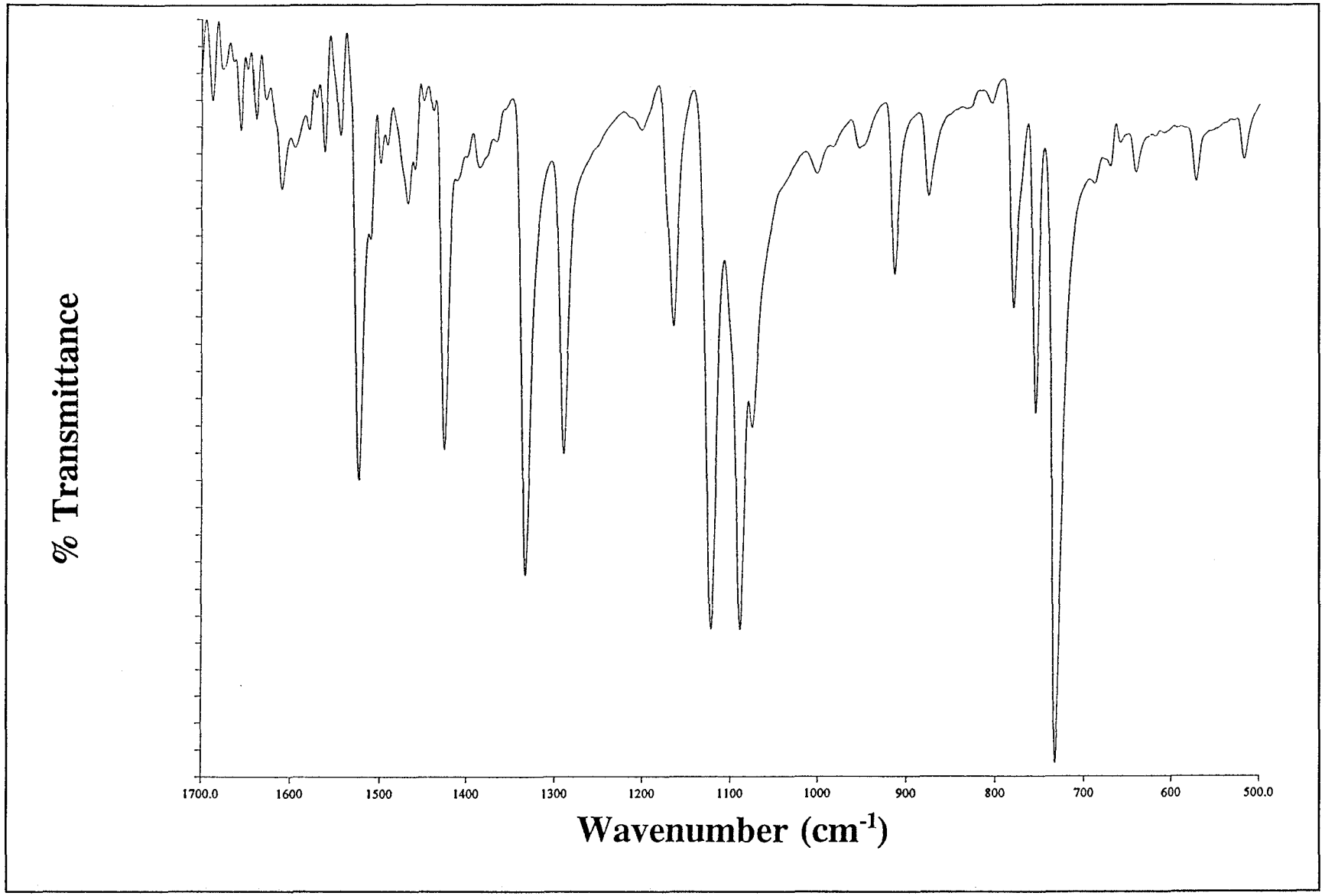

FIGURE 12: *Infrared spectrum of cobalt(II) phthalocyanine, $Co^{(II)}Pc$, using KBr disk.*

3.3 *Tetrasodium salt of oxomolybdenum(V) tetrasulfophthalocyanine*

3.3.1 Synthetic route for $[OMo^{(V)}(OH)TSPc]^{4-}$

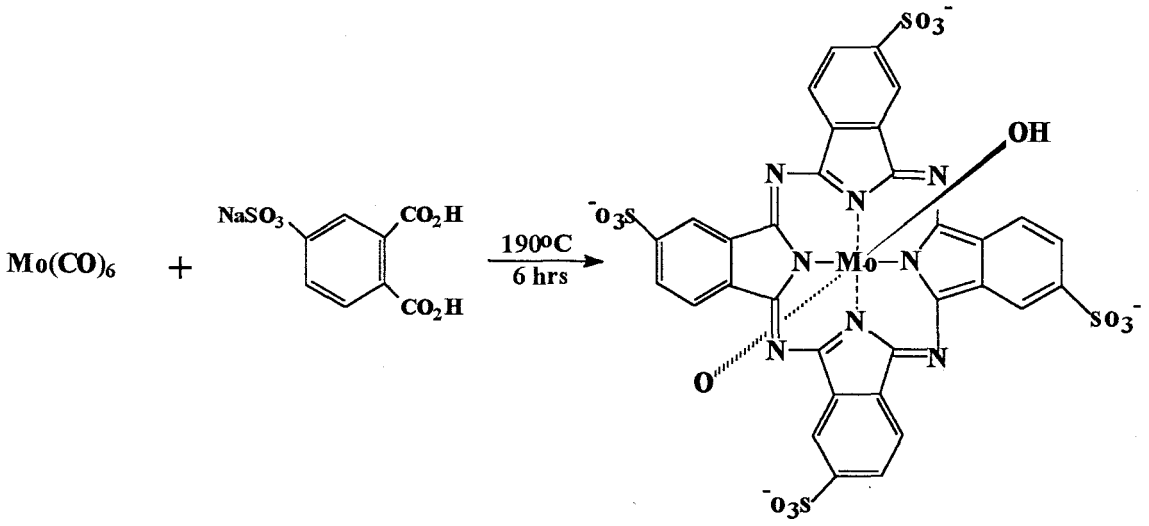

SCHEME 4

Scheme 4 presents the synthetic reaction of molybdenum hexacarbonyl with monosodium salt of 4-sulfophthalic acid as explained in the experimental section, forming molybdenum(V) tetrasulfonated phthalocyanine, $[OMo^{(V)}(OH)TSPc]^{4-}$, complex. The reaction follows the same synthetic route as that of $[Co^{(II)}TSPc]^{4-}$.

3.3.2 Redox properties of $[OMo^{(V)}(OH)TSPc]^{4-}$

Like all other sulphonated phthalocyanines, $[OMo^{(V)}(OH)TSPc]^{4-}$ is soluble in water, hence its use in solution-phase catalysis was investigated. Differential pulse voltammetric study of $[OMo^{(V)}(OH)TSPc]^{4-}$ in DMF containing tetrabutylammonium hexafluorophosphate (as electrolyte) by Ferraudi *et al* [59] revealed two major waves at -0.108 and -0.806 and two minor waves at -1.123 and -1.370 V (*vs* SCE). Therefore, in order to employ

$[OMo^{(V)}(OH)TSPc]^{4-}$ as a catalyst for the electrooxidation of cysteine in this study, it was found essential to investigate cyclic voltammetric behaviour for the oxidation of this complex. Cyclic voltammetry of $[OMo^{(V)}(OH)TSPc]^{4-}$ in DMSO, containing TEAP as a supporting electrolyte, revealed a voltammogram shown in **Fig. 13** below. $[OMo^{(V)}(OH)TSPc]^{4-}$ complex has a poor solubility in solvents like DMSO [59]. This therefore may account for the weak voltammetric peaks observed in DMSO **(Fig. 13)**.

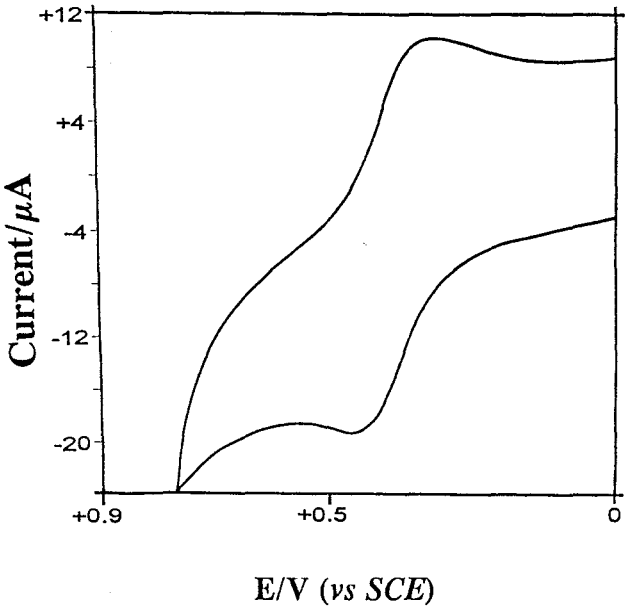

FIGURE 13: *Cyclic voltammogram of $[OMo^{(V)}(OH)TSPc]^{4-}$ in DMSO containing 0.1 mol dm^{-3} TEAP electrolyte, on glassy carbon electrode. Scan rate = 500 mV s^{-1} (vs SCE).*

The cyclic voltammogram exhibits a reversible couple with ΔE_p of approximately 60 mV. The ratio of peak current to square root of scan rate, $i_p/v^{1/2}$, was found to be constant and the ratio of anodic to cathodic peak currents was unity, which is typical of diffusion controlled reversible processes. A half-wave potential, $E_{1/2}$, of about 0.40 V (*vs* SCE) was obtained for the oxidation couple in **Fig. 13**. Reports have assigned the oxidation of $OMo^{(V)}(OH)Pc(2-)$ to

$[OMo^{(VI)}(OH)Pc(2-)]^+$ to be at the central metal, rather than at the ring, with an $E_{½}$ = 0.53 V (in DMSO, *vs* SCE) [58], whereas in DMF the $E_{½}$ of 0.51 V (*vs* SCE) has been reported [23]. Therefore, the fact that the potential of 0.40 V for the oxidation of $[OMo(OH)TSPc]^{4-}$ obtained in this work is in the range reported for molybdenum oxidation in MPc complexes [23] indicates that the oxidation couple in **Fig. 13** is due to central metal oxidation, whereby $[OMo^{(V)}(OH)TSPc]^{4-}$ is believed to undergo one electron oxidation to give $[OMo^{(VI)}(OH)TSPc]^{3-}$. The difference between the reduction potentials and $E_{½}$ values of $[OMo^{(V)}(OH)TSPc]^{4-}$ and $OMo^{(V)}(OH)Pc$ [58] is most probably due to the effect of the peripheral sulphonate groups in the former. For $[OMo^{(V)}(OH)TSPc]^{4-}$ in DMSO (with TEAP), no ring-based oxidation couples were observed within the potential range investigated.

3.3.3 Elemental and spectral analysis

Elemental analysis of $[OMo(OH)TSPc]^{4-}$ found H, 2.18%; C, 33.48% and N, 10.15%, whereas calculated for $MoC_{32}O_{14}N_8S_4H_{15}Na_4$ gave H, 2.21%; C, 33.71% and N, 9.83%.

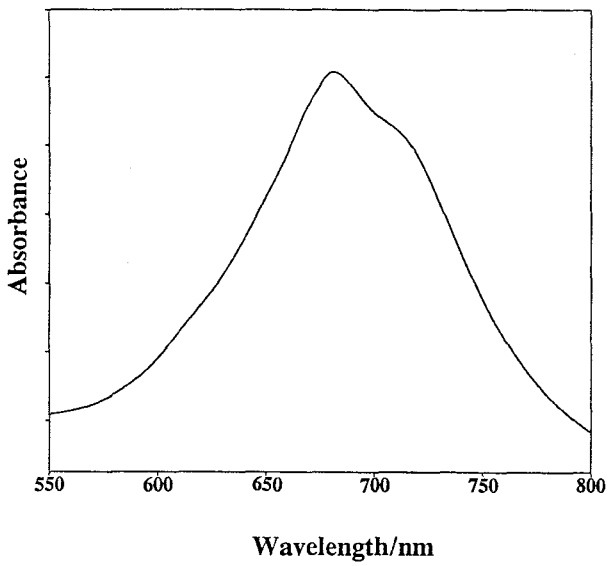

FIGURE 14: *Absorption spectrum of $[OMo(OH)TSPc]^{4-}$ in 0.05 mol dm^{-3} H_2SO_4.*

In 0.05 mol dm^{-3} sulphuric acid, UV-Vis absorption spectrum of $[OMo(OH)TSPc]^{4-}$ showed a strong band at 680 nm, suggesting that this complex is dimerised in aqueous solution [23]. A weak band due to monomeric species, was observed at 710 nm **(Fig. 14)** [23]. In the UV-vis spectrum of $[OMo^{(V)}(OH)TSPc]^{4-}$ in DMSO (not shown), an intense absorption due to monomeric species with λ_{max} at 696 nm, and a far less intense absorption band due to dimeric species at 630 nm were observed [59].

The IR spectrum of $[OMo^{(V)}(OH)TSPc]^{4-}$ closely resembles that of $OMo^{(V)}(OH)Pc$, except that for reasons already discussed, $[OMo^{(V)}(OH)TSPc]^{4-}$ exhibits fewer absorption bands than $OMo^{(V)}(OH)Pc$. The spectrum showed additional band at 967 cm^{-1}, which is in the region reported to be for Mo=O stretching vibration [69]. Based on these, the 967 cm^{-1} band is therefore assigned to molybdenum-oxygen vibration, ν(Mo=O). **Table 2** showed the ν(Mo=O) to be lower for $[OMo^{(V)}(OH)TSPc]^{4-}$ (966 cm^{-1}) than for $OMo^{(V)}(OH)Pc$ (973 cm^{-1}). This may be due to effect of peripheral sulphonate groups in the former. The band noted at 3436 cm^{-1} is attributed to a non-hydrogen bonded O-H stretching vibration [69].

3.4 Oxomolybdenum(V) phthalocyanine

3.4.1 Synthetic route for $OMo^{(V)}(OH)Pc$

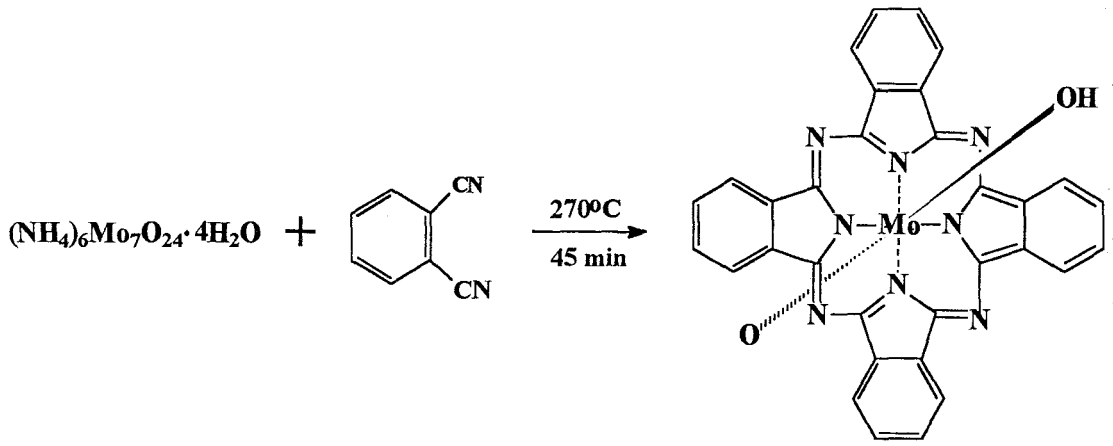

SCHEME 5

Synthetic scheme for the praparation of oxomolybdenum(V) phthalocyanine showing axial coordination of oxygen and hydroxyl, to balance the charge of the central metal, is shown in **scheme 5**. This complex is prepared as mentioned in the experimental section by reacting ammonium molybdate with phthalonitrile (1,2-dicyanobenzene).

3.4.2 Redox properties of $OMo^{(V)}(OH)Pc$

Fig. 15 shows the cyclic voltammogram of $OMo^{(V)}(OH)Pc$ in chloronaphthalene containing tetrabutylammonium perchlorate (TBAP) as the supporting electrolyte, and the half-wave potentials ($E_{1/2}$) are given in **Table 3** together with $E_{1/2}$ of OMo(OH)Pc as reported in literature [58]. The half-wave potentials assigned in **Table 3** are based on the work of Nyokong [58]. The cyclic voltammogram **(Fig. 15)** shows two quasi-reversible oxidation couples at ($E_{1/2}$ values) 0.40 and 1.40 V, and four reduction couples with $E_{1/2}$ values; -0.70, -1.0, -1.45 and -1.70 V (*vs* SCE). The first oxidation couple **(I)** is due to the oxidation of the central metal,

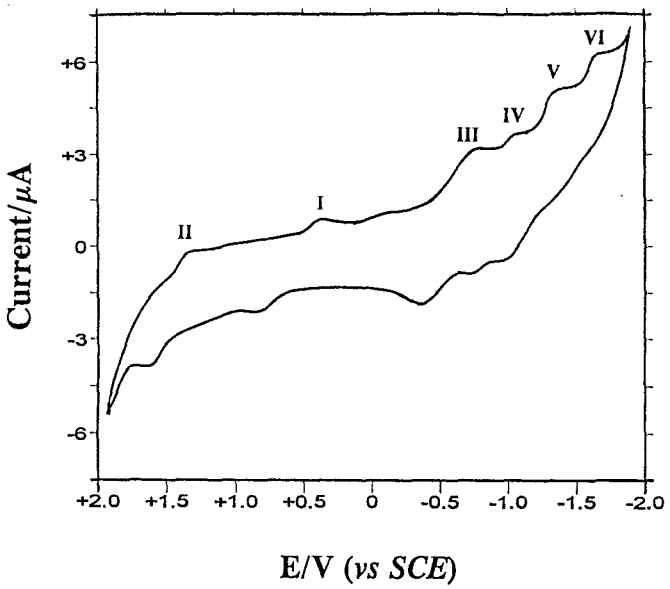

FIGURE 15: *Cyclic voltammogram of $OMo^{(V)}(OH)Pc$ in chloronaphthalene containing TBAP as an electrolyte, on GCE. Scan rate = 100 mV s^{-1} (vs SCE).*

$Mo^{(V)} \rightarrow Mo^{(VI)}$, and the second **(II)** couple is due to ring oxidation, represented by $Pc(2-) \rightarrow Pc(1-)$ [58]. The rest of the couples are as assigned in **Table 3**, by comparison with

TABLE 3: *The half-wave potentials ($E_{½}$) of $OMo^{(V)}(OH)Pc$ in chloronaphthalene containing TBAP (vs SCE).*

Redox couple	$E_{½}$/V (a) this work	$E_{½}$/V (b) Ref.[58]	Assignment
I	0.45	0.38	$Mo^{(V)} \rightarrow Mo^{(VI)}$
II	1.30	1.22	$Pc^{(2-)} \rightarrow Pc^{(1-)}$
III	-0.70	-0.74	$Mo^{(V)} \rightarrow Mo^{(IV)}$
IV	-1.0	-1.15	$Pc^{(2-)} \rightarrow Pc^{(3-)}$
V	-1.45	-1.69	$Mo^{(IV)} \rightarrow Mo^{(III)}$
VI	-1.70	-1.85	$Pc^{(3-)} \rightarrow Pc^{(4-)}$

(a) On glassy carbon working electrode and, (b) On platinum disk working electrode.

literature assignments. In this work, glassy carbon working electrode was used, compared to the platinum disk used on the work reported in reference [58]. This therefore may account for the difference in $E_{½}$ values reported in **Table 3**.

3.4.3 Elemental and spectral analysis

Elemental analysis of OMo(OH)Pc found H, 2.80%; C, 59.80% and N, 17.90%. Calculated for $OMoC_{32}H_{16}N_8OH$ gave H, 2.60%; C, 59.90% and N, 17.50%.

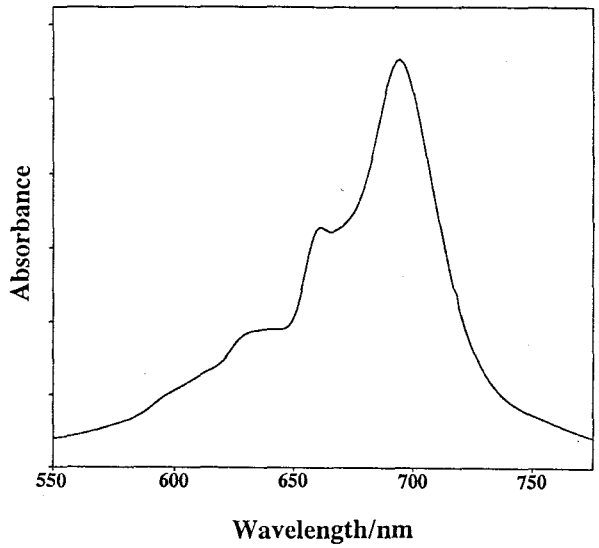

FIGURE 16: *Electronic absorption spectrum of OMo(OH)Pc in pyridine showing intense monomeric absorption behaviour.*

The UV-vis absorption spectra in pyridine revealed intense absorption at lower energy side and two shoulders towards higher energies **(Fig. 16)**. The intense band at 690 nm is due to monomeric species. Apart from the intense band at 690 nm, two small shoulders due to vibronic transitions were observed at 600 and 633 nm, and this is consistent with the spectra of $OMo^{(V)}(OH)Pc$ taken in DMSO as reported by Nyokong [58].

For reasons of symmetry, the IR spectrum of phthalocyanine complexes of related transition metals are expected to be similar [75]. From **Fig. 17**, $OMo^{(V)}(OH)Pc$ shows IR spectrum similar to those reported in literature [57,64,73]. The spectrum is also similar to the spectra of phthalocyanines of other transition metals **(Table 2)** [65], but with additional absorption bands observed at 3450 and 973 cm^{-1}. The band at 973 cm^{-1} is due to molybdenum-oxygen stretching vibrations, $\nu(Mo=O)$. This assignment is based on the data published in literature for Mo=O stretching vibrations in molybdenum compounds [57,58]. This has been further supported by the 972 cm^{-1} reported by Hill and Norgett [65] who reported that the vibrations of Mo=O stretch, the diamagnetism, and the absorption spectrum all indicate a very strong molybdenum-oxygen bond in molybdenum phthalocyanine. The presence of a strong Mo=O bonding therefore eliminates the possibility of formation of a dimeric compound with oxygen bridging [65]. The band at 3450 cm^{-1} can be attributed to an ν(O-H) [66]. The fact that molybdenum has two single bonds to nitrogen atoms, the presence of a double bond to oxygen and a single bond to OH, indicates that molybdenum is in the oxidation state of five, (V). Therefore, the complex can be conveniently be written as $OMo^{(V)}(OH)Pc$, which is supported by elemental analysis results.

The IR spectra of almost all metal phthalocyanines have been found to be independent of the central metal ion [73]. Therefore, in conclusion, the redox properties, UV-visible absorption and IR spectra of metal phthalocyanines reported here closely resembles the results which are characteristic of metal phthalocyanines reported in the literature, and confirm the purity of these phthalocyanine complexes.

FIGURE 17: *Infrared spectrum of oxomolybdenum(V) phthalocyanine, $OMo^{(V)}(OH)Pc$, using KBr disk.*

CHAPTER FOUR: ELECTROANALYIS OF *L*-CYSTEINE

4.1 Molybdenum(V) phthalocyanine complexes

4.2 Cobalt(II) phthalocyanine complex

4.3 General discussion on cysteine

4.1 Molybdenum(V) phthalocyanine complexes

4.1.1 Solution-phase catalysis of cysteine by $[OMo^{(V)}(OH)TSPc]^{4-}$

The cyclic voltammogram for the oxidation of $[OMo(OH)TSPc]^{4-}$ in 0.05 mol dm^{-3} sulphuric acid on an unmodified CPE showed a weak anodic peak at 0.44 V (*vs* Ag|AgC*l*), **Fig. 18(a)**, which is associated with the oxidation of $Mo^{(V)}$ to $Mo^{(VI)}$. Addition of 0.08 mol dm^{-3} cysteine to the $[OMo^{(V)}(OH)TSPc]^{4-}$ solution gave voltammogram shown in **Fig. 18(b)**.

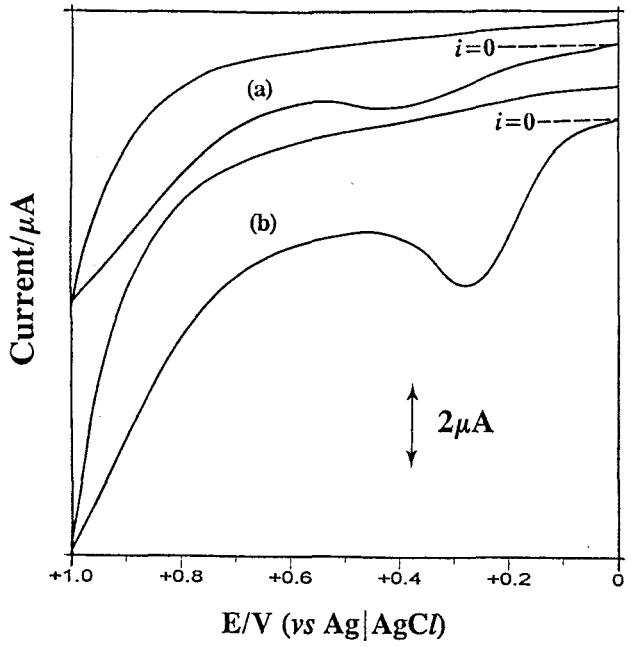

FIGURE 18: *Cyclic voltammograms of* ***(a)*** *0.003 mol* dm^{-3} $[OMo^{(V)}(OH)TSPc]^{4-}$ *in 0.05 mol* dm^{-3} H_2SO_4 *and,* ***(b)*** *same as in (a) but with 0.08 mol* dm^{-3} *cysteine added. All at unmodified carbon paste electrode, scan rate = 100 mV* s^{-1} *(vs Ag|AgCl).*

Addition of cysteine produced a marked increase in anodic current and a shift of anodic peak potential from 0.44 to 0.29 V (*vs* Ag|AgC*l*) **(Fig. 18)**. The observed anodic current decreased drastically after the first scan, probably due to depletion of cysteine concentration at or around the electrode surface. The initial anodic current was easily reproduced by stirring the solution.

The oxidation of cysteine, catalysed by $[OMo^{(V)}(OH)TSPc]^{4-}$, was found to be irreversible as evidenced by the absence of the cathodic wave on the reverse scan. This implies the formation of a stable intermediate or final product, cystine, which cannot be easily reduced back to the starting material. However, the formed product does not bind strongly to the electrode surface active sites because there was no apparent electrode poisoning noted; this is because cystine is soluble in acidic media. The unusual steep tailing in **Fig. 18(a)** could not be explained. However, on CoPc-CMCPE, this irregular shape has been reported to be due to irreversible coordination of the thiol to the MPc complex [2]. The initial anodic current for the oxidation of cysteine was found to depend on the concentration of cysteine added, with linearity prevailing in the range 0.02 to 0.08 mol dm^{-3} as shown in **Fig. 19**. Deviations from linearity were observed at higher concentrations of cysteine. This is likely to be due to competition for the electrode's active sites, when the electrode gets saturated, by cysteine molecules.

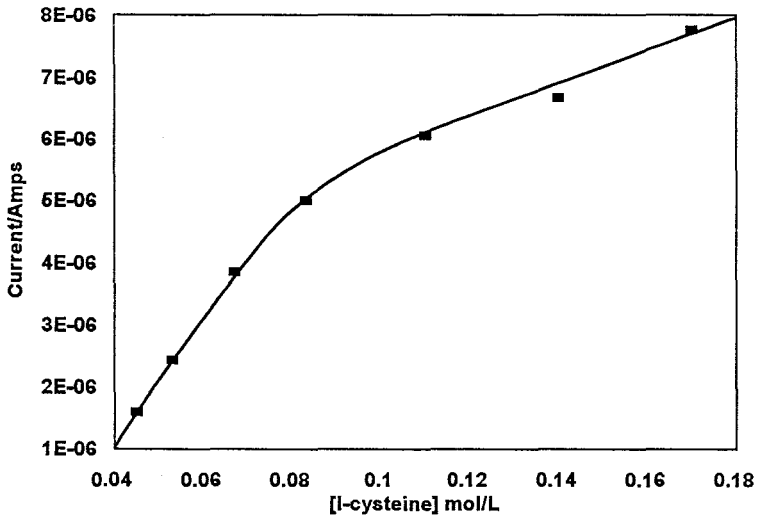

FIGURE 19: *Plot of anodic current dependence on the concentration of cysteine using $[OMo^{(V)}(OH)TSPc]^{4-}$ in 0.05 mol dm^{-3} H_2SO_4 on unmodified CPE (scan rate = 200 mVs^{-1}).*

In the absence of $[OMo^{(V)}(OH)TSPc]^{4-}$, there was no cysteine oxidation peak observed on unmodified carbon paste electrode within the potential range of the medium. As already mentioned, electrooxidation of $[OMo^{(V)}(OH)TSPc]^{4-}$ in solution occurs at 0.44 V, when cysteine is added the anodic peak was lowered to 0.29 V. Suggesting that the species being oxidised is not $[OMo^{(V)}(OH)TSPc]^{4-}$ complex only, but an adduct of $[OMo^{(V)}(OH)TSPc]^{4-}$ with cysteine, hence a shift of oxidation potential.

4.1.2 Absorption spectral studies of $[OMo^{(V)}(OH)TSPc]^{4-}$

To investigate the possible interaction of $[OMo^{(V)}(OH)TSPc]^{4-}$ with cysteine, absorption spectral studies were undertaken. Absorption spectra of $[OMo^{(V)}(OH)TSPc]^{4-}$ in 0.05 mol dm^{-3} sulphuric acid was recorded **(Fig. 20(a))**. Then cysteine was added to the same solution and the spectra taken again **(Fig. 20(b))**.

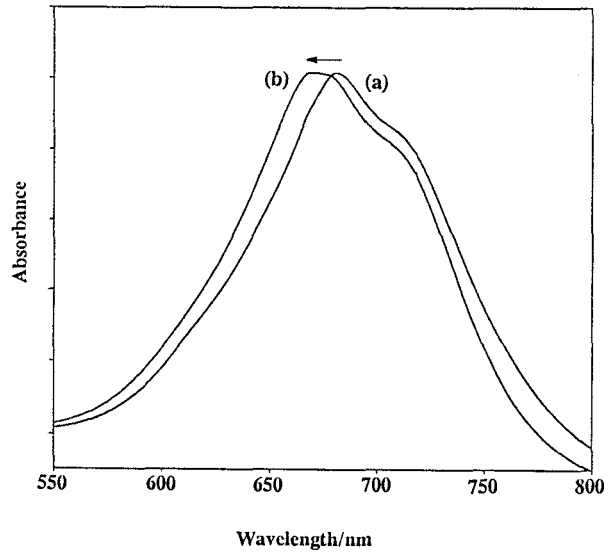

FIGURE 20: *Absorption spectral changes observed on addition of cysteine to the solution of $[OMo^{(V)}(OH)TSPc]^{4-}$ in 0.05 mol dm^{-3} sulphuric acid; (a) spectrum of $[OMo^{(V)}(OH)TSPc]^{4-}$ only and, (b) after addition of cysteine.*

In the presence of cysteine, spectral shift to higher energies was observed as shown in **Fig. 20**. This spectral shift, which occurred without a change in intensity, indicates the formation of an adduct between $[OMo^{(V)}(OH)TSPc]^{4-}$ and cysteine before electrochemical redox reaction takes place. The MPc complexes are known to use axial positions for coordinating the analyte during electrocatalysis. Therefore, cysteine is also likely to be axially coordinated to $[OMo^{(V)}(OH)TSPc]^{4-}$ giving $[OMo^{(V)}(OH)(RSH)TSPc]^{4-}$ species prior to electrooxidation. Molybdenum is known to coordinate up to 8 ligands [20]. For nonmetallated complexes such as tetrakis (4-trimethylammoniumphenyl) porphyrin (H_2TMAP), their interaction with cysteine probably results from an outer-sphere complex formed by H-bonding of RSH or RS^- with the cavity N-donors on the ring [76], suggesting ring-based catalytic redox process.

The suggested mechanism for the oxidation of cysteine by $[OMo^{(V)}(OH)TSPc]^{4-}$ is believed to involve a two-step electrocatalytic process. The initial step involves metal oxidation, whereby the adduct $[OMo^{(V)}(OH)(RSH)TSPc]^{4-}$ is oxidised to $[OMo^{(VI)}(OH)(RSH)TSPc]^{3-}$, followed by deprotonation and oxidation of cysteine, with ultimate regeneration of $[OMo^{(V)}(OH)TSPc]^{4-}$ catalyst. The oxidised cysteine is believed to form a thiol radical ($RS^{\bullet}$), two molecules of which couple together to form a disulphide, cystine, as per equations 13 to 15 [2]:

$$\mathbf{[OMo^{(V)}(OH)TSPc]^{4-} + RSH \rightarrow [OMo^{(V)}(OH)(RSH)TSPc]^{4-}} \quad \text{.....(13)}$$

$$\mathbf{[OMo^{(V)}(OH)(RSH)TSPc]^{4-} \rightarrow [OMo^{(VI)}(OH)(RSH)TSPc]^{3-} + e^-} \quad \text{..... (14)}$$

$$\mathbf{2[OMo^{(VI)}(OH)(RSH)TSPc]^{3-} \rightarrow 2[OMo^{(V)}(OH)TSPc]^{4-} + RSSR + 2H^+} \quad \text{.....(15)}$$

In aqueous solvents, $[OMo^{(V)}(OH)TSPc]^{4-}$ aggregates into dimeric species. However, for simplification, these dimeric effects have been left out in the proposed mechanism for the electrocatalytic oxidation of cysteine.

4.1.3 Heterogeneous catalysis using OMo(OH)Pc-CMCPE

The chemically modified carbon paste electrode (CMCPE) for use in heterogeneous catalysis of cysteine was achieved by incorporating $OMo^{(V)}(OH)Pc$ into a conductive matrix of nujol/graphite to produce a chemically modified electrode, as explained in the experimental section. The performance of OMo(OH)Pc-CMCPE was evaluated by cyclic voltammetry. The initial experiment investigated the effect of OMo(OH)Pc "loading" on the analytical performance of the chemically modified electrode. That is, varying the percentage amount of OMo(OH)Pc in CMCPE from 3 to 8% to determine the percentage amount that shows the highest catalytic activity. The electrode with 4% composition of $OMo^{(V)}(OH)Pc$ was found to have the highest sensitivity and reproducibility rate, and was therefore used as the working electrode for all the subsequent heterogeneous catalytic determination of cysteine.

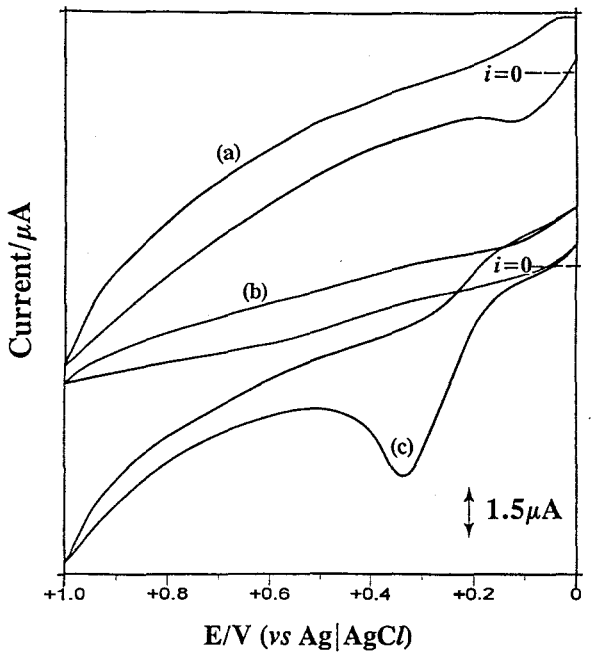

FIGURE 21: *Cyclic voltammograms of* ***(a)*** *4% $OMo^{(V)}(OH)Pc$ modified carbon paste electrode in blank 0.05 mol dm^{-3} H_2SO_4,* ***(b)*** *0.08 mol dm^{-3} cysteine on unmodified carbon paste electrode and,* ***(c)*** *0.08 mol dm^{-3} cysteine on 4% OMo(OH)Pc-CMCPE. Scan rate = 100 mV s^{-1}.*

Figure 21(a) shows the response of the OMo(OH)Pc-CMCPE in a blank solution of 0.05 mol dm^{-3} sulphuric acid. This showed a very weak anodic oxidation wave at 0.13 V (*vs* Ag|AgC*l*), corresponding to $Mo^{(V)}/Mo^{(VI)}$ transition. Addition of cysteine showed an increase in anodic current and a shift in potential from 0.13 to 0.33 V (*vs* Ag|AgC*l*) **(Fig. 21(c))**. A very weak and undefined cathodic peak at 0.17 V (*vs* Ag|AgC*l*) was noted on the reverse scan in the presence of cysteine **(Fig. 21(c))**. On unmodified carbon paste electrode, anodic oxidation of cysteine was not observed for potentials of up to 1.0 V **(Fig. 21(b)**. The anodic currents for the oxidation of cysteine, on 4% OMo(OH)Pc-CMCPE, were found to depend linearly on the concentration of cysteine ranging from 0.008 to 0.02 mol dm^{-3}, with deviations from linearity observed at higher concentrations **(Fig. 22)** of cysteine due to competition for the surface active sites of the electrode.

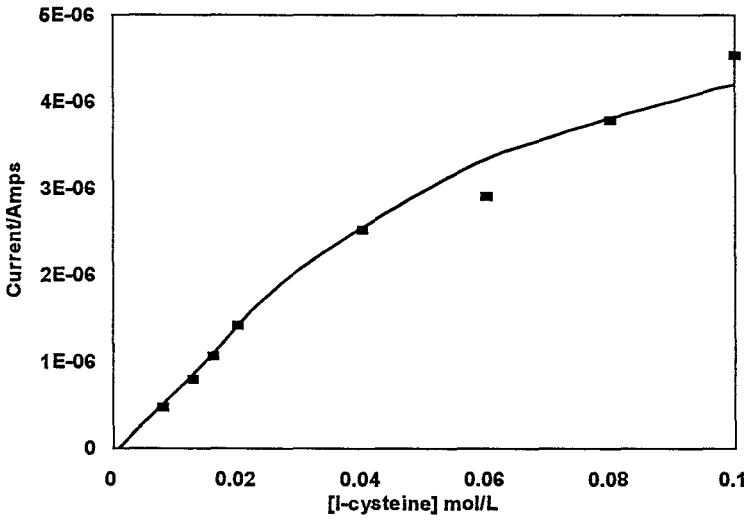

FIGURE 22: *Anodic peak currents vs concentration of cysteine (in 0.05 mol dm^{-3} H_2SO_4) on 4% OMo(OH)Pc modified carbon paste electrode (scan rate = 100 mV s^{-1}).*

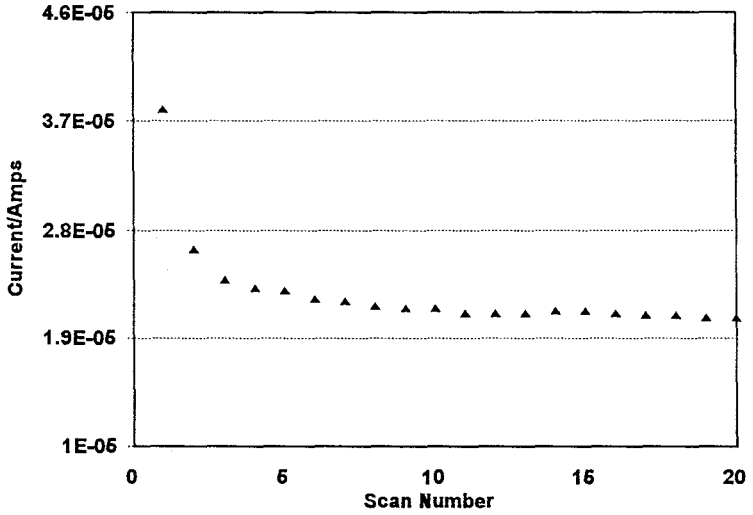

FIGURE 23: *The effect of cyclic voltammetric scan number on the anodic current for the oxidation of 0.1 mol dm^{-3} cysteine on 4% OMo(OH)Pc modified carbon paste electrode (electrolyte = 0.05 mol dm^{-3} H_2SO_4, scan rate = 300 mV s^{-1}).*

On investigating the effect of varying the scan number on anodic peak current, the initial peak current was followed by a sudden decrease in current magnitude which later stabilized after about four runs, and ultimately giving a stable and reproducible current after about 20 scans **(Fig. 23)**. This shows that the OMo(OH)Pc-CMCPE is stable towards the oxidation of cysteine.

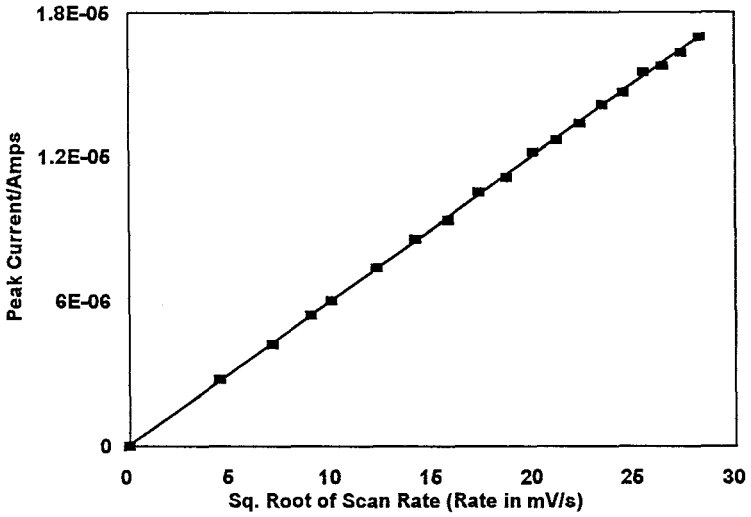

FIGURE 24: *Anodic currents vs square root of scan rate for the oxidation of 0.1 mol dm^{-3} cysteine on 4% OMo(OH)Pc modified carbon paste electrode. Electrolyte = 0.05 mol dm^{-3} H_2SO_4.*

A linear dependence of current on the square root of scan rate was observed for scan rates as high as 800 mV s^{-1}, indicating that mass transfer of cysteine is diffusion controlled as discussed in the introduction **(Fig. 24)**. The long-term stability of the electrode was investigated by regular use of the same 4% OMo(OH)Pc-CMCPE for a period of over 3 months. During this period no apparent deterioration was observed.

The heterogeneous oxidation of cysteine on OMo(OH)Pc-CMCPE can also be simply explained as a two-step process involving the oxidation of $OMo^{(V)}(OH)Pc$ to $[OMo^{(VI)}(OH)Pc]^+$ followed by reduction of $[OMo^{(VI)}(OH)Pc]^+$ by cysteine, with ultimate regeneration of $OMo^{(V)}(OH)Pc$. Cysteine oxidation possibly results in the disulphide compound, cystine. Many of investigative studies, on the oxidation of cysteine, have revealed cystine to be the major product of electrooxidation of cysteine by metallophthalocyanine complexes [10,77].

The change of the central metal in phthalocyanines is known to affect the product distribution only and not the type of products formed [78].

4.2 Cobalt(II) phthalocyanine complex

Heterogeneous catalysis using CoPc-CMCPE

The use of 2% and 5% $Co^{(II)}Pc$ chemically modified carbon paste electrode (CoPc-CMCPE) for electroanalysis of cysteine have been reported [2,6]. As already stated, in this work 4% CoPc-CMCPE was used for comparison with the work undertaken using 4% OMo(OH)Pc-CMCPE. A typical cyclic voltammogram for the oxidation of cysteine on 4% CoPc-CMCPE is as shown in **Fig. 25**. Cyclic voltammetry of 4% CoPc-CMCPE in blank 0.05 mol dm^{-3} H_2SO_4 revealed only a weak oxidation wave at 0.80 V (*vs* Ag|AgC*l*), corresponding to $Co^{(II)}/Co^{(II)}$ transition as observed before [2]. For electroanalysis on unmodified carbon

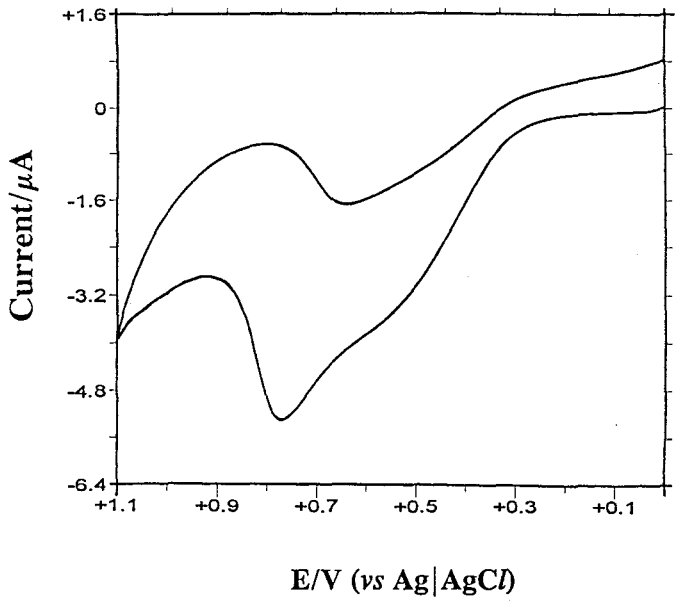

FIGURE 25: *Typical cyclic voltammogram for the oxidation of cysteine on CoPc modified CPE in 0.05 mol dm^{-3} H_2SO_4 (vs Ag|AgCl). Scan rate = 100 mV s^{-1}.*

paste electrode (CPE), there was no anodic oxidation wave observed for the direct electrooxidation of cysteine. Whereas, on CoPc-CMGCE there was a marked increase on the anodic currents associated with CoPc oxidation. The anodic currents from the first scan, for cysteine oxidation, were found to depend on the concentration of cysteine added. The current dependence on the concentration was linear for concentrations below 0.0005 mol dm^{-3} of cysteine **(Fig. 26(b))**, deviations from linearity were observed at concentrations higher than 0.0005 mol dm^{-3}, with currents starting to level off at 0.05 mol dm^{-3} of cysteine **(Fig. 26(a))**. This observation indicates loss of activity of the electrode at high concentrations of cysteine, probably due to competition for active sites on the electrode surface.

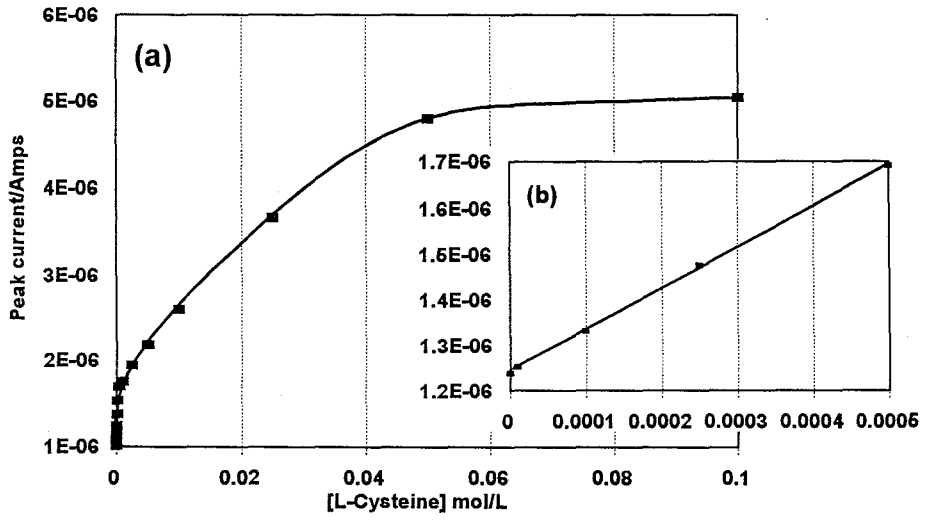

FIGURE 26: *Plot of the effect of cysteine concentration on the anodic currents for the oxidation of cysteine on CoPc modified CPE, for concentrations of (a) up to 0.1 and, (b) up to 0.0005 mol dm^{-3} cysteine (electrolyte = 0.05 mol dm^{-3} H_2SO_4, scan rate = 100 mV s^{-1}).*

The initial current, for the oxidation of cysteine on CoPc-CMCPE, was followed by a sharp decrease on subsequent scans as the cysteine gets depleted around the electrode [2]. These

sharp current drop stabilized after about 13 scans. The initial current was reproduced by stirring the solution, without necessarily renewing the electrode surface. The current decrease after the first scan formed a trough which was followed by an increase and stabilisation of current **(Fig. 27)**. These behaviour could not be explained.

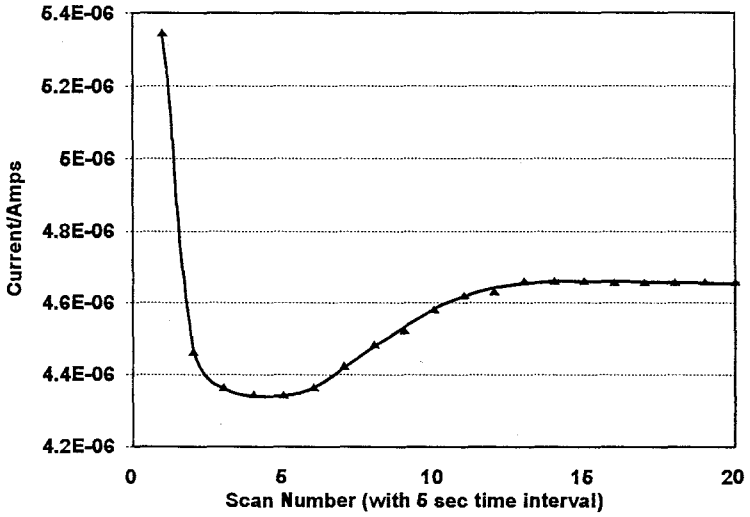

FIGURE 27: *The variation of anodic peak currents with scan number for the voltammetric response of 0.1 mol dm^{-3} cysteine on a CoPc modified CPE. Scan rate = 150 mV s^{-1}. Electrolyte = 0.05 mol dm^{-3} H_2SO_4 (vs Ag|AgCl).*

The variation of anodic peak current with the square root of scan rate was found to be linear for scan rate as high as 900 mV s^{-1}, which is consistent with the diffusion controlled electrode reactions **(Fig. 28)**. The potential required for the oxidation of cysteine was found to vary with the scan rate, increasing with increasing scan rate. This behaviour is typical of totally irreversible electrode reactions [3].

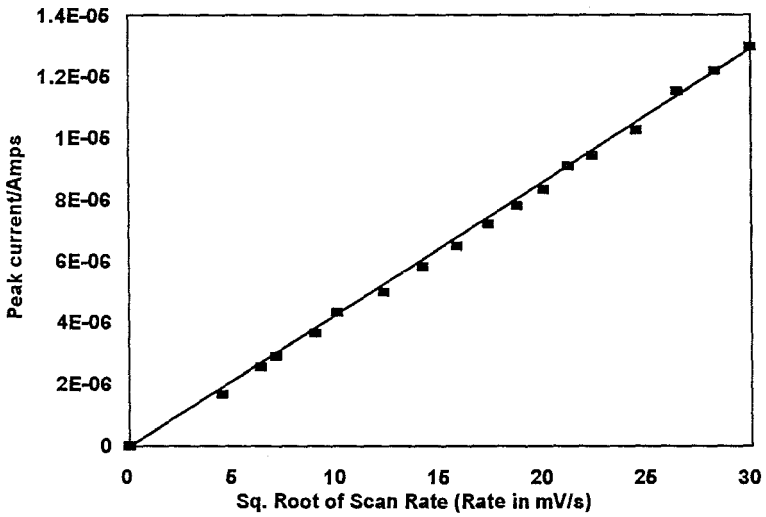

FIGURE 28: *Plot of anodic peak currents vs square root of scan rate on CoPc modified GCE, towards determination of 0.1 mol dm^{-3} cysteine in 0.05 mol dm^{-3} H_2SO_4 (vs Ag\|AgCl).*

In general, the results obtained were consistent with those reported in literature [2,6]. Halbert and Baldwin [2] further attributes the observations reported above to be that of a typical two-step electrocatalytic process initiated by electrooxidation of cobalt(II) to cobalt(III) followed by cysteine oxidation with ultimate reduction of $Co^{(III)}$, thus regenerating the $Co^{(II)}Pc$ catalyst as per equations 16 to 18:

$$Co^{(II)}Pc(RSH) \rightarrow Co^{(III)}Pc(RSH) + e^- \quad \text{.....(16)}$$

$$Co^{(III)}Pc(RSH) \rightarrow Co^{(II)}Pc + RS^{\cdot} + H^+ \quad \text{.....(17)}$$

$$2\,RS^{\cdot} \rightarrow RSSR \quad \text{.....(18)}$$

Cysteine is believed to loose a proton and an electron forming a radical. Two of these radicals then couple together to form a disulfide, cystine.

4.3 General discussion on cysteine

Table 4 shows the oxidation potential and detection limits for the oxidation of cysteine in 0.05 mol dm^{-3} sulphuric acid in the presence of phthalocyanines and tetrakis (4-trimethylammoniumphenyl) porphyrin (H_2TMAP). The electrooxidation of cysteine occurs at low potentials when catalysed by molybdenum(V) phthalocyanine complexes than in the presence of other complexes. For molybdenum complexes, cysteine is oxidised at a lower potential in the presence of $[OMo^{(V)}(OH)TSPc]^{4-}$ than when mediated by $OMo^{(V)}(OH)Pc$. These lowering of potential is important as it indicates the ease with which cysteine may be electrochemically detected in the presence of $[OMo^{(V)}(OH)TSPc]^{4-}$.

TABLE 4: *Detection limits and oxidation potential exhibited by different phthalocyanines and porphyrin towards detection of cysteine.*

Catalyst	E_p/V (vs Ag|AgCl)	Detection limit (mol dm^{-3})	Mode of catalysis	Reference
$OMo^{(V)}(OH)Pc$	0.33	10^{-3}	CMCPE	This work
$[OMo(OH)TSPc]^{4-}$	0.29	10^{-2}	solution	This work
$Co^{(II)}Pc$	0.77	10^{-7}	CMCPE	[2,6] & This work
$[Co^{(II)}TSPc]^{4-}$	0.82	10^{-8}	CMGCE	[16]
$[Co^{(II)}TSPc]^{4-}$	0.77	----	solution	[2]
H_2TMAP	0.60	----	solution	[76]

Even though molybdenum(V) phthalocyanine complexes have shown efficiency in lowering the potential needed for electrooxidation of cysteine, they have poor sensitivity. For instance, a much lower concentration of cysteine was detected by CoPc-CMCPE and CoTSPc-CMGCE than on molybdenum phthalocyanine complexes. For CoPc-CMCPE and CoTSPc-CMGCE, under similar conditions of MPc composition in CMCPEs and same electrolyte concentration,

detection limit as low as 10^{-7} mol dm^{-3} on CoPc-CMCPE and 10^{-8} mol dm^{-3} on CoTSPc-CMGCE have been reported [6,16], whereas detection limits of 10^{-3} and 10^{-2} mol dm^{-3} were obtained from the use of OMo(OH)Pc-CMCPE and $[OMo(OH)TSPc]^{4-}$ (in solution), respectively. The high sensitivity of CoPc-CMCPE has made evaluation of the performance of CoPc-CMCPE in the analysis of cysteine in human urine possible [6]. The concentration of cysteine in the urine sample of a normal individual is reported to be 10^{-5} mol dm^{-3} [6]. The poor detection limits of OMo(OH)Pc-CMCPE therefore limits its use only to analytes with high concentration of sulfhydryl compounds. However, the lowering of the oxidation potential is a significant development in the analysis of cysteine in situations where low energy, other than low detection limit, is desirable.

As already discussed, at high concentrations of cysteine deviations from linearity were observed, indicating a decrease in activity of OMo(OH)Pc-CMCPE and CoPc-CMCPE. This suggests that the active sites on the electrode surface were gradually being covered with cysteine and/or intermediates molecules, resulting in a decrease in the activity of the electrode. Catalytic oxidation of cysteine, on phthalocyanine modified electrodes, forms a disulphide (cystine). It is believed that the reduction of cystine occurs when two sulphur atoms interact with the electrode. But for steric reasons, it is unlikely that both sulphur atoms (of cystine) simultaneously interact with the metal centre of the phthalocyanine. The interaction is possibly via one sulphur atom at a time, inhibiting electron transfer. This could then explain why the oxidation of cysteine was found to be irreversible in this study.

CHAPTER FIVE: ELECTROANALYSIS OF PHENOLIC COMPOUNDS

5.1 Cresols, mono-chlorinated phenols and phenol

5.2 Polychlorinated phenols

5.3 Electroanalysis of all phenolic compounds using $[Co^{(II)}TSPc]^{4-}$

5.4 Overall discussion on all phenolic compounds

5.1 Cresols, mono-chlorinated phenols and phenol

5.1.1 Electroanalysis using CoPc-CMGCE

Cyclic voltammetric studies of cresols, phenol, 2-chlorophenol and 4-chlorophenol were conducted on a glassy carbon electrode coated (drop-dry method) with metal phthalocyanine.

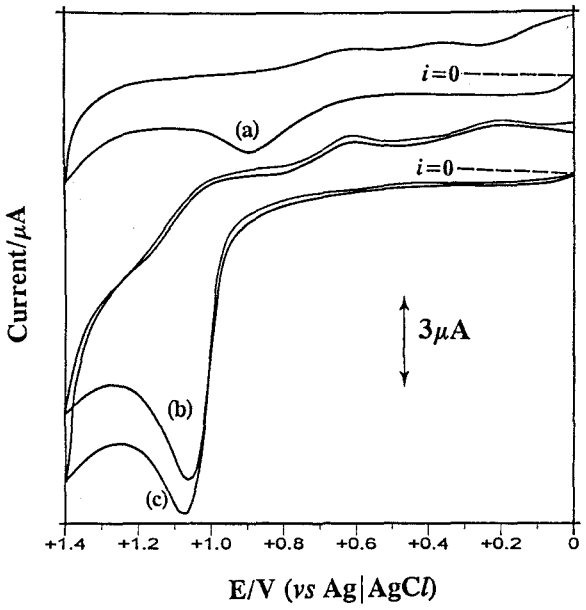

FIGURE 29: *Cyclic voltammograms of (a) CoPc coated GCE in the blank 0.05 mol dm^{-3} H_2SO_4, (b) phenol on uncoated GCE and, (c) phenol on CoPc coated GCE. Phenol concentration was 2.5 x 10^{-4} mol dm^{-3} in 0.05 mol dm^{-3} H_2SO_4 (scan rate = 100 mV s^{-1}).*

Fig. 29(a) shows the cyclic voltammogram of CoPc deposited on GCE in a blank 0.05 mol dm^{-3} sulphuric acid solution. The CoPc-CMGCE exhibited a single anodic wave at around 0.88 V (vs Ag|AgC*l*) when cycled in blank solution. This single anodic wave was accompanied by three relatively small and undefined reduction waves on the reverse scan. A similar observation was made by Halbert and Baldwin [2]. The anodic wave at 0.88 V (*vs*

Ag|AgCl) is associated with oxidation of the central metal in $Co^{(II)}Pc$ with the formation of $Co^{(III)}Pc$ [2]. The wave at 0.88V is surely due to the presence of CoPc on the electrode because voltammetric scan of the blank solution using bare GCE did not produce any voltammetric waves.

In cyclic voltammetric analysis of phenolic compounds, the MPc-CMGCE exhibited currents higher than those exhibited by the uncoated GCE. For example, **Fig. 29(b)** and **(c)** shows the cyclic voltammograms of phenol in 0.05 mol dm^{-3} sulphuric acid on uncoated and on CoPc-CMGCE, respectively, for the detection of phenol. Higher currents were observed for phenol on CoPc-CMGCE than on uncoated GCE. The enhanced currents were accompanied by a small positive shift (≈ 0.03 V) in oxidation potential. A similar positive shift of oxidation potential was also noted for other phenolic compounds under investigation. This positive shift of oxidation potential when CoPc was used as a mediator (compared to uncoated GCE) suggest the formation of an adduct between the adsorbed CoPc and the phenolic compounds, resulting in the oxidation occurring at slightly more positive potentials than noted for the uncoated GCE. An ideal catalytic electrode is expected to lower the oxidation potential and also bring about enhanced sensitivity and stability. The adduct formation has also been use to explain the catalytic activity of CoPc towards the oxidation of thionyl chloride [79]. In **Fig. 29(b)** and **(c)**, the small reduction waves on the reverse scan were attributed to p,p'-dihydroxydiphenyl compounds resulting from the tail-tail coupling of two phenoxy radicals, which is followed by intramolecular rearrangement as reported by Sharma *et al* [41]. Even though similar, but smaller, waves were observed in **Fig. 29(a)**, the fact that these waves were enhanced in the presence of phenol and were also noted for phenol on uncoated GCE leads to the conclusion that indeed these reduction peaks are due to the oxidation products of phenol as reported before [41].

Fig. 30(i) show voltammograms of cresols, and **Fig. 30(ii)** shows voltammograms of phenol, 2-chlorophenol and 4-chlorophenol, on CoPc-CMGCE. There is a significant difference between the shapes of voltammograms for cresols to that of phenol and mono-chlorophenols. Presumably this is due to electron-withdrawing or donating properties of groups attached to the benzene. Phenol and chlorophenols display voltammograms with broad peaks **(Fig. 30(ii))**, whereas in the presence of electron-donating groups, voltammograms with sharp peaks were observed **(Fig. 30(i))**. The shape of voltammograms for the cresols were found to depend on the scan rate, broadening at scan rates higher than 100 mV s^{-1}.

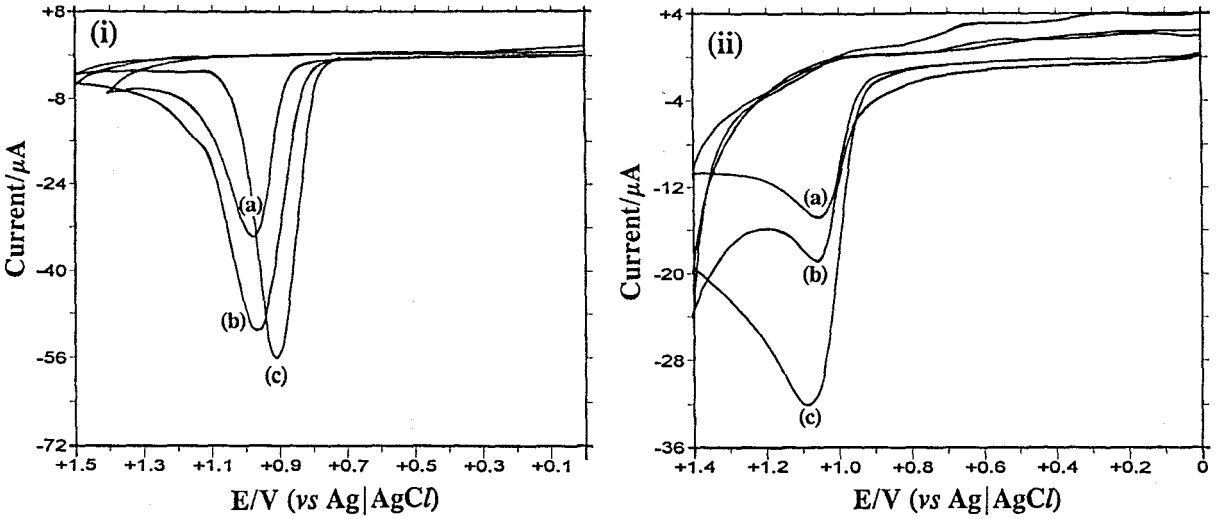

FIGURE 30: *Cyclic voltammograms of 0.0025 mol dm^{-3} of; **(i)** cresols: where (a) is p-cresol, (b) o-cresol and (c) m-cresol and, **(ii)** other phenolic compounds: i.e (a) 2-chlorophenol, (b) 4-chlorophenol and (c) phenol - on CoPc coated GCE. Electrolyte = 0.05 mol dm^{-3} H_2SO_4, scan rate = 100 mV s^{-1}.*

The stability of the CoPc-coated GCE, as compared to uncoated GCE, towards determination of phenolic compounds was investigated by studying the current response against the number of runs as shown in **Fig. 31**. A decrease in anodic peak current with run number was observed

on both the CoPc-CMGCE and the uncoated GCE. However, with similar concentrations of the phenolic compounds, higher currents were observed on the CoPc-CMGCE than on the uncoated GCE for all the compounds, indicating a higher sensitivity and stability of CoPc-CMGCE, compared to uncoated GCE **(Fig. 31)**.

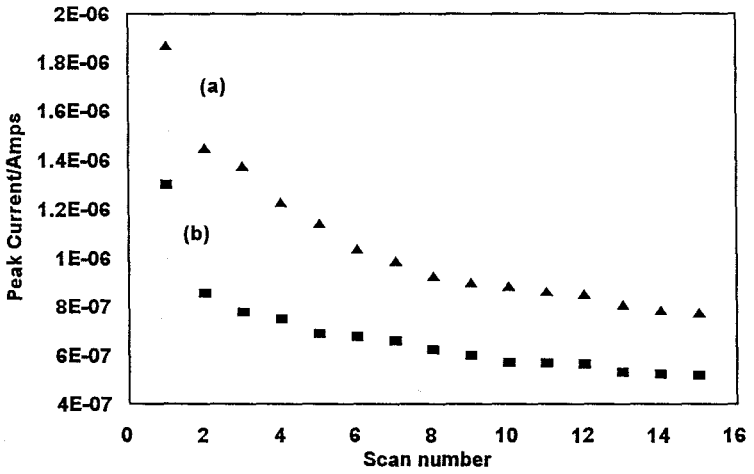

FIGURE 31: *The variation of anodic peak currents with scan number for the voltammetric response of 7.5 x 10^{-5} mol dm^{-3} 2-chlorophenol on (a) a CoPc-CMGCE and, (b) on uncoated GCE. Scan rate = 100 mV s^{-1}, electrolyte = 0.05 mol dm^{-3} H_2SO_4.*

For all the phenolic compounds under consideration, the CoPc-CMGCE was found to be more stable than the unmodified GCE for the oxidation of these species in that peak currents became less than 0.2 μA after fewer scans on uncoated GCE than on CoPc-CMGCE. In general there is a decrease in poisoning when the electrode is coated with phthalocyanine complexes. This is an important observation because the use of voltammetry for oxidative detection of phenolic compounds results in polymeric products which adhere to the electrode surface, thus causing a sudden decrease of current with increasing scan numbers on the conventional carbon electrodes. **Fig. 32** compares the decrease of current response for the cresols, phenol and

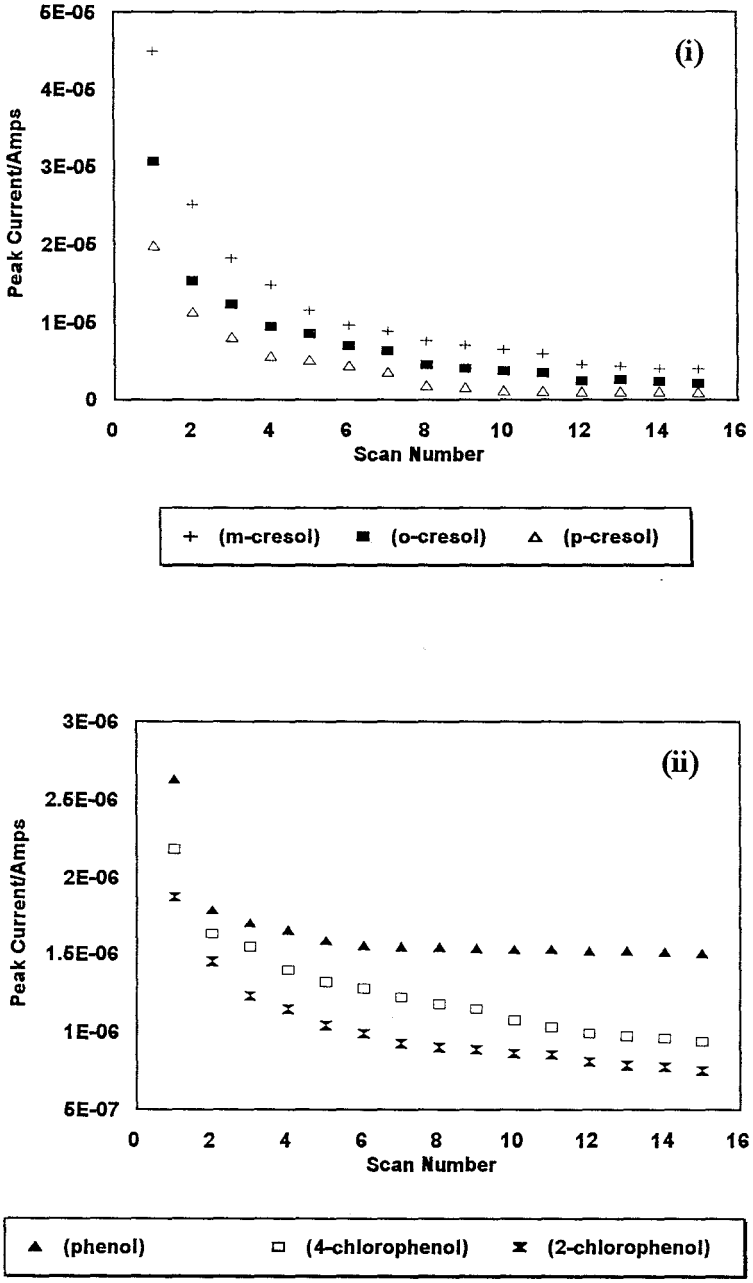

FIGURE 32: *Plots of anodic currents vs scan number for 7.5 x 10^{-5} mol dm^{-3} of (i) cresols and, (ii) phenol, 2-chlorophenol and 4-chlorophenol on CoPc coated GCE. Scan rate = 100 mV s^{-1}, electrolyte = 0.05 mol dm^{-3} H_2SO_4.*

chlorophenols with scan number on CoPc-CMGCE. The CoPc-CMGCE was found to be more stable towards the oxidation of phenol than towards the rest of the phenolic compounds under consideration in that even though a significant decrease in current was observed after the first scan on CoPc-CMGCE for phenol, the rate of decrease of the current slowed down considerably after about five scans (**Fig. 32(ii)**). Anodic peak currents higher than 1.0 μA were obtained for phenol even after 170 scans. On an uncoated glassy carbon electrode, the oxidation peak for phenol became less than 0.2 μA after about 20 scans. The relative number of scans that could be observed for the oxidation of the phenolic compounds on a CoPc-CMGCE compared to the number of scans observed on an unmodified GCE before the current became lower than 0.2 μA gives a good idea of the stability of the former electrode relative to the latter (**Table 5**). In general, it is apparent that CoPc-CMGCE is more stable towards the oxidation of phenol since the difference between the number of scans that could be observed on CoPc-CMGCE and uncoated GCE was much larger for phenol than for the rest of the compounds. The CoPc-CMGCE showed the least stability for the oxidation of the chlorinated phenols (**Table 5**).

TABLE 5: *Stability of CoPc modified against uncoated glassy carbon electrodes towards detection of different phenolic compounds (i.e number of voltammetric scans before the current becomes less than 0.2 μA), vs Ag|AgCl at 100 mV s^{-1}, electrolyte = 0.05 mol dm^{-3} H_2SO_4.*

COMPOUND	CoPc COATED GCE	BARE GCE
PHENOL	over 170	21
O-CRESOL	168	94
M-CRESOL	113	34
P-CRESOL	94	16
4-CHLOROPHENOL	52	12
2-CHLOROPHENOL	30	13

The decreased electrode fouling when CoPc-CMGCE was employed as the working electrode in the determination of phenolic compounds, compared to when uncoated GCE was used, suggests that the CoPc inhibits the formation of dimeric or polymeric oxidation products that are known to poison the electrode, making it more stable and usable even after many voltammetric scans. This decrease in electrode fouling could be due to some steric hindrance caused by the CoPc species, minimizing the adsorption of the oxidation products onto the CoPc coated electrode.

For each of the phenolic compounds under investigation, anodic peak currents (i_p) were found to be proportional to the square root of scan rate ($v^{1/2}$), for scan rates as high as 500 mV s^{-1}, indicating that the electrode process involves the diffusion of the phenolic compounds (**Fig. 33**).

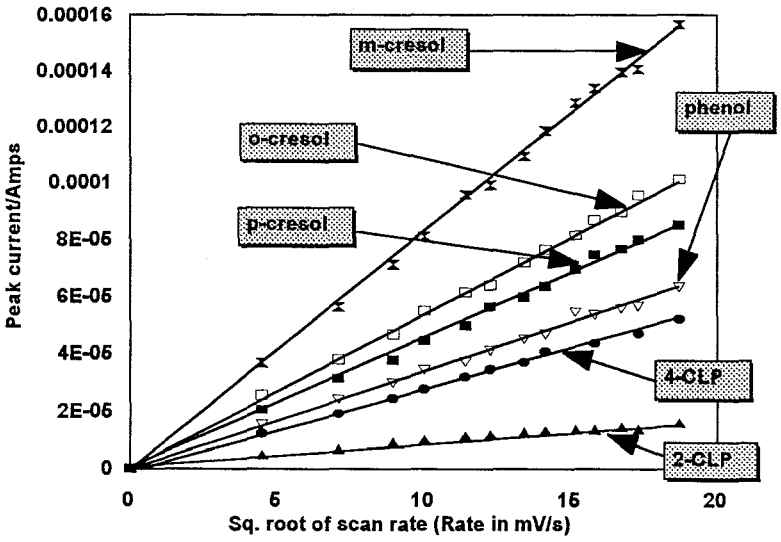

FIGURE 33: *Plot of anodic peak currents vs square root of scan rate for the oxidation of 7.5 x 10^{-5} mol dm^{-3} of m-cresol, o-cresol, p-cresol, phenol, 4-chlorophenol (4-CLP) and 2-chlorophenol (2-CLP) on CoPc coated GCE. Electrolyte = 0.05 mol dm^{-3} H_2SO_4.*

The voltammograms of all the phenolic compounds showed a characteristic shift of the peak potential with increasing scan rate, which is typical of totally irreversible systems [3]. From the plot of current against the square root of the scan rate, electrooxidation of m-cresol was found to exhibit the highest currents and 2-chlorophenol the lowest. This therefore suggests that CoPc-CMGCE has a higher catalytic activity towards m-cresol than the rest of the phenolic compounds. In principle, o-cresol was expected to exhibit the highest current density than the rest of phenolic compounds under consideration because of the electron-donating methyl group on the ortho position being very close to the functional hydroxyl group. However, o-cresol exhibited currents lower than those obtained from the electrooxidation of m-cresol. Presumably, the bulky methyl group on the ortho position in o-cresol sterically prevents o-cresol molecule from approaching the electrode closely, thus giving currents lower than those obtained from m-cresol. The 2-chlorophenol also experiences steric effect from the chlorine on the ortho position, which prevents it from approaching the electrode closely. Generally, chlorophenols exhibit low currents, relative to cresols, because of their size and the electronegative effect of chlorine. The magnitude of the current obtained from a redox process is determined by the rate at which the substrate is transferred to the electrode [1], suggesting that heavier molecules are prone to exhibiting low currents due to their slow movement towards or away from the electrode.

On comparing the oxidation potentials of all the phenolic compounds, phenol and chlorophenols were found to be oxidised at a relatively higher potentials than cresols (**Table 6**). The difference in oxidation potentials of these species can be attributed to the electron-donating and withdrawing effects of the substituents attached to the phenyl ring.

TABLE 6: *Oxidation potentials of different phenolic compounds at $Co^{(II)}Pc$ coated glassy carbon electrode (Concentration of phenolic compounds was 0.0025 mol dm^{-3} in all cases). Scan rate = 100 mV s^{-1}, electrolyte = 0.05 mol dm^{-3} H_2SO_4.*

Phenolic compounds	E_p/mV (*vs* Ag|AgCl)
PHENOL	1084
2-CHLOROPHENOL	1058
4-CHLOROPHENOL	1026
P-CRESOL	979
O-CRESOL	969
M-CRESOL	911
‡**Blank**	880

‡**Blank** = *electrolyte (0.05 mol dm^{-3} sulphuric acid) only, and the potential corresponds with the oxidation of $Co^{(II)}Pc$ to $Co^{(III)}Pc$ species.*

Generally, all the analysed phenolic compounds get oxidised at different potentials. The oxidation potential as noted in **Table 6** can therefore be arranged in the following order.

Phenol > 2-CLP > 4-CLP > p-cresol > o-cresol > m-cresol

Phenol exhibits the highest oxidation potential due to resonance stabilisation of electrons delocalised within the benzene ring. 2-chlorophenol gets oxidised at higher potential than 4-chlorophenol because of the effect of electron-withdrawing substituent, chlorine, on the ortho position and the steric effect also play an important role. In o-cresol, the electron-donating methyl is very close to the functional hydroxyl, and therefore o-cresol is expected to be oxidized at potential lower than that of m-cresol. In contrary, o-cresol was oxidized at a potential higher than that of m-cresol because of a steric effect. The bulky methyl group

prevents the hydroxyl group from approaching the electrode very closely, resulting in the oxidation occurring at a slightly more positive potential than noted for the m-cresol.

Cresols exhibit only one irreversible oxidation peak on the first scan, as reported by Sharma *et al* [45]. For o-cresol, m-cresol and phenol, Sharma *et al* [41,45] observed new oxidation couples on the second and subsequent scans. On an uncoated GCE, two new oxidation couples, for phenol, m-cresol and o-cresol, were observed in this work as has been observed before [41,45]. On CoPc-CMGCE, one oxidation peak during the first scan for the cyclic voltammetry of all cresols, phenol and chlorophenols was observed in this work. New oxidation peaks were observed on the second and subsequent scans for phenol, o-cresol and the chlorophenols, but not for m-cresol.

In acidic media, the initial electrode process for the oxidation of cresols and phenols is expected to be a one-electron oxidation process forming phenoxy radicals [41,45]. Coupling of these free phenoxy radicals is favoured in acidic media. Coupling of the free radicals of the phenolic compounds is expected to give new electroactive products, which after further oxidation and intramolecular rearrangements form dimeric and polymeric products. The new redox couples observed after the first scan for o-cresol, m-cresol and phenol were therefore assigned to electrooxidation of dimeric and polymeric products as proposed by Sharma *et al* [41,45]. Since no new oxidation couples were observed on return when CoPc-CMGCE was employed for the oxidation of m-cresol, it is likely that the CoPc complex on the electrodes inhibits coupling of m-cresol radicals, thus showing the highest catalytic activity towards determination of m-cresol, as showed in **Fig. 33** above.

Fig. 34 presents the first scan anodic peak current dependence on the concentration of phenolic compounds on CoPc-CMGCE. Of the cresols, m-cresols showed higher currents on the first scan than o-cresol and p-cresol considering the same concentration **(Fig. 34(a))**. Unsubstituted phenol showed higher current response on CoPc-CMGCE during the first scan than the chlorinated phenols for all concentrations studied **(Fig. 34(b))**. In general cresols exhibited higher current responses than phenol and chlorinated phenols, which can be attributed to the electron-donating effect of the methyl group as discussed earlier. In general, the current dependence on the concentrations was linear for all cresols, phenol and mono-chlorinated phenols for concentrations less than 0.001 mol dm^{-3}. Deviations from linearity were observed for concentrations exceeding 0.001 mol dm^{-3}, and a levelling off of the current was observed in some cases, for 2-chlorophenol in particular **(Fig. 34(b))**. This observation implies that the activity of the electrode is decreased at high concentrations of the phenolic compounds, probably due to competition for active sites on the electrode surface. It has also been reported [48] that the fouling of the electrode by the phenolic oxidation products is more persistent at higher concentrations of phenolic compounds.

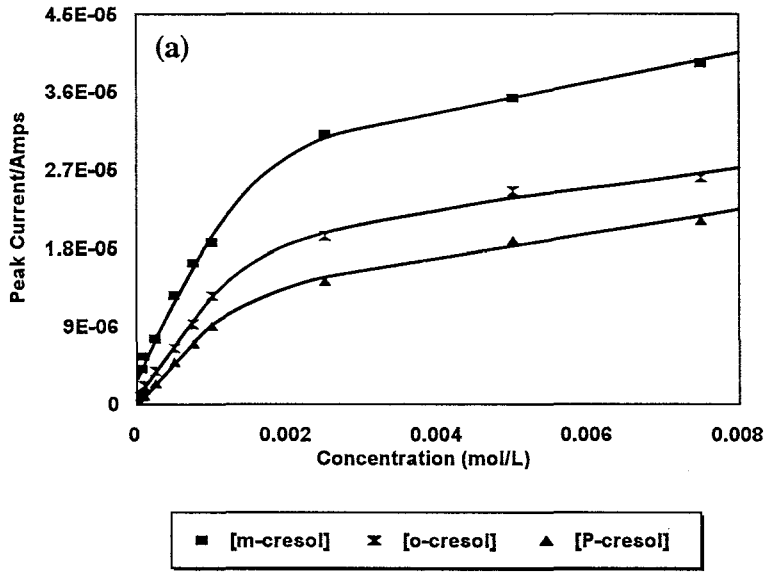

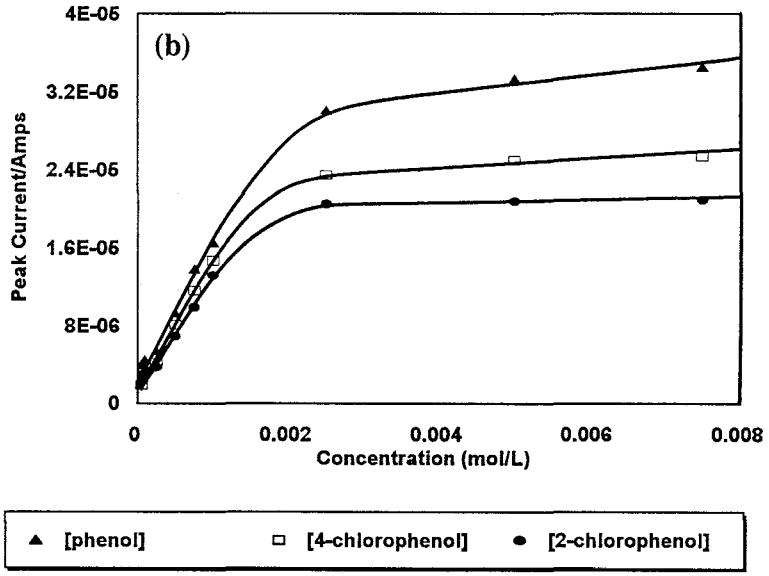

FIGURE 34: *Plots of anodic currents dependence on the concentrations of:* **(a)** *cresols (scan rate = 50 mV s^{-1}) and,* **(b)** *phenol, 4-chlorophenol and 2-chlorophenol (scan rate = 100 mV s^{-1}). All on CoPc coated GCE. Electrolyte = 0.05 mol dm^{-3} (vs Ag\|AgCl). The anodic currents are for the first scan only, following which the electrode was cleaned and coated again.*

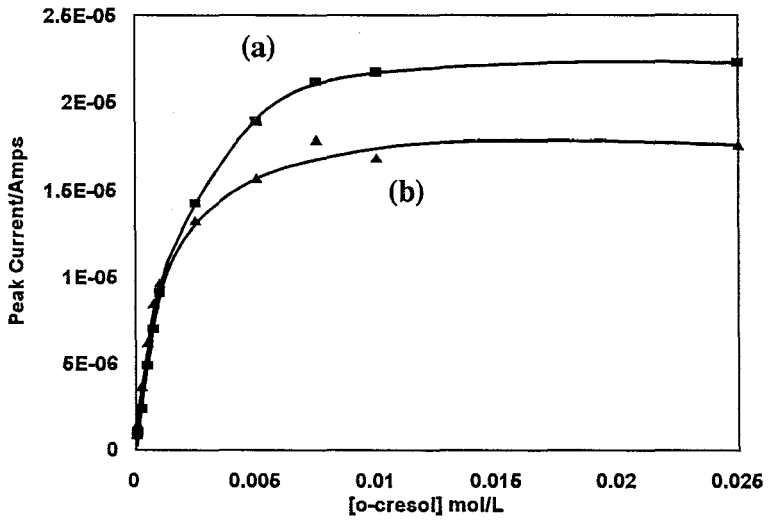

FIGURE 35: *Plot of current dependence on concentration on (a) CoPc coated GCE versus (b) uncoated GCE towards detection of o-cresol (electrolyte = 0.05 mol dm^{-3} H_2SO_4, scan rate = 100 mV s^{-1}).*

Fig. 35 shows a plot of CoPc-CMGCE versus uncoated GCE towards oxidative detection of o-cresol. This shows that at high concentrations of o-cresol, the uncoated GCE **(Fig. 35(b))** looses activity faster than the $Co^{(II)}Pc$ coated GCE **(Fig. 35(a))**. Suggesting that uncoated GCE becomes saturated, by the substrate molecules, faster than the $Co^{(II)}Pc$ coated GCE. Similar trend was observed for p-cresol, m-cresol, phenol, 2-chlorophenol and 4-chlorophenol.

5.1.2 Electroanalysis using other first row transition metals

The initial experiments investigated the catalytic activity of some of the first row transition metal and metal-free phthalocyanine complexes towards detection of phenolic compounds. The catalytic effect of metal phthalocyanine complexes of manganese, iron, cobalt, nickel, copper and zinc were investigated. All the MPcs investigated showed catalytic effects towards electrooxidation of phenolic compounds. **Table 7** shows the catalytic efficiency (CE), which is the ratio of the peak current of the catalytic wave over the peak current of the uncatalysed electrooxidation wave of the same concentration of the substrate [7], for different metal phthalocyanine complexes against different phenolic compounds. From **Table 7**, catalytic efficiency increases down and across the table. As noted for electroreduction of carbon dioxide [21] and electrooxidation of cysteine [17], electrocatalytic activity, hence catalytic efficiency, of MPc complexes was found to depend on the nature of the central metal ion (down the table). Across the table, it seems phenol compared to 2-chlorophenol and 4-chlorophenol, and p-cresol of the cresols show higher catalytic efficiencies corresponding to their high oxidation potential, **Table 7**. This can therefore be correlated with the electron-donating or withdrawing ability of the substituent on the phenyl ring. For the same concentrations, the currents observed for the oxidation of all phenolic compounds when the electrode was modified with CoPc were found to exhibit higher current densities, hence higher catalytic efficiencies, than when the electrode was modified with other phthalocyanine complexes, **Table 7**.

TABLE 7: *Catalytic Efficiency (CE) of different M(II)Pc-modified GCE towards oxidation of different phenolic compounds (vs Ag|AgCl), at 100 mV s^{-1}, in 0.05M H_2SO_4. (CE = ratio of $i_{(CoPc\text{-}CMGCE)}/i_{(bare\ GCE)}$)*

GCE	2-CLP	4-CLP	Phenol	o-cresol	m-cresol	p-cresol
$Zn^{(II)}Pc$	1.11	1.12	1.15	1.16	1.28	1.61
H_2Pc	1.12	1.19	1.29	1.40	1.46	1.58
$Cu^{(II)}Pc$	1.17	1.24	1.39	1.40	1.40	1.58
$Ni^{(II)}Pc$	1.23	1.65	1.62	1.65	2.08	2.44
$Fe^{(II)}Pc$	1.37	1.40	2.17	1.74	2.13	3.51
$Mn^{(II)}Pc$	1.85	2.31	2.55	3.06	3.45	3.63
$Co^{(II)}Pc$	1.91	2.72	3.05	3.27	3.99	4.15

A plot of catalytic efficiency against d-orbital electrons **(Fig. 36)** of metal ions of some of the first row transition metal phthalocyanines ($Mn^{(II)}Pc$, $Fe^{(II)}Pc$, $Co^{(II)}Pc$, $Ni^{(II)}Pc$, $Cu^{(II)}Pc$ and

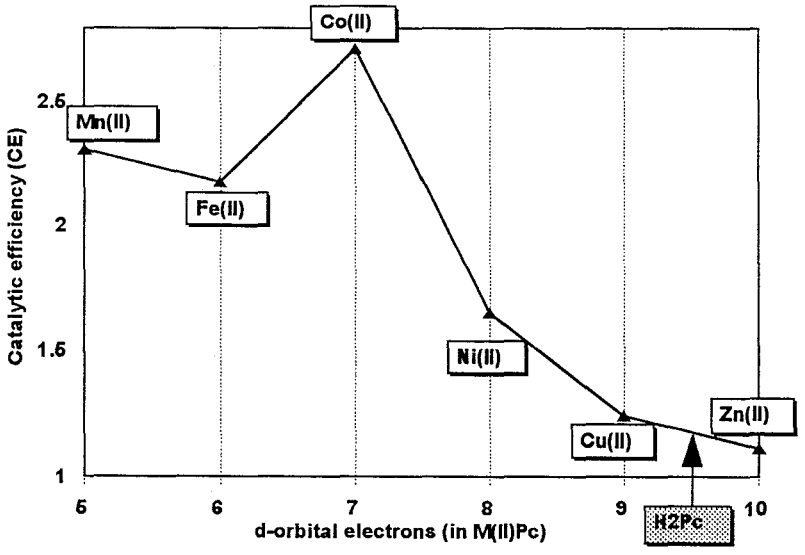

FIGURE 36: *Plot of catalytic efficiency (CE) against d-orbital electrons of some of the first row transition metal(II) ions of metal(II) phthalocyanines towards detection of 0.001 mol dm^{-3} 4-chlorophenol on MPc coated GCE (electrolyte = 0.05 mol dm^{-3} H_2SO_4, scan rate = 100 mV s^{-1}). Similar trend was observed for all other monosubstituted phenolic compounds.*

$Zn^{(II)}Pc$), in detection of 4-chlorophenol, shows dependence of catalytic efficiency on d-orbital electron. This can therefore be explained in terms of difference in their d-orbital electronic configuration.

In MPc catalysis, metal phthalocyanines use axial coordination sites for catalysis. As discussed in the introduction, $Co^{(II)}Pc$ shows higher catalytic activity due to the partly occupied $\mathbf{e_{1g}}$ $(\mathbf{d_z^2})$ orbital with electrons lying along the z-axis, and with proper symmetry to interact with the substrate, phenolic compounds. This suggests that the partly occupied $\mathbf{e_{1g}}$ $(\mathbf{d_z^2})$ orbital of the metal atom of the phthalocyanine plays a major role in electrocatalysis [15,21]. In addition, the cobalt(II) state is more stable over a much wider potential range [18], thus making it the best catalyst for electrooxidation of phenolic compounds. H_2Pc (non-metallated Pc) was found to have catalytic efficiency within the range of CuPc and ZnPc **(Fig. 36)**. The similarity of the catalytic efficiencies of H_2Pc, CuPc and ZnPc is an evidence that CuPc and ZnPc have electro-inactive metal centres, and their redox activities are based on the phthalocyanine ring, rather than at the central metal.

The general trend for the improvement of the current response of the GCE by phthalocyanines is as follows;

$Co^{(II)}Pc$ > $Mn^{(II)}Pc$ > $Fe^{(II)}Pc$ > $Ni^{(II)}Pc$ > $Cu^{(II)}Pc$ > H_2Pc > $Zn^{(II)}Pc$ > bare GCE

This trend shows that MPc complexes with an electroactive metal centres, CoPc, MnPc and FePc [21], enhanced the currents for the oxidation of the phenolic compounds to a larger extent than those exhibiting only ring-based redox processes. This observation suggests that electron transfer reactions centred on the central metal may play a role in enhancing the

oxidation currents of the phenolic compounds. It is generally accepted that electron transfer reactions to or from MPc complexes are involved during the catalysis of reactions using these complexes. For example, catalytic oxidation of cysteine on CoPc-modified carbon electrodes is thought to involve the $Co^{(III)}Pc/Co^{(II)}Pc$ couple [2], thus resulting in enhancement of the oxidation currents of this couple in the presence of cysteine or other sulfhydryl compounds. **Table 6** showed that the oxidation peak potentials of the phenolic compounds are observed at more positive potentials than observed for the $Co^{(II)}Pc \rightarrow Co^{(III)}Pc$ peak, but based on the fact that there is enhancement of the oxidation currents of the phenolic compounds on MPc modified GCE, it is suggested that the electron transfer reaction takes place between the phenolic compounds and MPc complexes according to equations 15 and 16:

$$\mathbf{M^{(II)}Pc \rightarrow [M^{(III)}Pc]^{+} + e^{-}} \quad \text{..... (19)}$$

$$\mathbf{[M^{(III)}Pc]^{+} + Ph \rightarrow M^{(II)}Pc + Ph\ oxidation\ products} \quad \text{..... (20)}$$

Where **Ph** = o-cresol, m-cresol, p-cresol, phenol, 2-chlorophenol and 4-chlorophenol.

5.2 Polychlorinated phenols

Electroanalysis using CoPc-CMGCE

Polychlorinated phenols, 2,4,6-trichlorophenol (TCP) and pentachlorophenol (PCP), have extremely low solubility in aqueous solvents. The solubility of chlorinated phenols in water and persistency in the environment can be correlated with their degree of substitution; that is, the solubility of chlorinated phenols decrease with an increasing degree of substitution. For instance, monochlorinated phenols dissolves reasonably well in water, whereas the solubility of pentachlorophenol in water has been found to be negligible. However, in the presence of

1.0 mol dm^{-3} sodium hydroxide, solubility of trichlorophenol and pentachlorophenol improved dramatically. Sodium hydroxide, which is a strong base, presumably deprotonates the functional hydroxyl group, thus improving the solubility of such phenols. This indicates that the pH of the solution influences the bond scission for species subject to acid-base reactions.

Cyclic voltammetric study of trichlorophenol and pentachlorophenol in 0.05M sulphuric acid (supporting electrolyte) and 1.0 mol dm^{-3} sodium hydroxide on CoPc-coated GCE exhibited current densities lower than those from uncoated GCE. For example, **Fig. 37** shows the high current obtained from the use of uncoated electrode **(Fig. 37(b))** as compared to the low current obtained from CoPc-CMGCE **(Fig. 37(a))** for the determination of PCP. The unusual tailing of voltammogram obtained on CoPc-CMGCE is attributed to an irreversible coordination of PCP to CoPc as discussed earlier **(Fig. 37(a))**.

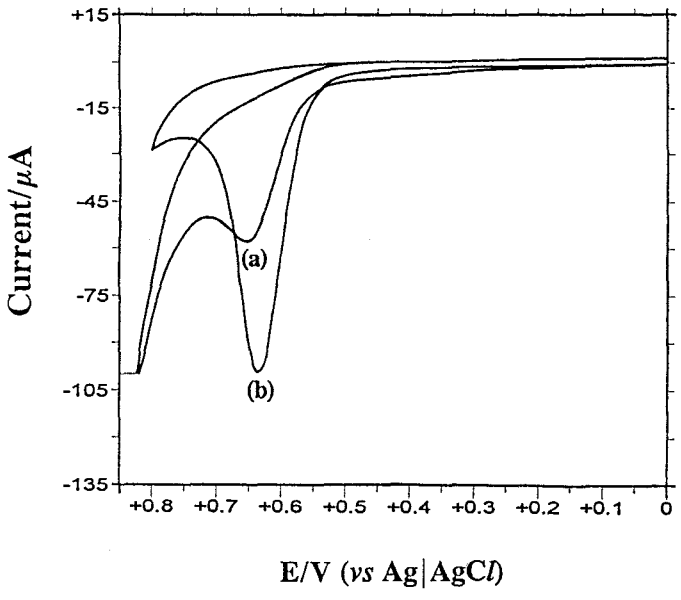

FIGURE 37: *Cyclic voltammograms of 0.1 mol dm^{-3} pentachlorophenol (PCP) on (a) CoPc-CMGCE and, (b) on uncoated GCE. Electrolyte = 0.05 mol dm^{-3} H_2SO_4. Scan rate = 100 mV s^{-1} (vs Ag|AgCl).*

Lower currents were also observed on $[Co^{(II)}TSPc]^{4-}$ electrochemically deposited on GCE, as compared to uncoated GCE. However, for the sake of determining the electrochemical behaviour of TCP and PCP on $Co^{(II)}Pc$ coated GCE for ease of relating with the results of monosubstituted phenolic compounds, the data obtained on the use of $Co^{(II)}Pc$ towards oxidation of TCP and PCP is presented. In solution, metallophthalocyanines with electroactive metal centres binds to water or hydroxide, depending on the pH of the media [4]. Therefore, during the cyclic voltammetry of trichlorophenol and pentachlorophenol, in 0.05 mol dm^{-3} sulphuric acid and 1.0 mol dm^{-3} sodium hydroxide, on CoPc-CMGCE, the hydroxide presumably binds strongly to the axial catalytic sites in $Co^{(II)}Pc$, thus reducing the catalytic activity of the CoPc-CMGCE. Hence why currents obtained from CoPc-CMGCE were lower than those from the uncoated GCE.

The anodic peak currents, for the first scan, of the catalysed redox reaction were found to depend on the concentration of PCP and TCP, with linearity prevailing over the low concentration range ($< 10^{-2}$ mol dm^{-3}), **Fig. 38**. In general, the anodic currents for the determination of TCP were higher than those for the determination of PCP at all concentrations. This can be attributed to more electron withdrawing substituents on the latter than the former, **Fig. 38**.

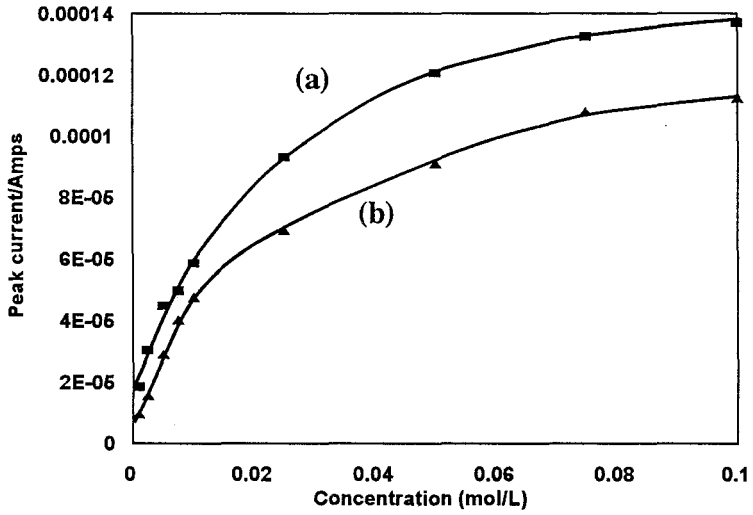

FIGURE 38 *Variation of anodic peak currents with varying concentrations of:* ***(a)*** *2,4,6-trichlorophenol and,* ***(b)*** *pentachlorophenol, in 0.05 mol dm^{-3} H_2SO_4 and 1.0 mol dm^{-3} NaOH (scan rate = 100 mV s^{-1}) - on CoPc coated GCE.*

The magnitude of anodic peak currents also increased linearly with square root of scan rate, for scan rates as high as 1000 mV s^{-1}, suggesting diffusion controlled process **(Fig. 39)**. The anodic peak currents for the electrooxidation of TCP were still found to be higher than those obtained from the oxidation of PCP, at all scan rates. This is due to high inductive effect caused by more electron-withdrawing substituents on the phenyl in PCP.

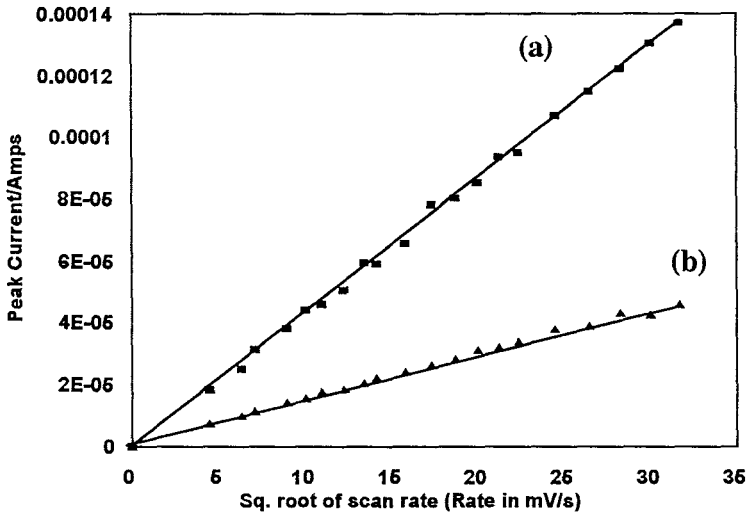

FIGURE 39: *Variation of anodic peak currents against square root of scan rate towards detection of 0.001 mol dm^{-3} of; (a) trichlorophenol and, (b) pentachlorophenol (in 0.05 mol dm^{-3} H_2SO_4 and 1.0 mol dm^{-3} NaOH), on CoPc coated GCE.*

In principle, the presence of an electronegative non-leaving substituent on the ortho and para positions of trichlorophenol and pentachlorophenol are expected to inhibit the formation of dimeric and polymeric oxidation products responsible for electrode fouling. This was then expected to enhance the stability of CoPc-CMGCE towards determination of these compounds. However, this was not the case because at 10^{-3} mol dm^3, which is the lowest detectable concentration of PCP and TCP, the electrode fouling was found to be more persistent than exhibited by other phenolics, at the same concentration. This therefore indicates that the size of the analyte molecule also determines its rate of movement towards or away from the electrode, which in turn determines the magnitude of the current density obtained [80]. Electrode fouling also depends on the size of the analyte molecule and not only on the adsorption of the oxidation products. This means that the larger TCP and PCP molecules

occupy more of the available space on the electrode, thus deactivating the electrode more faster than phenol, mono-chlorinated phenols and cresols.

5.3 *Electroanalysis of all phenolic compounds using $[Co^{(II)}TSPc]^{4-}$*

5.3.1 Catalytic activity of $[Co^{(II)}TSPc]^{4-}$ species in solution

Solution-phase catalysis in the presence of water soluble $[Co^{(II)}TSPc]^{4-}$ complex in solution was made in 0.05 mol dm^{-3} sulphuric acid on an unmodified GCE.

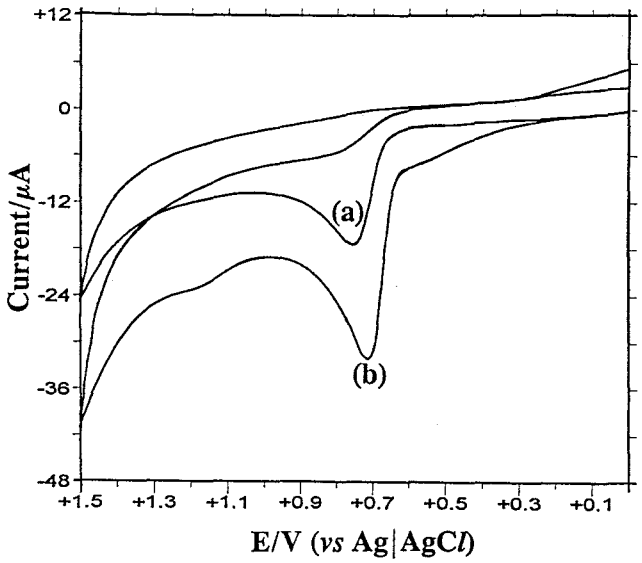

FIGURE 40: *Cyclic voltammograms of 0.001 mol dm^{-3} p-cresol in (a) absence and, (b) in the presence of $[CoTSPc]^{4-}$ in solution on uncoated GCE (scan rate = 100 mV s^{-1}, electrolyte = 0.05 mol dm^{-3} H_2SO_4).*

Fig. 40 shows cyclic voltammograms for the detection of p-cresol in the absence, and when $[Co^{(II)}TSPc]^{4-}$ is added to the solution. A considerable increase in current was observed in the presence of $[Co^{(II)}TSPc]^{4-}$, thus confirming that the this species catalyses the oxidation of p-

cresol (**Fig. 40(b)**), and all other phenolic compounds under consideration. $[Co^{(II)}TSPc]^{4-}$ readily adsorbs onto the electrode [2], therefore, it is possible that the adsorbed species are responsible for catalysis in this respect. The lowest concentration of the phenolic compounds detected by a CoPc-CMGCE was of the order of 10^{-6} mol dm^{-3}, whereas for solution-phase catalysis in the presence of $[Co^{(II)}TSPc]^{4-}$ the lowest concentration detected was of the order of 10^{-3} mol dm^{-3}. It is important to note that for aqueous solution in the presence of $[Co^{(II)}TSPc]^{4-}$, the currents for the oxidation of the phenolic compounds decreased rapidly after the first scan. And in contrast to the observation on CoPc-CMGCE, a decrease, rather than an increase, in peak potentials for the oxidation of the phenolic compounds was observed on a GCE in the presence of $[Co^{(II)}TSPc]^{4-}$ in solution. The plot of i_p against $v^{½}$ was found to be linear for solution-phase catalysis, indicating a diffusion controlled process.

The current and potential dependence on the concentration of $[Co^{(II)}TSPc]^{4-}$ in solution was investigated by varying the concentration of $[Co^{(II)}TSPc]^{4-}$ in solution and keeping the concentration of the phenolic compounds (under consideration) and the electrolyte constant, on uncoated GCE in 0.05 mol dm^{-3} sulphuric acid. The magnitude of the anodic peak current was found to depend directly on the concentration of $[Co^{(II)}TSPc]^{4-}$ in solution, **Fig. 41**.

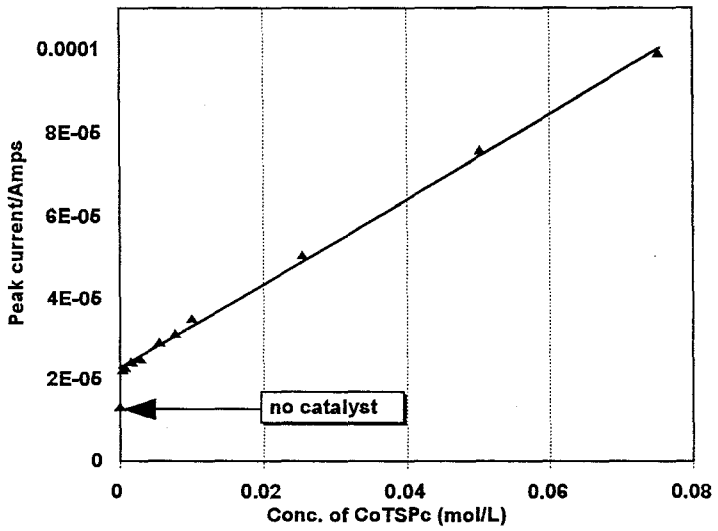

FIGURE 41: *Plot showing the relationship between anodic peak currents and the concentration of the catalyst towards detection 0.001 mol dm^{-3} 4-chlorophenol in 0.05 mol dm^{-3} H_2SO_4, using uncoated GCE (scan rate = 100 mV s^{-1}).*

An indirect relationship between the oxidation peak potential and the concentration of $[Co^{(II)}TSPc]^{4-}$ was observed. That is, as the current increased with an increasing concentration of $[Co^{(II)}TSPc]^{4-}$, the oxidation potential decreased further, compared to the potential obtained from uncatalysed process. For example, the presence of 10^{-3} mol dm^{-3} of $[Co^{(II)}TSPc]^{4-}$ in solution containing 0.001 mol dm^{-3} 4-chlorophenol in 0.05 mol dm^{-3} sulphuric acid reduced the potential for the oxidation of 4-chlorophenol by 0.10 V (*vs* Ag|AgC*l*), at 100 mV s^{-1}. Generally, similar trends were observed for other phenolic compounds. The decrease of oxidation potential with increasing catalyst concentration was observed for up to about 0.1 mol dm^{-3} of $[Co^{(II)}TSPc]^{4-}$. At concentrations exceeding 0.1 mol dm^{-3}, the oxidation peak potential started increasing, with voltammetric peaks becoming broader. In addition to the anodic oxidation peak, in detection of 4-chlorophenol, extra anodic and cathodic waves, associated

with the redox activity of $[Co^{(II)}TSPc]^{4-}$ in solution were observed at concentrations above 0.1 mol dm^{-3} of $[Co^{(II)}TSPc]^{4-}$.

5.3.2 Electroanalysis using $[CoTSPc]^{4-}$ chemically modified GCE

Electrochemical deposition process

According to Martin and Foss [11], chemisorption is an adsorptive interaction between an adsorbate and the electrode surface in which electron density is shared by the adsorbed molecule and the electrode surface. In the case of MPc complexes, the π-electron density is shared between the electrode and the adsorbate molecule. It is therefore apparent that chemisorption requires direct contact between the chemisorbed molecule and the electrode surface. It is believed that the highest achievable coverage is usually a monolayer, and the deposition reaction is rarely irreversible [11]. The mode of attachment of phthalocyanine complexes to the electrode surface during electrodeposition is still a mystery, but films adhere strongly to the electrode surface, provided that the solvent from which the complexes are deposited is not a good solvent for that particular complex [80].

Fig. 42 shows cyclic voltammograms of repetitive scanning of $[Co^{(II)}TSPc]^{4-}$ in the range 0 to 1.3 V in 0.05 mol dm^{-3} sulphuric acid. Three anodic oxidation waves were observed, with the gradual increase in peak current and a shift to higher potentials of the wave around 0.54 V, and a slight increase of a reversible wave at $E_{½}$ = 0.68 V and, a decrease of the wave at 1.10 V (*vs* Ag|AgC*l*) upon successive scans. The wave at $E_{½}$ = 0.68 V has been assigned to the central metal oxidation, whereby $[Co^{(II)}TSPc(2-)]^{4-}$ is oxidised to $[Co^{(III)}TSPc(2-)]^{3-}$ and the wave at 1.10 V is due to the oxidation of the phthalocyanine ring from $[Co^{(III)}TSPc(2-)]^{3-}$ to $[Co^{(III)}TSPc(1-)]^{2-}$. The wave at 0.54 V has been attributed to the splitting

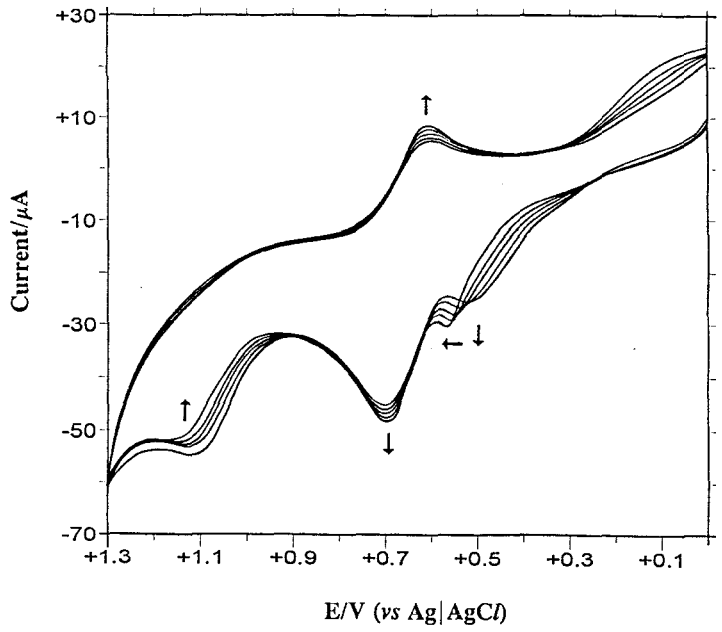

FIGURE 42: *Cyclic voltammograms of repetitive scans during electrodeposition of 0.001 mol dm^{-3} [CoTSPc]$^{4-}$ onto GCE. Scan rate = 100 mV s^{-1}, electrolyte = 0.05 mol dm^{-3} H_2SO_4).*

due to stabilisation of the mixed valence species [23] as discussed earlier. The currents of these three oxidation waves were found to depend on the concentration of $[Co^{(II)}TSPc]^{4-}$ and scan rate, indicating that the rate of electrodeposition of $[Co^{(II)}TSPc]^{4-}$ is diffusion controlled. The gradual increase of metal oxidation wave at $\mathbf{E}_{½}$ = 0.68 V indicates the formation of a conductive phthalocyanine film by electrodeposition on the electrode surface forming $[Co^{(II)}TSPc]^{4-}$ chemically modified GCE. Repetitive scanning from 0.0 to 0.90 V did not encourage film formation. It is only the cycling to potentials exceeding ring oxidation potential which induced film formation [48,62,80]. Repetitive cyclic voltammograms of $[Co^{(II)}TSPc]^{4-}$ was made until there was no apparent change in the peak heights, after about the 25th scan. Upon removing the electrode from $[Co^{(II)}TSPc]^{4-}$ solution, a purple film was

observed on the electrode surface. The surface coverage after the 25th scan, calculated from the charge under the anodic curve using equation 7 ($\mathbf{Q = nFA\Gamma}$), was found to be, $\Gamma \approx 1.37 \times 10^{-9}$ mol cm^{-2}.

During electrodeposition of dimethyl ester of metalloprotoporphyrin, $(Fe^{(III)}PP)_2O$ in organic solvents, Macor and Spiro [80] observed an increase and a decrease of the ring and metal oxidation waves, respectively. In contrast, in this work, voltammograms for the electrodeposition of $[Co^{(II)}TSPc]^{4-}$ showed a gradual increase of the metal oxidation wave at $\mathbf{E}_{½} = 0.68$ V and a decrease of the peak due to ring oxidation at 1.10 V, **Fig. 42**. Assuming that the $[Co^{(II)}TSPc]^{4-}$ molecule lies flat on the electrode surface, the increase of the first wave (due to the metal oxidation) upon successive scan indicates direct involvement of the central metal during electrochemical deposition process. Therefore, this suggests that the film growth is probably via interaction of the oxidized species, already deposited, with the $[Co^{(II)}TSPc]^{4-}$ molecules in solution. However, the data does not provide information on whether the monomeric or dimeric species are deposited.

The oxidation couple at $\mathbf{E}_{½} = 0.68$ V continued to be observed even after the removal of the electrode from the $[Co^{(II)}TSPc]^{4-}$ solution, rinsing the surface, and immersing it into a blank electrolyte solution (0.05 mol dm^{-3} sulphuric acid). This suggests that the redox process, noted above, is due to the adsorbed $[Co^{(II)}TSPc]^{4-}$.

Electroanalysis using CoTSPc-CMGCE

Generally, reactions catalysed by $[Co^{(II)}TSPc]^{4-}$ electrochemically deposited on GCE exhibited anodic currents higher than those obtained from solution-phase catalysis using $[Co^{(II)}TSPc]^{4-}$ on uncoated GCE for the determination of cresols, phenol, 2-chlorophenol and 4-chlorophenol

in acidic media. **Fig. 43** shows the cyclic voltammograms of 2-chlorophenol on uncoated and on $[Co^{(II)}TSPc]^{4-}$ electrochemically deposited on GCE. CoTSPc-CMGCE enhanced the anodic current and the oxidation potential shifted from 1.04 V to 0.91 V (*vs* Ag|AgC*l*), for electrooxidation of 2-chlorophenol, **Fig. 43.**

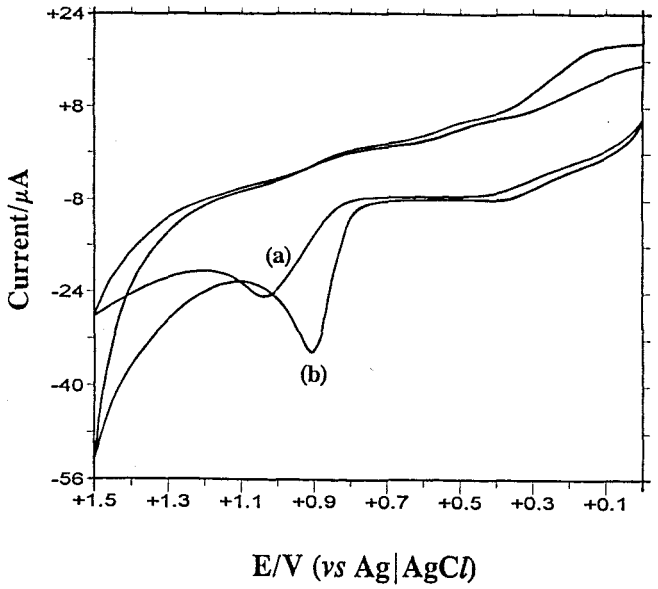

FIGURE 43: *Cyclic voltammograms of 0.001 mol dm^{-1} 2-chlorophenol on (a) uncoated GCE and, (b) on CoTSPc-CMGCE, in 0.05 mol dm^{-3} H_2SO_4. Scan rate = 100 mV s^{-1} (vs Ag|AgCl).*

According to Countanceau *et al* [81], electrocatalytic processes involving phthalocyanines complexes are very difficult to study in alkaline media because of the weak conductivity or non-conductivity of the phthalocyanine film in such conditions. Electroanalysis of phenolic compounds at higher pH values was also undertaken in pH 7 phosphate buffer. The uncoated GCE was found to exhibit higher anodic currents than CoPc coated GCE. Apart from weak conductivity of phthalocyanines in alkaline media, phosphate is known to form complexes with

transition metals [82]. It is therefore likely that phosphate competes for active sites with phenolic compounds during electrocatalysis.

Generally, a linear relationship between the current and the square root of the scan rate for determination of phenolic compounds on CoTSPc-CMGCE was observed, indicating that the oxidation of phenolic compounds on $[CoTSPc]^{4-}$-CMGCE is diffusion controlled. An increase of oxidation potential with increasing scan rate was also observed, which is typical of totally irreversible redox reactions [3].

5.3.3 Absorption spectral studies

Interaction of phenolic compounds and sodium hydroxide with $[Co^{(II)}TSPc]^{4-}$

To investigate the interaction of phenolic compounds with the water soluble $[Co^{(II)}TSPc]^{4-}$, UV-visible absorption spectroscopy was employed. It is well established that metal(II) tetrasulfonated phthalocyanine complexes form aggregates in solution [22,25,63]. The electronic spectra of these species have been explained in terms of monomer/dimer equilibria. The lower energy absorption near 670 nm has been attributed to the monomeric species while the higher energy peak near 620 nm is due to the dimeric species [22,24,63], as discussed in the introduction.

Fig. 44 shows the electronic absorption spectra of $[Co^{(II)}TSPc]^{4-}$ in 0.05 mol dm^{-3} sulphuric acid, before and after addition of 4-chlorophenol. The same spectral change were observed for the addition of any of the phenolic compounds to the solution of $[Co^{(II)}TSPc]^{4-}$ in 0.05 mol dm^{-3} sulphuric acid. The spectra before the addition of the phenolic compounds (**Fig. 44(a)**) shows the absorption band due to dimeric species at 624 nm and a weak band due to monomeric species at 666 nm. Addition of any of the phenolic compounds to the solution of

$[Co^{(II)}TSPc]^{4-}$ resulted in the decrease in the peak due to the dimeric species and a gradual increase with time in the intensity of the monomeric peak. An increase in the absorption due to monomeric species was observed before [25] when oxygen was bubbled through alkaline solutions of $[Co^{(II)}TSPc]^{4-}$ and this was attributed to the formation of an adduct between oxygen and $[Co^{(II)}TSPc]^{4-}$ [25]. The test on the effect of residual oxygen was performed by monitoring

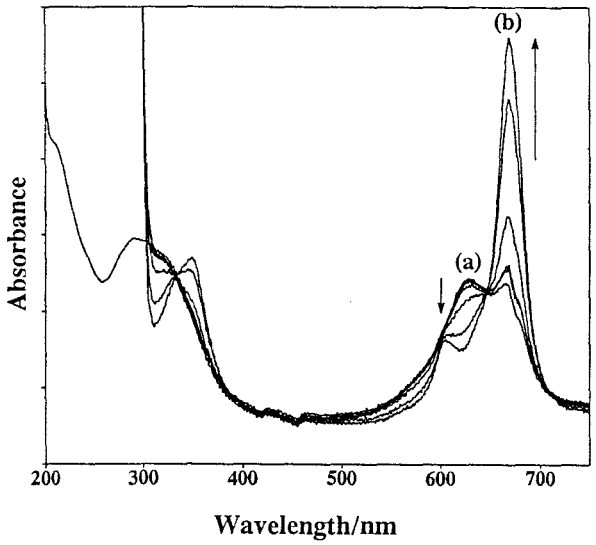

FIGURE 44: *Absorption spectral changes observed upon addition of 4-chlorophenol to the solution of [CoTSPc]$^{4-}$ in 0.05 mol dm^{-3} H_2SO_4. Spectra of (a) [CoTSPc]$^{4-}$ only and, (b) after addition of 4-chlorophenol, spectra monitored with time for up to 90 hours.*

the spectra of unpurged solution of $[Co^{(II)}TSPc]^{4-}$ in acidic solution in the absence of phenolic compounds. No changes in spectra were observed. Thus, the spectral changes shown in **Fig. 44** are due to the interaction between 4-chlorophenol and $[Co^{(II)}TSPc]^{4-}$ and not to the effects of oxygen. In comparison with the interaction between $[Co^{(II)}TSPc]^{4-}$ and oxygen in basic media discussed before [25], the spectral changes shown in **Fig. 44** are therefore associated with the formation of an adduct between 4-chlorophenol and the $[Co^{II}TSPc]^{4-}$ species. The

spectral changes give evidence for the presence of $[Co^{(II)}TSPc]^{4-}$ rather than $[Co^{(III)}TSPc]^{3-}$. The formation of the latter would be accompanied by a shift in the Q band of the monomeric species to lower wavelengths [77]. Upon addition of 4-chlorophenol to $[CoTSPc]^{4-}$ solution in water only, a gradual increase in the intensity of the monomeric peak was observed. Similar increase of the monomeric peak was also observed upon addition of 4-chlorophenol to $[CoTSPc]^{4-}$ in 0.05 mol dm^{-3} H_2SO_4, as discussed above. However, in water only, a slight shift of the Q band to higher wavelengths was noted, **Fig. 45.**

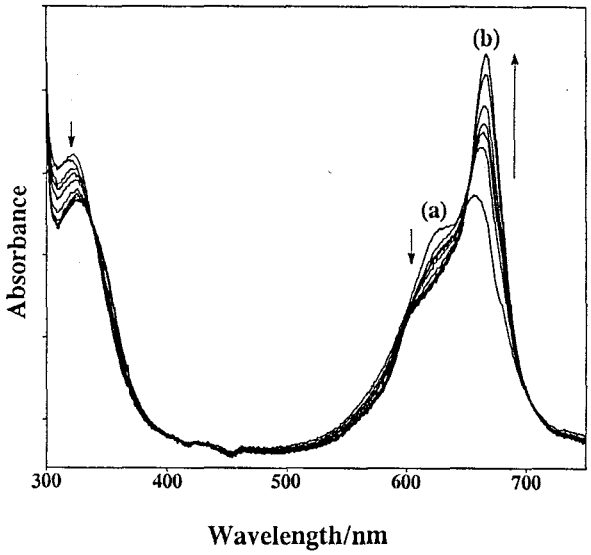

FIGURE 45: *Absorption spectral changes observed when 4-chlorophenol was added to the solution of [CoTSPc]$^{4-}$ in water only (compare with* ***Fig. 44****), Changes were monitored with time for up to 90 hours also.*

As mentioned earlier, electrocatalytic processes involving phthalocyanines complexes are very difficult to study in alkaline media because of the weak conductivity or non-conductivity of the phthalocyanine film in such conditions [81]. For instance, the presence of sodium hydroxide was found to inhibit catalytic activity of cobalt phthalocyanine complexes towards

electrooxidation of trichlorophenol and pentachlorophenol (section 5.2). Therefore, to investigate the possible interaction between sodium hydroxide and $[Co^{(II)}TSPc]^{4-}$, absorption spectra of $[Co^{(II)}TSPc]^{4-}$ with and without sodium hydroxide was taken (**Fig. 46**). Addition of sodium hydroxide to the solution of $[Co^{(II)}TSPc]^{4-}$ resulted in an increase of absorption due to monomeric species, the increase was found to depend on the concentration of sodium hydroxide as shown in **Fig. 46**. Gruen and Blagrove [25] attributes this behaviour to the

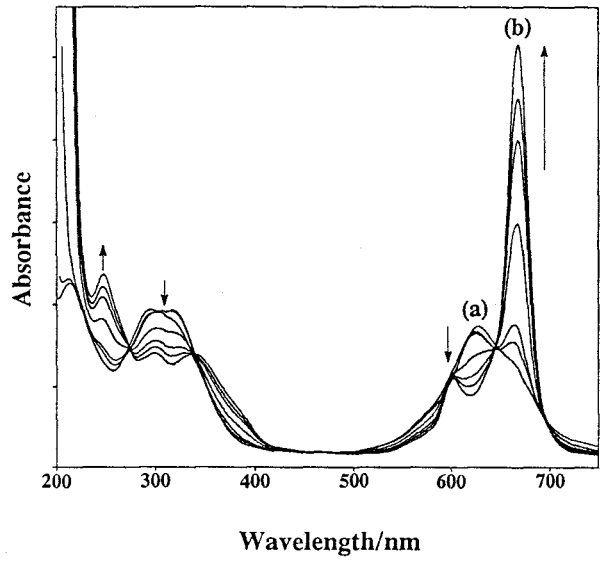

FIGURE 46: *Absorption spectral changes observed upon varying the concentration of NaOH added to the solution of [CoTSPc]$^{4-}$ in 0.05 mol dm^{-3} H_2SO_4. Where (a) is the spectra without and, (b) with NaOH (0.1, 0.2, 0.4, 0.6, 0.8 and 1.0 mol dm^{-3} concentrations) added.*

reversible formation of an oxygen adduct of $[Co^{(II)}TSPc]^{4-}$ in alkaline solution. It is alleged that deoxygenation can be achieved by bubbling the solution with nitrogen. However, bubbling the solution with nitrogen continuously for more than 24 hours resulted in an insignificant reduction in the intensity of the monomeric absorption band. This indicates that $[Co^{(II)}TSPc]^{4-}$ in solution exists with water or hydroxide as the axial ligands, depending on the

pH of the solution [4]. Therefore, the changes observed when sodium hydroxide is added to $[Co^{(II)}TSPc]^{4-}$ are tentatively attributed to the formation of an adduct between hydroxide and $[Co^{(II)}TSPc]^{4-}$, with hydroxide ion coordinating very strongly to the axial catalytic sites. This therefore accounts for the weak conductivity of cobalt phthalocyanine complexes in alkaline media.

5.4 Overall discussion on all phenolic compounds

Redox couples obtained from the phthalocyanine complexes adsorbed, electrodeposited onto the glassy carbon electrode or incorporated into the conductive matrix, as in CoPc-CMGCE, CoTSPc-CMGCE and CoPc-CMCPE, respectively, were found to be less reversible than when $[Co^{(II)}TSPc]^{4-}$ was used in solution-phase catalysis. This is claimed to be a factor which tends to reduce the catalytic efficiency (in terms of enhancing redox currents at similar concentrations) of adsorbed complexes. Similar observations have been made by Andrieux and Saveant [7].

Cobalt tetrasulfonated phthalocyanine was employed in determining catalytic efficiency of homogeneous and heterogeneous catalysis by using $[Co^{(II)}TSPc]^{4-}$ in solution and electrochemically deposition on GCE as already discussed. **Table 8** compares the catalytic efficiency of solution-phase and electrodeposited $[Co^{(II)}TSPc]^{4-}$ towards detection of different phenolic compounds. As **Table 8** shows, higher catalytic efficiencies were observed for solution-phase catalysis, except for phenol, trichlorophenol and pentachlorophenol. This deviation could not be explained.

TABLE 8: *Catalytic efficiency of $[CoTSPc]^{4-}$ in detection of different phenolic compounds. Where catalytic efficiency (CE) = ratio of current from catalysed reaction to that of uncatalysed process.*

Phenolic compounds	CATALYTIC EFFICIENCY	
	Solution-phase	Electrodeposited
2-CHLOROPHENOL	1.68	1.22
4-CHLOROPHENOL	1.49	1.27
PHENOL	1.70	1.70
O-CRESOL	1.49	1.28
M-CRESOL	1.87	1.48
P-CRESOL	1.77	1.43
TRICHLOROPHENOL	0.60	0.68
PENTACHLOROPHENOL	0.52	0.59

Catalysis by metal phthalocyanines occurs through indirect electrochemical oxidation of the substrate (cysteine and phenolic compounds) which involves the initial oxidation of the phthalocyanine complexes and the subsequent reaction of the oxidised MPc species with cysteine or phenolic compounds. This approach facilitate oxidation of cysteine and phenolic compounds at potentials closer to the thermodynamic values. The phthalocyanine complexes are thus termed redox-activated catalysts [83].

An attempt to use CoPc chemically modified carbon paste electrode (CoPc-CMCPE) for the detection of phenolic compounds was made. Even though the CoPc-CMCPE was found to posses some catalytic activity for the reaction, the catalytic effect was not as pronounced as

that observed for the oxidation of cysteine on the same electrode. CoPc-CMCPE showed higher activity towards the oxidation of cysteine, suggesting that CoPc-CMCPE reversibly binds both the reactants and the products of cysteine. Whereas, the rapid loss of activity of CoPc-CMCPE, towards the oxidation of phenolic compounds, is attributed to the formation of a stable adduct between CoPc (in carbon paste) and the phenolic compound molecules which then blocks the CoPc active sites, preventing new molecules from interacting and reacting.

For electroanalysis using $[Co^{(II)}TSPc]^{4-}$ as a catalyst, comparison of potentials obtained for the catalytic oxidation of the phenolic compounds on CoTSPc-CMGCE and those obtained for solution catalysis employing the same catalyst, reflected higher oxidation potential for the surface bound $[Co^{(II)}TSPc]^{4-}$ relative to the potentials of this species in solution. Catalysts that result in a larger lowering of the potentials for the oxidation of phenolic compounds are essential since they make the electrochemical determination of these species more feasible.

CHAPTER SIX: CONTROLLED POTENTIAL COULOMETRY

6.1 General background

6.2 Analysis of products of electrolysis of chlorinated phenols

CHAPTER SIX: CONTROLLED POTENTIAL COULOMETRY

6.1 General background

Electrolysis at controlled potential is an experimental technique which is widely used in the study and elucidation of electrode reaction mechanisms. Controlled potential coulometry is usually performed in a stirred solution with the electrode maintained at a constant potential, such that the single electrode reaction occurs. The potential of the electrode is chosen so that the rate of the reaction given as $\mathbf{C} \pm \mathbf{ne}^- \rightarrow \mathbf{R}$ is controlled by the rate of mass transfer of **C** from the bulk of the solution to the electrode. Under these conditions, the rate of the reverse reaction is considered negligible [84].

6.2 Analysis of products of electrolysis of chlorinated phenols

As a way of investigating possible ring cleavage or dechlorination of phenolic compounds during electrooxidation, chlorinated phenolic compounds were exhaustively electrolysed under the conditions outlined in the experimental section. Initially, the phenolic compounds gave colourless solutions in acetonitrile. However, after electrolysis, 2-chlorophenol produced a yellowish-brown product, a white crystalline product was obtained from electrolysis of pentachlorophenol and 4-chlorophenol and trichlorophenol gave a brown, oily product. The physical appearance of these products was different from that of the starting compounds, suggesting that some form of reaction has taken place during electrolysis process. The current was also found to decrease exponentially with time as electrolysis proceeds. The final products obtained were then subjected to NMR and IR spectral analysis.

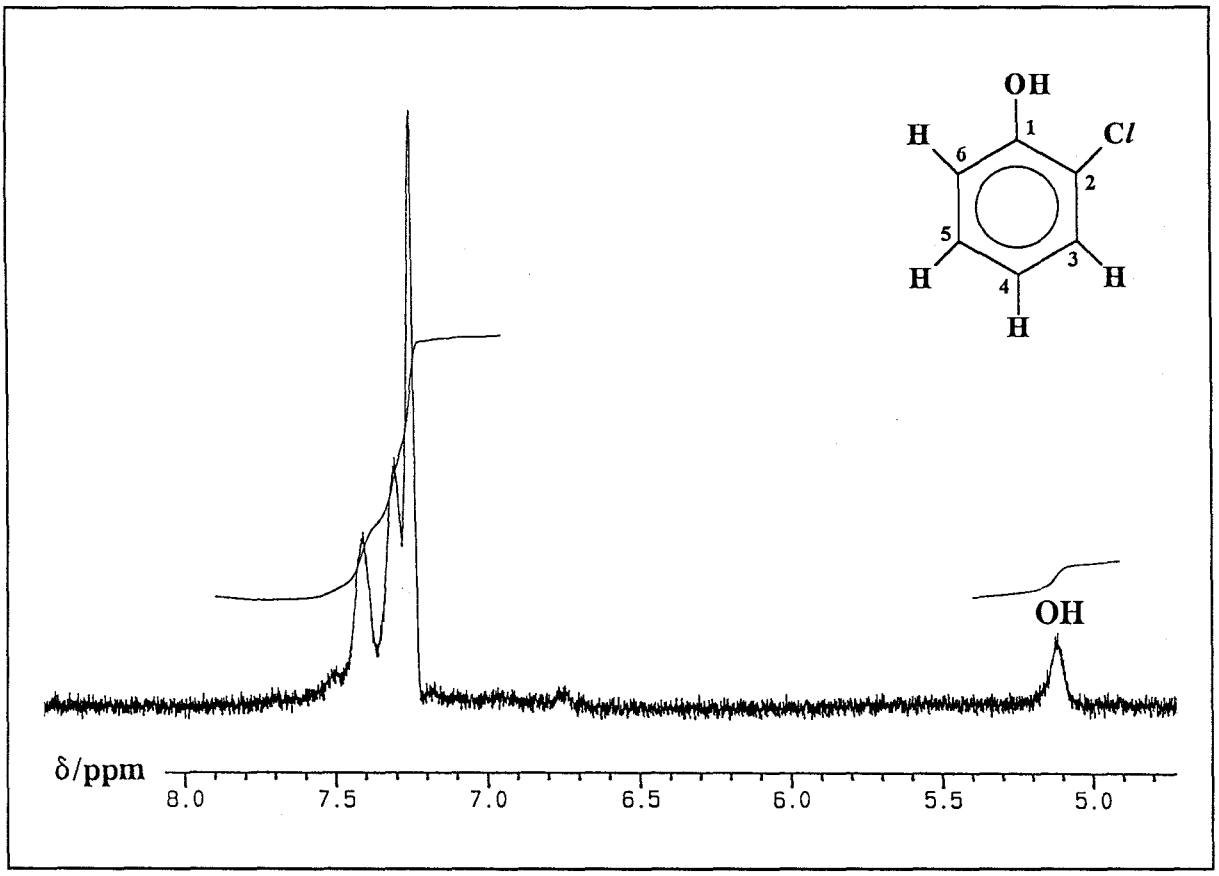

FIGURE 47: *^1H NMR (400 MHz, $CDCl_3$) spectrum of the oxidation product(s) of 2-chlorophenol.*

For 2-chlorophenol, **Fig. 47** shows the **^1H** NMR spectrum of the product(s) in chloroform ($CDCl_3$). The spectrum revealed the proton chemical shifts at δ 5.11 and 7.29 ppm. The resonance at δ 5.11 ppm arises from the proton on the hydroxyl functional group on the benzene ring, whereas the chemical shift centred at δ 7.29 ppm exhibited a multiplet arising from spin-spin splitting of protons on positions 3, 4, 5 and 6 of the benzene ring **(Fig. 47)**. This splitting behaviour is typical of the ortho-substituted phenols [85].

^1H NMR analysis of the oxidation products of 4-chlorophenol revealed resonance at δ 5.11 ppm due to the resonance of the proton on the hydroxyl functional group of the phenyl. Two

additional singlet resonance signals were observed in the aromatic region of the spectrum **(Fig. 48(a))**. The resonance signal at δ 7.18 ppm is from the chemically equivalent H-3 and H-5 phenyl protons, whereas the resonance observed upfield (δ 6.76 ppm) is from H-2 and H-6 phenyl protons, which are also chemically equivalent. The ^{13}C NMR spectrum **Fig. 48(b))** revealed resonance signals at δ 154.00 and 125.75 ppm arising from the resonance signals of C-4 and C-1 carbons respectively. The C-4 carbon resonance signal occurs further downfield than C-1 carbon signal because of deshielding by chlorine which is more electronegative than oxygen. Two additional resonance signals due to the chemically equivalent carbons were observed at δ 129.53 ppm (for C-3 and C-5) and at δ 116.67 ppm (due to C-2 and C-6) **(Fig. 48(b))**. Further upfield (aliphatic region), there were no carbon or proton resonance signals observed. The IR data provided further evidence of the presence of hydroxyl (ν_{max} 3340 cm^{-1}) functional group, the aromatic C-H (ν 2928 cm^{-1}) and C-C aromatic skeletal (ν 1591 cm^{1}) vibrations, thus indicating the presence of a benzene ring.

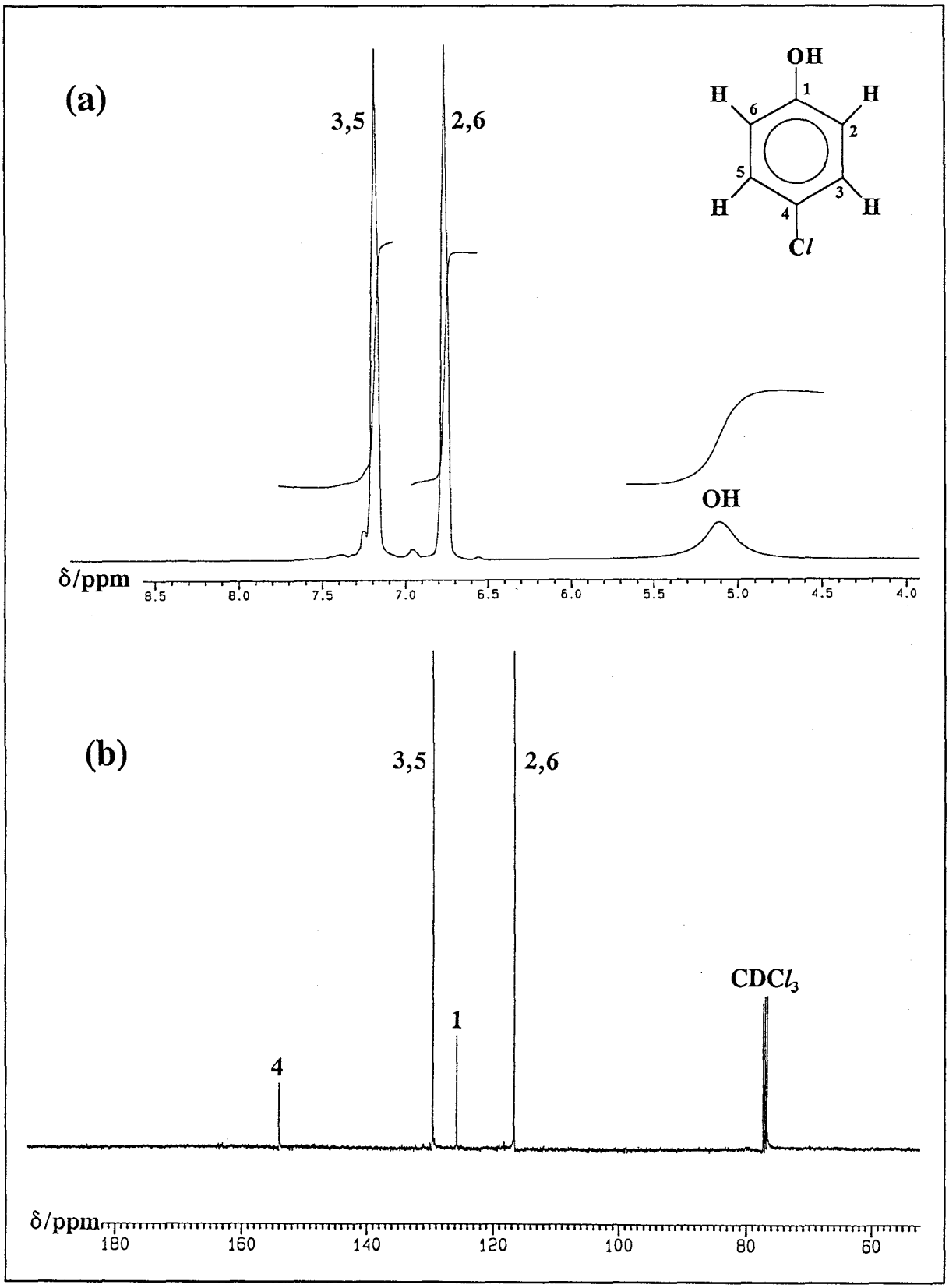

FIGURE 48: *(a) ^{1}H and, (b) ^{13}C, (400 MHz, $CDCl_3$) spectra of the oxidation products of 4-chlorophenol.*

The ^{1}**H** NMR spectrum of the oxidation products of 2,4,6-trichlorophenol **(Fig. 49)** exhibited the O-H proton resonance signal at δ 5.72 ppm and two additional intense signals in the aromatic region of the spectrum, at δ 7.52 and 7.25 ppm. The resonance at δ 7.52 ppm arises from the resonance of the chemically equivalent H-3 and H-5 aromatic protons, whereas the δ 7.25 ppm was undefined, but is most likely to be the solvent ($CDCl_3$) signal, because the concentration of trichlorophenol used in NMR analysis was very low. The additional and less intense signals within the same region of the spectrum were undefined; however it is believed that they may be caused by impurities. The nature of the product was also confirmed by IR absorption bands at 3517 cm^{-1} due to ν(O-H). The ν(ArC-H) at 1655 and 1591 cm^{-1} and the ν(ArC-C) also proved that the benzene ring is still intact.

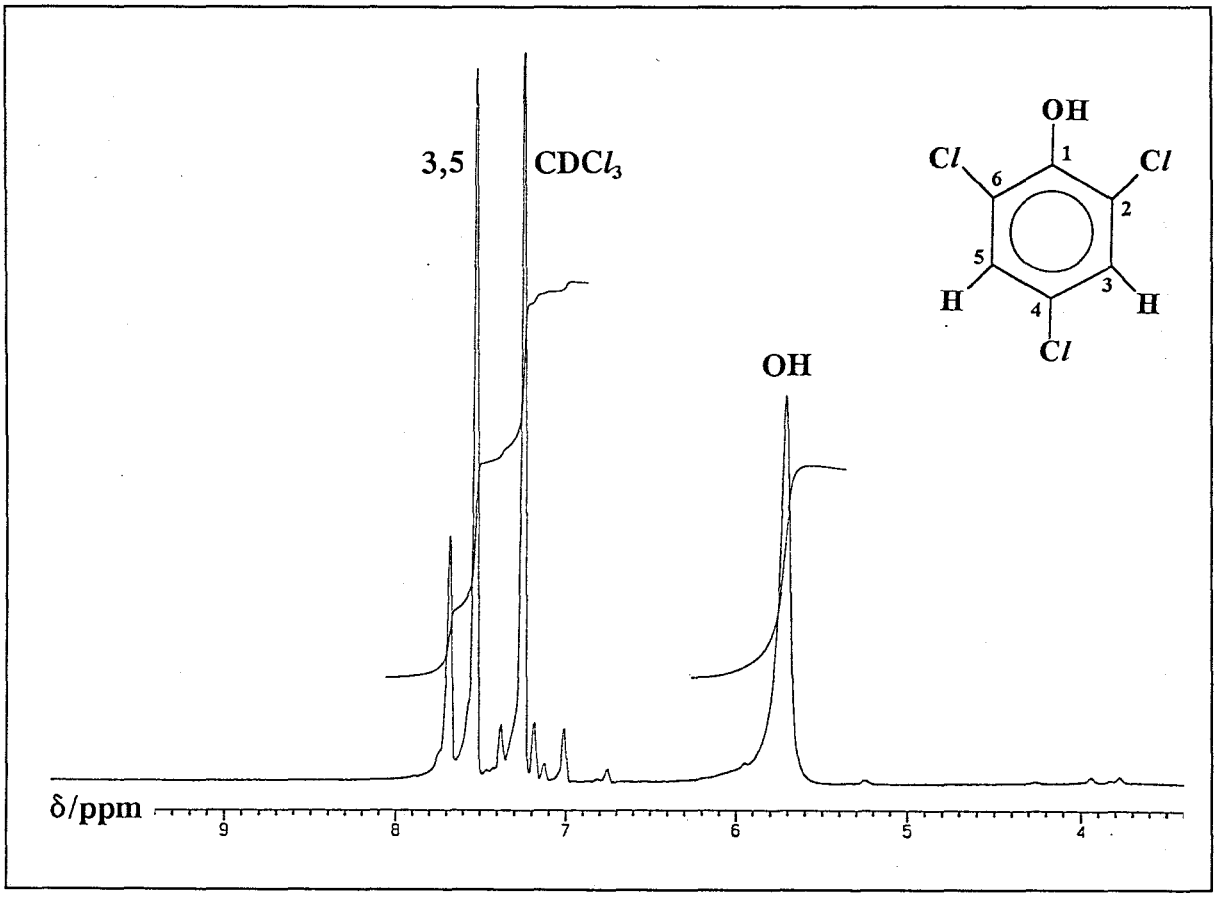

FIGURE 49: *^{1}H NMR (400 MHz, $CDCl_3$) spectrum of the oxidation product(s) of 2,4,6-trichlorophenol.*

The ^{1}H NMR spectrum of the oxidation products of pentachlorophenol revealed the chemical shift due the proton resonance signal from the OH functional group only, and no resonance signals in the aromatic region, indicating that all the five benzene carbons are still occupied by the chlorine molecules and the sixth position by the functional OH group, hence one proton resonance signal. The ^{13}C NMR spectrum shown in **Fig. 50** revealed the aromatic C-4 and C-1 carbon resonance signals at δ 148.14 and 125.09 ppm respectively. Two additional aromatic resonance signals from the four carbons were observed at δ 131.50 and 119.73 ppm. The chemical shift at δ 131.50 ppm is due to resonance of the chemically equivalent C-2 and C-6, and the δ 119.73 ppm arises from the resonance of C-3 and C-5 phenyl carbons. The occupation of five phenyl positions by chlorine molecules was confirmed by the absence of aromatic ν(C-H) in the IR spectrum of the oxidation products of pentachlorophenol.

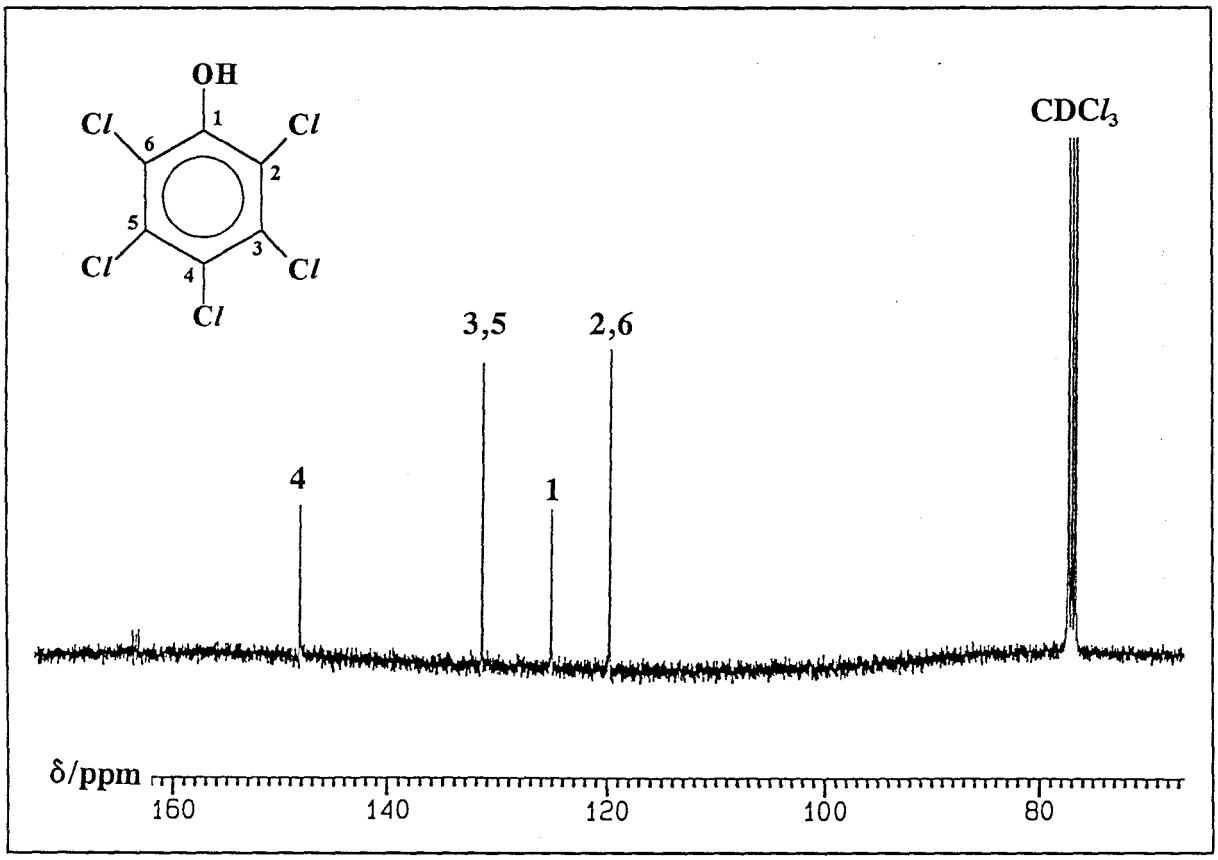

FIGURE 50: *^{13}C NMR (400 MHz, $CDCl_3$) spectrum of the oxidation products of pentachlorophenol.*

The NMR spectra shown in **Fig. 47**, **48**, **49** and **50** for the oxidation products of 2-chlorophenol, 4-chlorophenol, trichlorophenol and pentachlorophenol, respectively, were similar to the NMR spectra of the species before oxidation [85]. However, cyclic voltammetry for chlorophenols, phenol and o-cresol showed peaks which were assigned to the formation of polymeric products. The ^{1}H and ^{13}C NMR spectral analysis, and IR data also demonstrates the presence of a six carbon membered ring. Indicating that even after exhaustive electrolysis, the phenyl group remained intact. This also proves that dechlorination does not occur during electrooxidation of chlorinated phenols. As already stated, during electrooxidation, phenolic compounds loose a proton and an electron, forming phenoxy radicals as intermediate products. However, the presence of chemical shift δ 5.11 ppm (on ^{1}H NMR spectra) and the IR stretching vibrations around ν3500 cm^{-1} indicates the presence of OH, which is probably a terminal OH of polymeric or dimeric products, suggesting that the radical has gained back a proton, possibly as a result of intramolecular rearrangements of dimeric or polymeric oxidation products. However, these results are inconclusive as to the actual nature of the products formed. This therefore calls for further investigation into the possible formation of polymeric oxidation products, of 2-chlorophenol and 4-chlorophenol in particular, because trichlorophenol and pentachlorophenol are not expected to form dimers or polymers because of steric effect. The use of elemental analysis and mass spectrometry might prove useful in investigating the possible formation of polymeric or dimeric products. This is because NMR is only able to identify a single basic unit of a polymer and not a polymeric chain made of a replicate organic units.

CHAPTER SEVEN: CONCLUSION

7.1 General conclusion

7.2 Future work

CHAPTER SEVEN: CONCLUSION

7.1 General conclusion

In conclusion, this research undertaking has shown that the presence of metal complex catalysts, such as phthalocyanines, on the electrode surface and in solution enhances the oxidation of cysteine and phenolic compounds, and also improves the stability of the ordinary glassy carbon electrode.

For the electrooxidation of cysteine, practically no oxidation takes place on the carbon paste electrode when phthalocyanines are absent (in the potential range 0 to 1.0 V, *vs* Ag|*AgCl*). But in the presence of molybdenum and cobalt phthalocyanines the oxidation was found to occur at readily accessible potentials. This then suggests that cysteine oxidation in this potential range can then be entirely attributed to catalysis by phthalocyanine complexes, and this is likely to occur via the sulphur atom in the cysteine and a $\mathbf{d}_z^2$ orbital in the metal phthalocyanines. Molybdenum phthalocyanines were found to lower the potential for the detection of cysteine, and the potentials were found to be lower than those reported for other MPc catalysts. The OMo(OH)Pc- and CoPc-modified carbon paste electrodes were found to be stable over long periods of time, thus making molybdenum phthalocyanines promising in the development of catalysts for the oxidative determination of cysteine.

The factors that control the activity of metal phthalocyanines are not fully understood. However, this research undertaking has established that parameters such as redox potentials and electronic structure of the central metal play a significant role. For example, it has been discovered that the cysteine oxidation process takes place at potentials very close to M(III)/M(II) redox potential of the central metal ion of the phthalocyanine ring.

The electrooxidation of phenolic compounds on MPc-coated glassy carbon electrodes indicated that phthalocyanines of metals that do not exhibit redox process (nickel, copper and zinc) show very low activity. The catalytic activity of metallophthalocyanines with redox active metal centres (manganese, iron and cobalt) can be correlated with the ability of these metal phthalocyanines to bind extraplanar ligands. The ability to bind extraplanar ligands depends on the electronic structure of the central metal. The redox potentials were also found to be related to the electronic structure of the central metal in metallophthalocyanines, which could then serve to explain the difference in the activities of phthalocyanines of different metals. Cobalt phthalocyanine has shown a remarkable catalytic activity for the oxidation of phenolic compounds. Phthalocyanines of other metals show much less activity, which demonstrates that the electronic structure and energy levels in the metal play a key role in determining the catalytic activity. The catalytic role of phthalocyanines is further explained by Zagal [79] who postulated that if the electronic level of uncoated electrode and the reactant molecule lie too far apart, the transition of electrons is improbable. This therefore implies that the phthalocyanine catalyst acts as a mediator, providing intermediate electronic levels, thus increasing the probability of electron transfer. It has also been established that to exhibit higher catalytic activity, the phthalocyanines should have intrinsic redox activity in the potential region of the reaction and they should not bind the reactant strongly.

Since oxidation of phenolic compounds on CoPc-CMGCE were found to occur at different potentials, the difference in potential may be used to selectively determine these species on CoPc-CMGCE. The CoPc-CMGCE was also found to have higher selectivity than uncoated GCE, in that the difference in the potentials of the various phenolic compounds was higher on the former. The reason why MPc-coated GCE have a much higher selectivity than ordinary carbon and metal plates may be attributed to specific geometric structure of MPcs, in which

a metal is coordinated in the centre of the plane Pc ring, whereas in the case of uncoated or unmodified electrodes, the surface structure is random and offers all sorts of reaction (adsorption) sites. Therefore, such a surface would lead to the production of a variety of electrolysis products, as a result of which the selectivity is very low.

Generally, unmodified electrodes were found to display faster response times than the modified electrodes at all pH values. Response time is the time required by the electrode to reach a steady reading. And the response time of CoPc-CMGCE was found to depend on the pH of the media, increasing with increasing pH. The response time was also found to depend on the thickness of the CoPc complex on GCE.

Up to this stage, it can be concluded that electrooxidation of chlorinated phenols follows the same mechanism as shown in **scheme 1**. However, it is most likely that the intermediate phenoxy radicals do couple together to form dimeric products which then undergo intramolecular rearrangements and further oxidation, forming long chain polymers as reported for the oxidation of phenol and cresols [41,45]. For trichlorophenol and pentachlorophenol, steric effect is likely to hinder the formation of polymers as discussed earlier.

7.2 Future work

NMR and IR spectral analysis of the electrolysis products of chlorinated phenols has indicated that even after exhaustive electrolysis the benzene ring remains intact, without showing any dechlorination. However, this does not provide information on the nature of the products formed. These therefore calls for further investigation into the nature of products formed, possibly by subjecting electrolysis products to elemental and mass spectral analysis, which are

likely to provide information which will lead to the ultimate elucidation of the mechanism followed by the electrooxidation of chlorinated phenols. The mechanism for electrooxidation of cresols and phenol has been suggested by Sharma *et al* [41,45].

Coating of glassy carbon electrodes with $Co^{(II)}Pc$ lowers the current response for the analysis of TCP and PCP, hence more work on catalysts that will improve the GCE for the detection of TCP and PCP is needed. Also, even though for other phenolic compounds an enhancement of oxidation currents is observed on MPc modified electrodes, the stability of the modified electrode still need improvement so that there is no decrease in current response on repetitive scanning.

Molybdenum phthalocyanine lowers the potential for the oxidation of cysteine, in solution or in the matrix of the carbon paste electrode. This is an important development. However, molybdenum phthalocyanine complexes show lower sensitivity for cysteine determination than CoPc species in that concentrations as low as 10^{-7} mol dm^{-3} may be determined on the latter and the lowest concentration that can be determined on molybdenum phthalocyanine electrodes is of the order of 10^{-3} mol dm^{-3}. There is thus a need for catalysts that can both lower the potential and improve the sensitivity for the detection of cysteine on carbon electrodes. There is also a need to determine cysteine in biological systems using the modified carbon electrodes.

Studies on electrochemical dechlorination and degradation of TCP and PCP would be useful in the detoxification of these compounds.

REFERENCES

APPENDIX

References

1 Delahay P, ***Instrumental Analysis***, 1st edn., McMillan Co. (USA) 1957, p67, 81, 91-93.

2 Halbert M K and Baldwin R P, ***Anal. Chem.***, **57** (1985) 591 - 595.

3 Wang J, ***Analytical Electrochemistry***, 1st edn., VCH publishers (New York), (1994). pp86-87, 91, 162-166, 198.

4 Zagal J, Sen R K and Yeager E, ***J. Electroanal. Chem.***, **83** (1977) 207 - 213.

5 Bard A J and Faulkner L R, ***Electrochemical Methods - Fundamentals and Applications***, 1st edn., John Wiley & sons (USA) 1980.

6 O'Shea T J and Lunte S M, ***Anal. Chem.***, **66** (1994) 307 - 311.

7 Andrieux C P and Saveant J M, ***J. Electroanal. Chem.***, **93** (1978) 163 - 168.

8 Kenball C, in Basolo F and Burwell R L (editors), ***Selectivity and Poisoning in Catalysis: Progress in Research***, 1st edn., Plenum publishing Co Ltd (London) 1973, p85 - 89.

9 Xu F, Li H, Cross S J and Guarr T F, ***J. Electroanal. Chem.***, **368** (1994) 221 - 225.

10 Zagal J, Fierro C and Rozas R, ***J. Electroanal. Chem.***, **119** (1981) 403 - 408.

11 Martin C R and Foss C H, in Kissinger P T and Heineman W R (editors), ***Laboratory Techniques in Electroanalytical Chemistry - "Chemically Modified Electrodes"***, 2nd edn., Marcel Dekker Inc. (New York) 1996, p403 - 442.

12 Nyokong T, ***S. Afr. J. Chem.***, **48** (1995) 23 - 29.

13 Taube R, ***Pure and Appl. Chem.***, **38** (1974) 427 - 438.

14 Randin J P, ***Electrochim. Acta***, **19** (1974) 83 - 85.

15 Vasudevan P, Phougat N and Shukla A K, ***Appl. Organometallic Chem.***, **10** (1996) 591 - 604.

16 Limson J and Nyokong T, ***Electroanalysis***, **9: 3** (1997) 255 - 260.

17 Zagal J H and Herrera P, ***Electrochim. Acta***, **30** (1985) 449 - 454.

18 Rollman L D and Iwamoto R T, ***J. Am. Chem. Soc.***, **90** (1968) 1455 - 1463.

19 Green J M and Faulkner L R, ***J. Am. Chem. Soc.***, **105** (1983) 2950 - 2955.

20 Cotton F A and Wilkinson G, ***Advanced Inorganic Chemistry***, 4th edn., John Wiley & sons (New York) 1980, p620, 845.

21 Meshitsuka S, Ichikawa M and Tamaru K, ***J. Chem. Soc. - Chem. Commun.***, (1974) 158 - 159.

22 Stillman M J and Nyokong T, in Leznoff C C and Lever A B P (editors), ***Phthalocyanines: Properties and Applications***, Vol.1, Ch.3. 1st edn., VCH publishers (New York) 1989.

23 Lever A B P, Milaeva E R and Speier G, in Leznoff C C and Lever A B P (editors) ***Phthalocyanines: Properties and applications***, Vol.3, Ch.1. 1st edn., VCH publishers (New York) 1993.

24 Milgrom L R, ***The colours of life: An introduction to the chemistry of porphyrins and related compounds***, 1st edn. Oxford University Press (New York) 1997, p195.

25 Gruen L C and Blagrove R J, ***Aust. J. Chem.***, **26** (1973) 319 - 323.

26 Blagrove R J and Gruen L C, ***Aust. J. Chem.***, **25** (1972) 2553 - 2558.

27 Morrison R T and Boyd R N, ***Organic Chemistry***, 5th edn., Allyn & Bacon (London) 1987, p1345 - 1352.

28 a) Stankovich M and Bard A J, ***J. Electroanal. Chem.***, **75** (1977) 487 - 505.
b) Kolthoff I M, Stricks W and Tanaka N, ***J. Am. Chem. Soc.***, **77** (1955) 4739 - 4742.
c) Stricks W and Kolthoff I M, ***J. Am. Chem. Soc.***, **75** (1953) 5673 - 5681.
d) Kolthoff I M and Barnum C, ***J. Am. Chem. Soc.***, **63** (1941) 520 - 526.
e) Bianco P and Haladjian J, ***Electrochim. Acta***, **25** (1980) 1317 - 1320.

29 a) Pradáč J and Koryta J, ***J. Electroanal. Chem.***, **17** (1968) 167- 175.
b) Kolthoff I M and Barnum C, ***J. Am. Chem. Soc.***, **62** (1940) 3061 - 3065.
c) Samec Z, Malycheva Zh, Koryta J and Pradáč J, ***J. Electroanal. Chem.***, **65** (1975) 573 - 586.
d) Davis D G and Bianco E, ***J. Electroanal. Chem.***, **12** (1966) 254 - 260.

30 Korfhage K M, Ravichandran K and Baldwin R P, ***Anal. Chem.***, **56** (1984) 1514 - 1517.

31 Christophersen M J and Cardwell T J, ***Anal. Chim. Acta***, **323** (1996) 39 - 46, and references therein.

32 Armentrout D N, McLean J D and Long M W, ***Anal. Chem.***, **51: 7** (1979) 1039 - 1045.

33 Kilner E and Samuel D M, ***Applied Organic Chemistry***, edn., McDonald (London) 1960, 484p.

34 Dennison M J, Hall J M and Turner A P F, ***Anal. Chem.***, **67** (1995) 3922 - 3927, and references therein.

35 Jáuregui O and Galceran M T, ***Anal. Chim. Acta***, **340** (1997) 191 - 199.

36 Emerson E, ***J. Org. Chem.***, **8** (1943) 417 - 428.

37 Martin F and Otto M, ***Fres. J. Anal. Chem.***, **352** (1995) 451 - 455.

38 Busto O, Olucha J C and Borrull F, ***Chromatographia.***, **32: 9/10** (Nov. 1991) 423-428.

39 Shoup R E and Mayer G S, ***Anal. Chem.***, **54** (1982) 1164 - 1169.

40 Wang J and Chen Q, ***Anal. Chim. Acta***, **312** (1995) 39 - 44.

41 Sharma L R, Singh G and Sharma A, ***Ind. J. Chem.***, **25A** (1986) 345 - 349.

42 Hedenburg J F and Freiser H, ***Anal. Chem.***, **25: 9** (Sept. 1953) 1355 - 1358.

43 Gaylor V C and Elving P J, ***Anal. Chem.***, **25: 7** (July 1953) 1078 - 1082.

44 Ruzgas T, Emnéus J, Gorton L and Marko-Varga G, ***Anal. Chim. Acta.***, **311** (1995) 245 - 253.

45 Sharma L R, Singh G and Sharma A, ***B. Electrochem.***, **4: 7** (1988) 679 - 682.

46 Wang J and Lin M H, ***Anal. Chem.***, **60** (1988) 499 - 502.

47 Koile R C and Johnson D C, ***Anal. Chem.***, **51** (1979) 741 - 744.

48 Wang J and Li R, ***Anal. Chem.***, **61** (1989) 2809 - 2811.

49 Poon M and McCreery R L, ***Anal. Chem.***, **59** (1987) 1615 - 1620.

50 Tse Y, Janda P, Lam H and Lever A B P, ***Anal. Chem.***, **67** (1995) 981 - 985.

51 Chebotareva N and Nyokong T, ***J. Appl. Electrochem.***, **27** (1997) 975 - 981.

52 Sorokin A and Meunier B, ***Chem., Eur. J.***, **2: 10** (1996) 1308 - 1317.

53 Sorokin A, Séris J and Meunier B, ***Science***, **268** (1995) 1163 - 1166.

54 Mylonas A and Papaconstantinou E, ***J. Photochem. Photobio. A: Chem.***, **94** (1996) 77 - 82.

55 Nensala N and Nyokong T, ***Polyhedron***, **16: 17** (1997) 2971 - 2976.

56 Weber J H and Busch D H, ***Inorg. Chem.***, **4:4** (1965) 469 - 475.

57 Edmondson S J and Mitchell C H, ***Polyhedron***, **5** (1986) 315 - 317.

58 Nyokong T, ***Polyhedron***, **13: 2** (1994) 215 - 220.

59 Ferraudi G, Nyokong T, Feliz M, Perkovic M and Rilema D P, ***Inorg. Chim. Acta***, **215** (1994) 27 - 32.

60 Farrel N P, Murray A J, Thornback J R, Dolphin D H and James B R, ***Inorg. Chim. Acta***, **28** (1978) L144 - L146.

61 Gagne R R, Koval C A and Lisensky G C, ***Inorg. Chem.***, **19** (1980) 2855 - 2857.

62 Tse Y, Janda P, Lam H, Zhang J, Pietro W J and Lever A B P, ***J. Porphyrins and Phthalocyanines***, **1** (1997) 3 - 16.

63 Lever A B P, Hempstead M R, Leznoff C C, Liu W, Melnik M, Nevin N A and Seymour P, ***Pure Appl. Chem.***, **58: 11** (1986) 1467 - 1476.

64 Shurvell H F and Pinzuti L, ***Can. J. Chem.***, **44** (1966) 125 - 136.

65 Hill H A O and Norgett M M, ***J. Chem. Soc.***, (1966) 1476 - 1480.

66 Kroenke W J and Kenney M E, ***Inorg. Chem.***, **3: 5** (1964) 696 - 698.

67 Kendall D N, ***Anal. Chem.***, **25: 3** (1953) 382 - 389.

68 Jones R A, ***Aust. J. Chem.***, **16: 1** (1963) 93 - 100.

69 Nakamoto K, ***Infrared and Raman Spectra of Inorganic and Coordination Compounds***, 3rd edn., John Wiley (New York) 1978, 448p.

70 Pavia D L, Lampman G M and Kriz G S, ***Introduction to Spectroscopy***, 1st edn., Saunders College publishing (USA) 1979, 367p.

71 Li H and Guarr T F, ***J. Chem. Soc.***, (1989) 832- 834.

72 Ebert A A and Gottlieb H B, ***J. Am. Chem. Soc.***, **74** (1952) 2806 - 2810.

73 Galindo S and González-Tovany L, ***Rev. Mex. Fís.***, **32** (1986) 435 - 453.

74 Matsuda Y and Murakami Y, ***Coord. Chem. Rev.***, **92** (1988) 157 - 192.

75 Elvidge J A and Lever A B P, ***J. Chem. Soc.***, (1961) 1257 - 1265.

76 Pang D and Wang J, ***J. Electroanal. Chem.***, **358** (1993) 235 - 246.

77 Cookson F J, Smith T D, Boas J F, Hicks P R and Pilbrow J R, ***J. Chem. Soc.***, (1977) 109 - 114.

78 Furuya N and Matsui K, ***J. Electroanal. Chem.***, **271** (1989) 181 - 191.

79 Zagal J H, ***Coord. Chem. Rev.***, **119** (1992) 89 - 136.

80 Macor K A and Spiro T G, ***J. Am. Chem. Soc.***, **105** (1983) 5601 - 5607.

81 Coutanceau C, Crouigneau P, Leger J H and Lamy C, ***J. Electroanal. Chem.***, **379** (1994) 389 - 397.

82 Plummer D T, ***An Introduction to Practical Biochemistry***, 3rd edn., McGraw Hill (London) 1987, p44.

83 Fisher B and Eisenberg R, ***J. Am. Chem. Soc.***, **102** (1980) 7361 - 7363.

84 Geske D H and Bard A J, ***J. Phys. Chem.***, **63** (1959) 1057 - 1062.

85 Pouchert C J, ***The Aldrich Library of NMR Spectra***, 2nd edn., Aldrich (USA) 1983. 1196p.

Appendix 1

Publications accruing from this work

The following papers have been published as a result of this work;

1. Tsukutlane J Mafatle and Tebello Nyokong, ***Journal of Electroanalytical Chemistry,*** -"Electrocatalytic oxidation of cysteine by Molybdenum(V) phthalocyanine complexes", **408** (1996) 213 - 218.

2. T Mafatle and T Nyokong, ***Analytica Chimica Acta,*** - "Using cobalt(II) phthalocyanine to improve the sensitivity and stability of glassy carbon electrodes for the detection of cresols, chlorophenols and phenol", **354** (1997) 307 - 314.

----------o0o----------